Workshop on Quantitative EPR

Dave Barr, Sandra S. Eaton, and Gareth R. Eaton
At the 31st Annual International EPR Symposium, Breckenridge, Colorado
July 27, 2008

Additional contributors to this booklet include
Ralph T. Weber, Patrick Carl, Peter Höfer,
Richard W. Quine, George A. Rinard, and Colin Mailer

Abstract
There is a growing need in both industrial and academic research to provide meaningful and accurate quantitative results from EPR experiments. Both relative intensity quantification of EPR samples and the absolute spin concentration of samples are often of interest. This workshop will describe and discuss the various sample-related, instrument-related and software-related aspects for obtaining useful quantitative results from your EPR experiments. Some specific items to be discussed include: choosing a reference standard, resonator considerations (Q, B_1, B_m), power saturation characteristics, sample positioning, and finally, putting all the factors together to provide a calculation model for obtaining an accurate spin concentration of a sample.

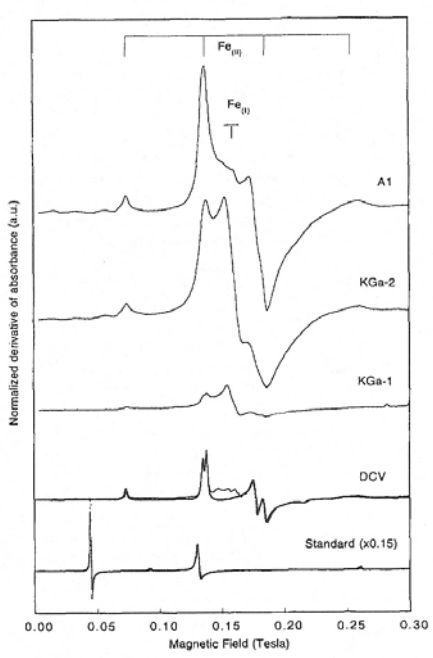

How many spins?

This graphic is intended to represent the fact that interpreting EPR spectra in terms of the number of spins in the sample ultimately depends on the use of the analytical balance for gravimetric determination of concentrations. The particular balance pictured is one that was used by Dr. Chester Alter, former Chancellor of the University of Denver, who determined atomic weights in the laboratory of Theodore William Richards (Nobel Prize 1914).

Quantitative analysis of a spectrum such as that shown (Fe^{3+} in kaolinite (Balan et al. 2000)) requires also computational simulation of the Fe^{3+} EPR spectrum, as outlined in the 2006 Workshop.

Table of Contents

Introduction

Quantitative EPR can be subdivided into two main categories for the common EPR applications: intensity and magnetic field/microwave frequency measurement.

Intensity is important for spin counting. This information is important for kinetics, mechanism elucidation, and a number of industrial applications. It is also important for studying magnetic properties.

Magnetic field/microwave frequency is important for g and A value measurements that reflect the electronic structure of the radicals or metal ions. (see the 2006 Workshop on Computation of EPR Parameters and Spectra.)

This Workshop might at first glance seem to be a step back from some of the topics discussed in some of the prior Workshops, but actually quantitative "routine CW EPR" is one of the most difficult aspects of EPR, and requires deep understanding of the spectrometer and the spin system.

Prior Workshops

- 1987 Workshop on the Future of EPR
  The Future of EPR Instrumentation, G. R. Eaton and S. S. Eaton, *Spectroscopy* **3**, 34-36 (1988).
- 1992 Workshop on the Future of EPR
  The Future of Electron Paramagnetic Resonance Spectroscopy, S. S. Eaton and G. R. Eaton, Spectroscopy, 8 20-27 (1993).
  The Future of Electron Paramagnetic Resonance Spectroscopy, S. S. Eaton and G. R. Eaton, Bull. Magn. Reson. 16, 149-192 (1995).
- 1999 First Pulsed EPR Workshop
- 2000 Workshop on Pulsed EPR
- 2001 Multifrequency EPR Workshop – Downloadable from Bruker Web Site
- 2002 Workshop on EPR of Aqueous Samples - Downloadable from Bruker Web Site
- 2003 Workshop on Measuring Electron-Electron Distances by EPR - Downloadable from Bruker Web Site
- 2004 Workshop on EPR Imaging- Downloadable from Bruker Web Site
- 2005 Workshop on Selecting an EPR Resonator
- 2006 Workshop on Computation of EPR Parameters and Spectra - Downloadable from Bruker Web Site

The 2008 Workshop will focus on CW quantitative EPR. The same fundamentals apply to quantitative pulsed EPR, but the detailed considerations are enough different that only CW will be discussed in the 2008 Workshop. Aspects of quantitative EPR have been embedded in each of the prior workshops, and we will refer back to them, and incorporate material from them, at appropriate points.

Chapter 1 – Why Should Measurements be Quantitative?

Even if the question is simply "is there a radical present?" you need to know, e.g., whether <1% or 100% of the species are in the radical form or in a particular metal oxidation state. There are many examples in the literature in which an impurity or a slight dissociation resulted in the EPR signal observed. One of the most dramatic in recent years was the EPR signal that was incorrectly attributed to C_{60}^-, which was full-scale when the true anion signal was not seen in the baseline because it was so much broader.

This Workshop will focus on radicals in condensed phases, and primarily at X-band. Gas phase EPR is a special area. Those interested should refer to the comprehensive 1975 review (Westenberg 1975).

Among the common type of measurements in which intensity quantitation is essential are:

- How many spins are there in a biological sample?
- What is the spin state of a metal complex as a function of temperature?
- What is the age of an archeological artifact?
- What is the radiation dose?
- What will be the shelf life of foods and beverages?

Line width quantitation is essential for:

- Oxymetry
- Molecular motion
- Relating line width to relaxation times and hyperfine couplings.

Magnetic field quantitation is essential for:

- Measurement of g values
- Measurement of hyperfine splittings
- Comparison of either with computation of these parameters.

1.1 Examples of Applications of Quantitative EPR

Burns and Flockhart (1990) reviewed several applications of quantitative EPR, including assays for drugs in body fluids (free radical assay technique - FRAT), radiation dosimetry, molybdenum in sea water, Fe, Mn, and even assays for diamagnetic metals by use of spin-labeled ligands. Two reviews on quantitative EPR and quality control in EPR that are a bit hard to find are appended (Eaton and Eaton 1980; 1992).When the goal is to measure the paramagnetic component of a complicated mixture, EPR may be more selective than other common analytical techniques. It is a strength of EPR that it can be applied to samples whose scattering properties or opacity would prevent quantitative optical techniques, samples whose mix of other metals would make colorimetric, gravimetric, etc. elemental analysis a challenging separations exercise, and EPR can be applied nondestructively to species such as radiation defects that would not persist through many other types of analytical procedures. Thus, it is not surprising that many reviews of EPR target the analytical community (Saraceno et al. 1961; Molin et al. 1966; Alger 1968; Randolph 1972; Goldberg and Bard 1983; Burns and Flockhart 1990; Eaton and Eaton 1990; 1997; Blakley et al. 2001). Whether one is measuring cigarette smoke, protein redox, or

beer stability, the answers provided by EPR can be accurate within a few percent, or wrong by more than a factor of two, depending on how carefully one follows the guidance set forth in this Workshop. A few examples will drive home this point.

1.1.1 Effect of Q

Blakley et al. (2001) showed that there were large differences in apparent free radical concentration in identical samples depending on the resonator used in the analysis, because the standard and the sample had different effects on resonator Q. Adding 0.1 M PBN (n-tert-butyl-α-phenylnitrone) to a benzene solution of tempo decreased the resonator Q from 4400 to 2600. Only after comparing samples in which radicals were trapped by PBN with standards containing the same concentration of PBN was radical concentration agreement achieved on all three spectrometers tested.

1.1.2 Dynamic Range

Distances between unpaired electrons in the range of ca. 4-12 Å can be measured by determining the relative intensity of the half-field transition to the intensity of the transitions in the $g \approx 2$ region (Eaton and Eaton 1982; Eaton et al. 1983). The relevant formula is

$$\text{relative intensity} = \frac{(19.5 \pm 0.5)(9.1)^2}{r^6 \nu^2}$$

where r is the distance in Å and ν is the microwave frequency in GHz.

The relative intensity of the half-field transition is very small. For example, at 8Å the relative intensity is about 7×10^{-5}. This would be very demanding of the S/N and dynamic range of the spectrometer. However, since the area, and not the line shape, is desired, larger than normal modulation amplitude can be used to improve the S/N. Further, the half-field transition is less easily saturated than is the $g \approx 2$ signal, so higher microwave power can be used for the half-field transition. Integration of these signals requires care about background corrections. Paying close attention to these matters, each of which is discussed in more detail later in these notes, provides accurate results for an important and useful measurement.

Another aspect of dynamic range in EPR is illustrated by the spectra of radical species derived from C_{60}. After many studies it has been learned that there is a radical impurity in most preparations of C_{60}. In the early days, the spectrum of this radical impurity was incorrectly identified as the spectrum of C_{60}^-. The problem was that this spectrum is very narrow, so when it was full scale, the spectrum of the anion was weak enough that it was possible to miss it. Figure 1-1 shows the broad spectrum of C_{60}^- when the narrow spectrum is off-scale (Schell-Sorokin et al. 1992).

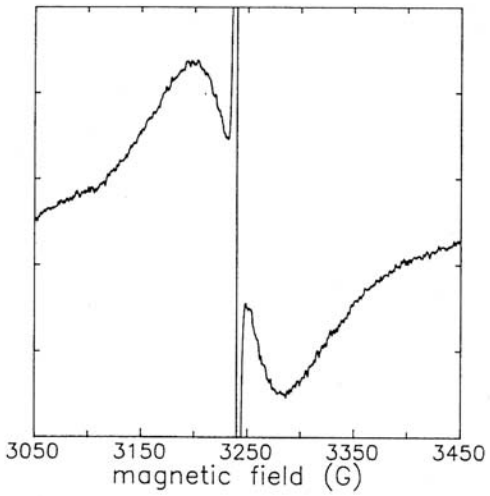

Fig. 4. Continuous wave X-band (9.1 GHz) ESR spectrum of ≈0.2 mM $Ca(C_{60})_2$ in MeTHF at 295 K obtained with 20 mW microwave power, 5 G modulation amplitude, and 400 G sweep width.

Figure 1-1 CW EPR spectrum of the C_{60} anion radical with a sharp impurity signal superimposed. From Schell-Sorokin et al. 1992.

Not all samples to which one might want to apply quantitative EPR are "clean." One interesting problem is to correlate the EPR spectrum in Figure 1-2 to the age of a blood stain (Fujita et al. 2005). The ratio of the signal labeled H to that labeled g4 provided a linear log-log plot up to 432 days, as shown in Figure 1-3 (Fujita et al. 2005).

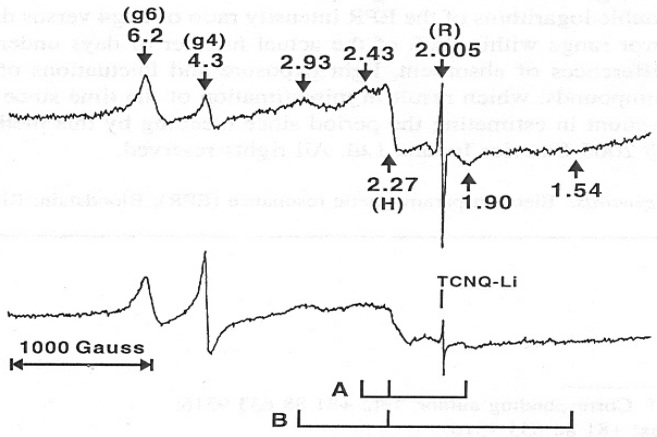

Fig. 1. EPR spectra at 77 K of dried human blood on filter paper on the 1st day (upper) and 775th day (bottom) after extraction. Tetracyanoquinod-imethane-lithium salt (TCNQ-Li, g = 2.00252) was used as standard for g-value calculation.

Figure 1-2. EPR of a blood stain.

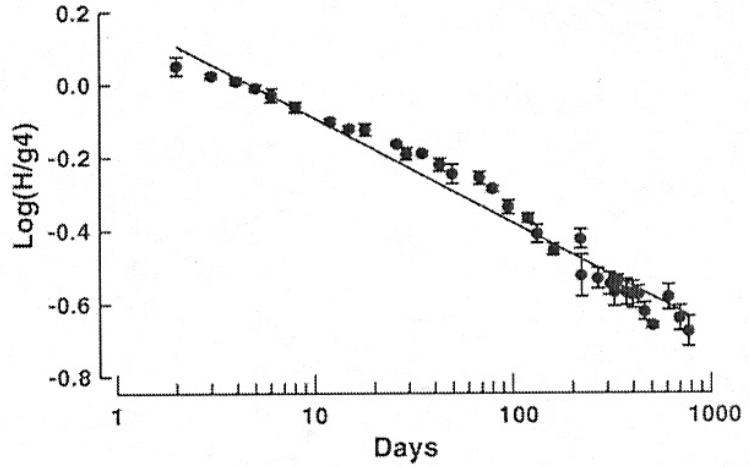

Fig. 3. Logarithmic plot of the intensity ratio (H/g4) of the two different EPR signals as a function of the age of dried human bloodstains. Data are mean values ± S.D. for three individual blood samples.

Figure 1-3. EPR intensity vs. age of dried human blood stains.

1.1.3 Radiation Dosimetry

Almost anything used in the operating room is sterilized either with γ rays or e-beam. Many other items, such as food and mail are also treated with radiation. The preferred method of measuring the radiation dose used for sterilization is EPR radiation dosimetry using alanine as the dosimeter. To ensure sterility (and avoid the legal liability if goods are not sterile) and to run a cost-effective business, the radiation dose measurement must be reliable, reproducible, accurate, and often performed by unskilled laborers. Also the results must be easily transferred to a LIMS system for auditing purposes.

The Bruker e-scan benchtop EPR spectrometer has been specifically designed for such applications. The resonator incorporates a special sample holder that reproducibly positions the alanine film dosimeter in the resonator. The sample holder also has a reference marker so that variations in instrument response can be used to normalize the intensity. A bar-code reader is incorporated so that the individual dosimeters are identified and the results logged properly into the quality control database.

Through careful control of sample positioning, size, and properties, a reproducibly of better than 0.5 % is attained.

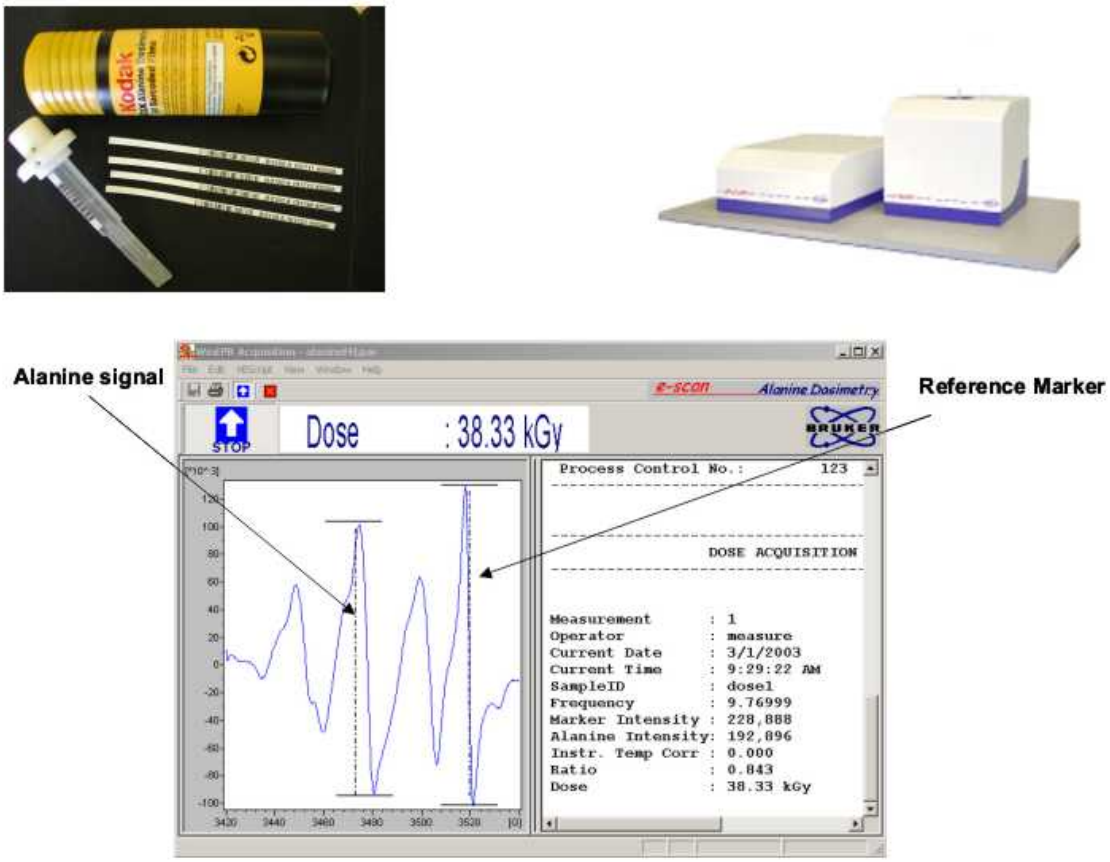

Figure 1 -4 E-scan with film holder and bar-coded film.

In vivo radiation dosimetry is an important application of quantitative EPR. For a review of current efforts, see Swartz et al. (2006).

1.1.4 Use of accurate line width information

Current effort in many laboratories (refer to the 2004 Workshop on EPR Imaging) seeks to use quantitative EPR to measure O_2 concentration in vivo. This is a case in which accuracy of line width information is more important than amplitude or g value. Some papers since the 2004 Workshop illustrate successful steps in this field. Halpern and coworkers have carefully calibrated the EPR method against the standard (invasive) fluorometric probe method that requires inserting a fiber optic probe into the animal. There is good agreement, and the EPR method has the advantages that it is 3-dimensional rather than just a spot measurement, and EPR does not damage the tissue that it measures (Elas et al. 2006). Presley et al. (2006) used EPR oximetry to measure cellular respiration.

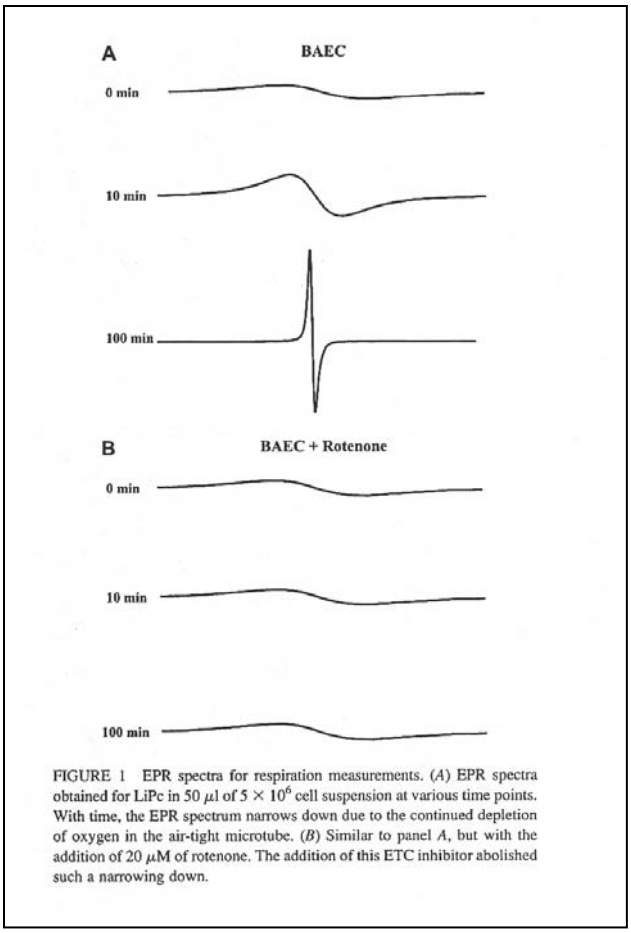

FIGURE 1 EPR spectra for respiration measurements. (*A*) EPR spectra obtained for LiPc in 50 μl of 5×10^6 cell suspension at various time points. With time, the EPR spectrum narrows down due to the continued depletion of oxygen in the air-tight microtube. (*B*) Similar to panel *A*, but with the addition of 20 μM of rotenone. The addition of this ETC inhibitor abolished such a narrowing down.

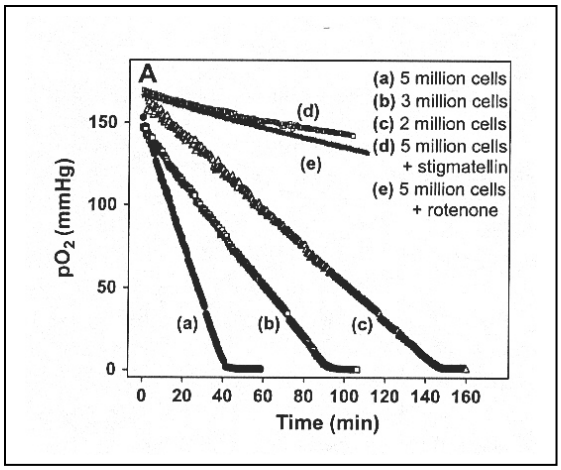

Figure 1-5 The line width of the X-band EPR spectrum of LiPc microcrystals in a suspension of bovine aortic endothelial cells (BAEC) decreased with time as the cells consumed the oxygen that broadened the EPR signal of the LiPc. The EPR measurements were made with sufficient accuracy to define three phases of cellular respiration (Presley et al. 2006).

1.1.5 Catalysis and Mineralogy

Many applications of quantitative EPR to catalysis and mineralogy were summarized by Dyrek et al. (1994; 2003).

Chapter 2 - Introduction to Quantitative EPR

Although most people attending this Workshop are familiar with EPR, we repeat some "elementary" aspects of EPR in order to comment about quantitative aspects.

2.1 General Expression for CW EPR Signal Intensity

The general expression for CW EPR signal intensity is:

$$V_S = \chi'' \eta Q \sqrt{P Z_0}$$

where V_S is the signal voltage at the end of the transmission line connected to the resonator, η (dimensionless) is the filling factor (Poole 1967), Q is the loaded quality factor of the resonator, Z_0 is the characteristic impedance of the transmission line, and P is the microwave power to the resonator produced by the external microwave source (Rinard et al. 1999a; 2004). The magnetic susceptibility of the sample, χ'', is the imaginary component of the effective RF susceptibility. Optimizing the EPR measurement involves optimizing each of these crucial parameters. Key variables on which we will focus this discussion of quantitative EPR are χ'', Q and η.

2.2 The EPR Transition

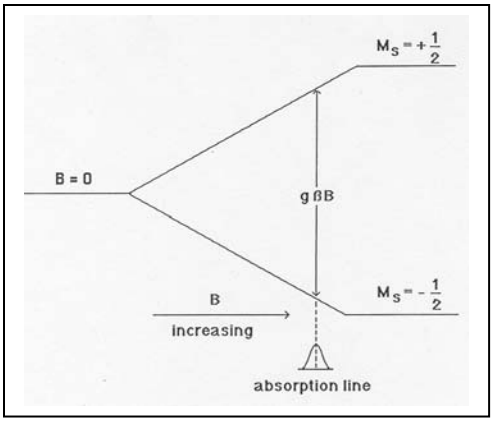

Figure 2-1 Sketch of the magnetic-field-dependent splitting of the energy levels for a single unpaired electron.

Pulsed EPR is fairly easy to understand. The usual vector diagram shows that the B_1 vector that is perpendicular to the spin magnetization (taken to be along the z direction) turns the magnetization into the xy plane. The magnetization in the xy plane induces a voltage in a detector coil (without loss of generality, this voltage could be in the conducting surfaces of a cavity or split ring resonator), which then is detected (i.e., rectified – converted to dc), amplified, and displayed. The magnetization in the xy plane changes with time due to T_2 relaxation (randomization in the xy plane) and T_1 relaxation (return to the z direction). After a single pulse, the induced voltage is the free induction decay (FID) and after two pulses there is an echo in addition to the FID after each of the pulses. There is additional discussion of the comparison of pulsed and CW EPR in the Appendix. See also the chapter by Jeschke (2007).

How do we relate the pulsed EPR vector picture to the CW picture? At field/frequency resonance, the CW B_1 is turning the spins as in the pulse case, but only by a very little amount. There is a voltage induced in the conductor of the resonator, as in the pulse case. The voltage is

proportional to the angle by which the spins were turned by B_1. If the CW signal is not "saturated" the T_1 and T_2 are short enough that relaxation back to the z axis is fast relative to other time constants of the experiment (such as field modulation). Hence, we can view the signal as always almost at equilibrium. If the microwave power is too high for the T_1, the B_1 turns the spins too far away from the z axis for the T_1 to return the magnetization very far within the time scale of the signal measurement, and the induced voltage is less than proportional to B_1, so the detected EPR signal does not increase linearly with square root of incident power. With small B_1 repeatedly perturbing the spin magnetization by very small amounts, the voltage induced in the resonator is very small. In order to distinguish the signal from the noise, one encodes the signal by modulating the magnetic field. Assuming that the noise is not correlated with the modulation, phase-sensitive detection at the modulation frequency greatly improves the S/N.

When the relaxation rate is fast enough (T_1 is short enough) that relaxation-dependent processes are not observed in the EPR signal, it becomes useful to take a different view of the EPR absorption. The T_1 relaxation converts microwave energy to heat via the spin-lattice relaxation process. For example, the electron magnetic moment could couple with the orbital angular momentum, which couples to thermal motion of the molecule. Conversion of microwave energy to heat appears, phenomenologically, to be microwave energy dissipation in a resistor. As shown in the section on resonator Q, this resonant absorption of microwaves looks like a change in resistance of the resonator, and hence a lowering of the resonator Q at resonance. "Critically coupling" the resonator matches it to the transmission line, so when the microwave power is absorbed at EPR resonance, the resonator becomes mis-matched, and power is reflected from the resonator. The reflected power is encoded at the modulation frequency, so discussion in terms of reflected power becomes equivalent to discussion in terms of induced voltage.

Interpretation of the schematic energy level diagram for an EPR transition (Figure 2-1) in the context of quantitative EPR requires (a) that the EPR spectrometer be constructed such that the microwave B_1 ($h\nu = g\beta B$) is actually perpendicular to the main magnetic field, B_0, (b) the temperature of the sample is known, so that the Boltzmann population of the two levels is known, (c) the magnitude of B_1 and its distribution over the sample is known, (d) the Q of the resonator is known, and some other experimental parameters, such as the modulation amplitude, are defined, as discussed below. Similarly, if the feature that is to be measured quantitatively is the line width, sketched as an absorption line in the Figure, one has to know that the magnetic field is homogeneous and scanned reproducibly without significant jitter.

2.2.1 Hyperfine Splitting

If the measurement of interest is the hyperfine splitting, then the additional energy levels shown in Figure 2-2 are important. A key thing to note about the energy levels in Figure 2-2 is that they are parallel only at magnetic fields that are large relative to the splitting. As will be emphasized later for nitroxyl radicals, the energy levels are not parallel at low magnetic fields, such as those used for in vivo studies.

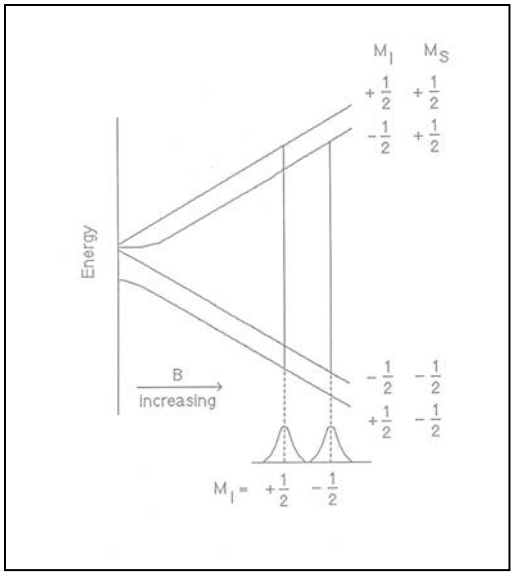

Figure 2-2 Schematic energy level diagram showing the splitting of the two energy levels in Figure 2-1 into 4 energy levels due to interaction of the electron spin with a nuclear spin of ½. The result is 2 allowed transitions.

Nitroxyl radicals, with I = 1 ^{14}N, have 6 energy levels in the high field approximation, resulting in 3 allowed transitions. The resulting absorption spectrum is shown in Figure 2-3. This figure also reveals 6 additional lines of lesser intensity. These are often called ^{13}C "sidebands," but really they are the spectrum of the part of the nitroxyl sample that is composed of molecules with ^{13}C instead of ^{12}C. The observed spectrum is the superposition of the spectra due to all of the isotopic species present in the sample.

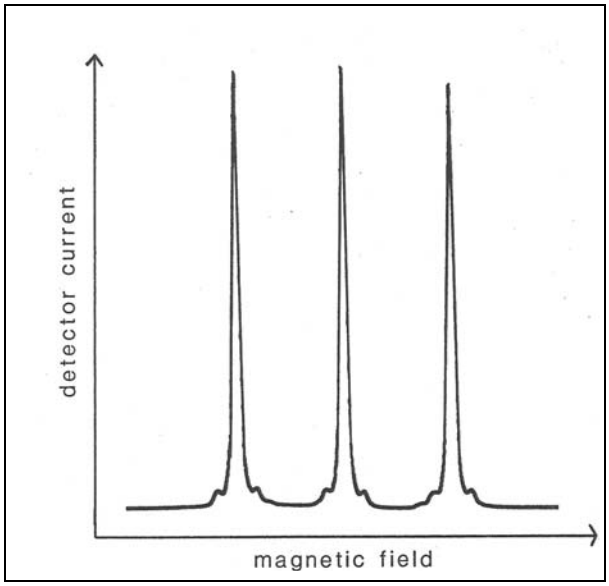

Figure 2-3 X-band CW EPR absorption spectrum of a nitroxyl radical with natural abundance C and N isotopes.

2.3 Derivative Spectra

In Figures 2-1, 2-2, and 2-3 the EPR spectra are sketched as absorption spectra. Most EPR spectra are recorded as first-derivative spectra, because they are obtained by using magnetic field modulation and phase-sensitive detection at the modulation frequency. The principle is sketched in Figure 2-4.

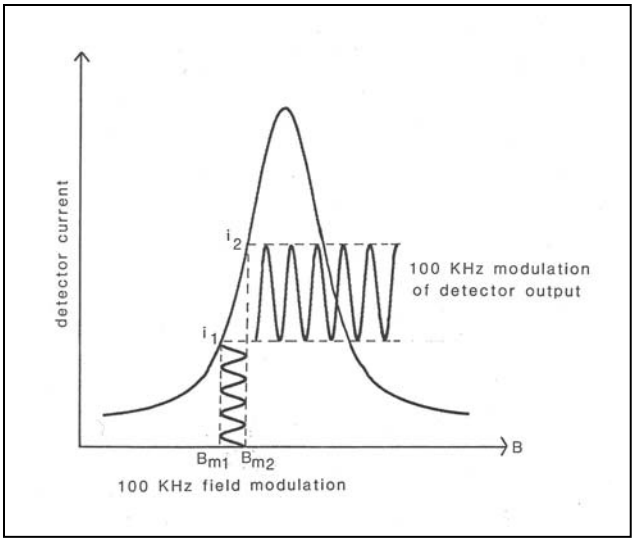

Figure 2-4 As the main magnetic field is scanned slowly through the EPR line, a small additional oscillating magnetic field, B_m, is applied in the same direction as the main field, B. B_m is commonly at 100 kHz. As B_m increases from the value B_{m1} to B_{m2}, the crystal detector output increases from i_1 to i_2. If the magnitude of B_m is small relative to line width, the detector current oscillating at 100 kHz has a peak-to-peak value that approximates the slope of the absorption curve. Consequently, the output of the 100 kHz phase-sensitive detector is the derivative of the absorption curve. This is how EPR spectra are recorded as derivative curves.

If the amplitude of the modulation is not "small" relative to the line width, then the spectrum is not the true derivative of the absorption spectrum. In addition, whenever there are two frequencies in a system, there will be sums and differences of these frequencies. Since the modulation frequency is small relative to the RF/microwave frequency, it appears as "sidebands" on the observed EPR transition. 100 kHz corresponds to ca. 35 mG, so these sidebands usually are hidden under the envelope of the EPR line. If the EPR line is very narrow, then the sidebands can be observed. For example, if K instead of Na is used to reduce TCNE, the lines are narrow enough to see the 100 kHz sidebands (J. S. Hyde and D. Leniart, Varian, 1972). See Poole for more details about modulation broadening. Schweiger and coworkers (Kälin et al. 2003) described the modulation experiment in great detail.

An advantage of derivative spectroscopy is that it emphasizes rapidly-changing features of the spectrum, thus enhancing resolution. However, a slowly changing part of the spectrum has nearly zero slope, so in the derivative display there is "no intensity." An example of how this has entered into the language of EPR is shown in Figure 2-5 where a high-spin Fe(III) spectrum is displayed. The solid line in this Figure is the derivative spectrum as recorded by the EPR spectrometer. It is common to describe this as have "a peak" at ca. g = 2 (near 3300 G in this

case) and "a peak" at ca. g = 6 (near 1100 G in this case). However, the absorption spectrum (the dashed line in the Figure) has intensity all the way from g = 6 to g = 2.

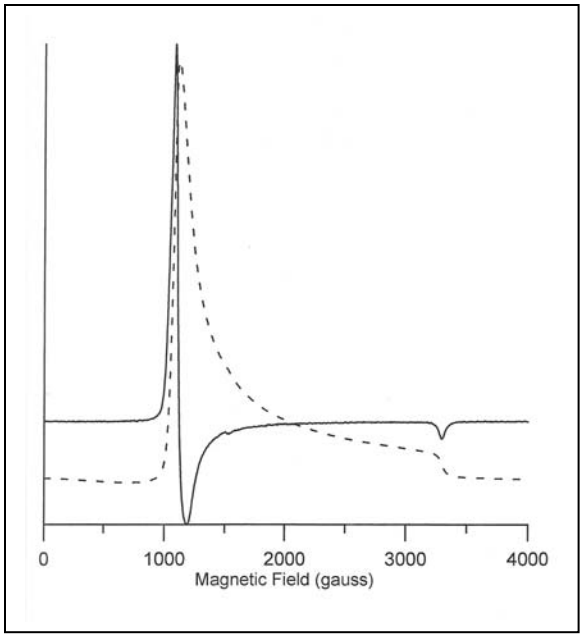

Figure 2-5 The dashed line is an X-band absorption spectrum of a high-spin Fe(III) sample. The solid line is the derivative as recorded by the EPR spectrometer.

2.4 The CW EPR Line Width

The CW EPR line width of free radicals in fluid solution is usually dominated by unresolved hyperfine interactions. In more viscous solvents and/or at higher field, the line width may be determined by intermediate tumbling rates (Freed 1976; Budil et al. 1996). In frozen solution and in solids, the line width may be determined by g and a anisotropy and distributions in these parameters, often caused by differences in environment, that is called g-strain and a-strain. Hyde and coworkers have shown how the balance of these effects leads to S-band as the frequency of choice for optimum resolution of hyperfine in Cu(II) complexes (Hyde and Froncisz 1982).
For those cases in which the line width is determined by electron spin relaxation, the line will be Lorentzian, and the relation between line width, ΔB, and the electron spin relaxation times is given by the following equations:

$$\Delta B^2 = \frac{4}{3}\frac{1}{\gamma^2 T_2^2}\left(1 + \gamma^2 B_1^2 T_1 T_2\right)$$

$$\Delta B^2 = \frac{4}{3}\left(\frac{1}{\gamma^2 T_2^2} + B_1^2 \frac{T_1}{T_2}\right)$$

$\gamma = 1.7608 \times 10^7$ rad s^{-1} G^{-1}

Thus, if B_1 is very small, only the first term in parentheses matters, and this reduces to:

$$\Delta B = \frac{2}{\sqrt{3}\gamma T_2} = \frac{6.56 \times 10^{-8}}{T_2} \text{ G when } T_2 \text{ is in seconds.}$$

This is a very handy formula for estimating limits on relaxation times. Recall that $T_1 \geq T_2$. For example, when $T_2 = 1$ μs, the peak-to-peak derivative line width is 0.0656 G. Since the line is relaxation-determined, it is Lorentzian. Note that in this limit T_1 does not affect the line width. Together with the expression for the saturation factor, and an estimate of B_1 in the resonator, this estimate of relaxation times helps select the power to use, as discussed in Ch. 3. See (Eaton and Eaton 2000b) and (Bertini et al. 1994a) for reviews of relaxation times.

However, if B_1 is not small, then the second term in parentheses contributes to the line width, which increases proportional to B_1. The longer T_1, the lower the power at which increasing the power broadens the line.

2.5 Second Derivative Operation

With magnetic field modulation and phase-sensitive detection, the voltage at the detector can be expressed in a Fourier series (Noble and Markham 1962; Russell and Torchia 1962; Wilson 1963; Poole 1983). The ν_m term is the first derivative, and the component detected at $2\nu_m$ is the second derivative. Note that whereas the amplitude of the first derivative EPR signal is proportional to the modulation amplitude, A, the amplitude of the second derivative EPR signal is proportional to the square of the modulation amplitude. If you integrate a first derivative spectrum twice (I_1) and a second derivative spectrum three times (I_2) the results are related by $I_2 = I_1 A/4$, if the actual absorption signal areas are identical (Wilson 1963).

It is also possible to obtain a second derivative of the EPR signal by using two modulation frequencies and two phase detectors. This follows directly from the discussion of how the first derivative lineshape is obtained, since everything stated there would remain true if the original signal were the first derivative. Thus, modulation at 100 kHz and 1 kHz, followed by phase detection at 100 kHz, yields a first derivative spectrum with a 1 kHz modulation signal on it, and then phase detection at 1 kHz yields the second derivative spectrum. If you go one step further and use the second harmonic of the high frequency modulation plus a low frequency modulation, you get the third derivative display.

Derivatives can also be generated with computer manipulation of digitally stored data. However, straight-forward numerical derivative computation causes such a noisy looking derivative (due to the discrete nature of the data array) that it is not very useful unless the original data were virtually noise-free or unless extensive multi-point averaging is used. Much more useful is the pseudomodulation technique developed by Hyde and coworkers (1992). This function is in Xepr.

2.6 What Transitions Can We Observe?

When the spectrometer is set up to observe the allowed transitions such as those sketched in Figures 2-1 and 2-2, and the spin system is S = ½ with some number of nuclear spin interactions, then the observation is limited by the relaxation times and the relation of the external magnetic field to the hyperfine-split width of the spectrum. At X-band and above, and for common hyperfine splittings, all of the expected lines will be observed and the relative intensities will be

as expected. However, at low microwave/RF frequencies and low magnetic fields, some of the expected lines may not be within the accessible magnetic field range, so hyperfine lines will be "missing." Examples are provided by figures in Belford et al. (1987), which are reproduced in Figures 2-6 and 2-7.

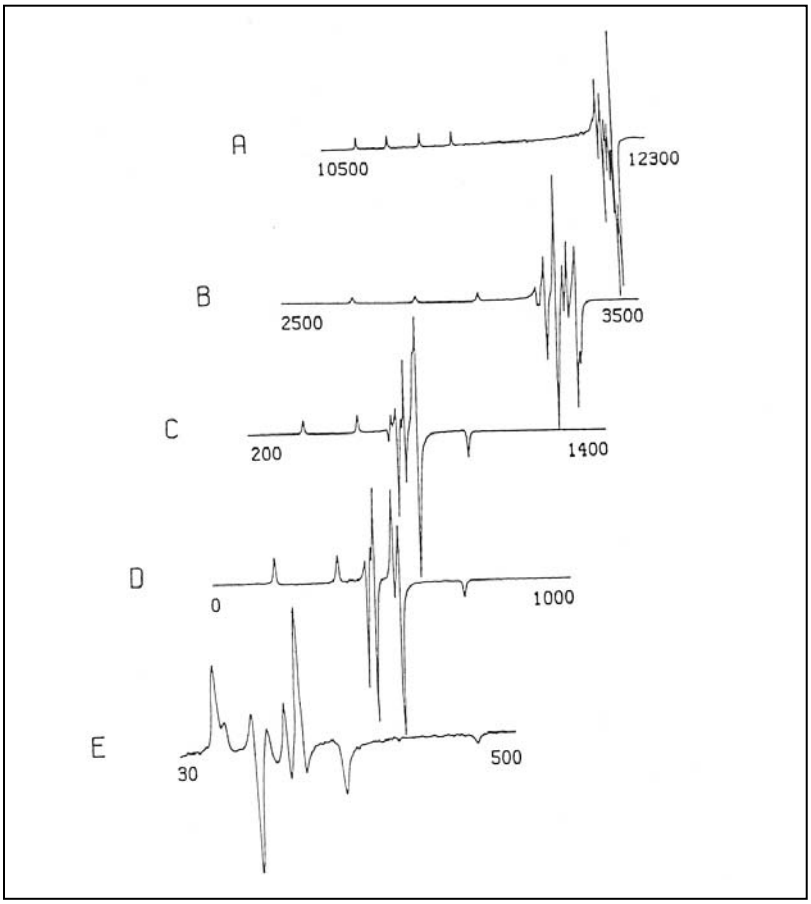

Figure 2-6 EPR spectra of ^{63}Cu doped into $Pd(acac)_2$ at various microwave frequencies. Magnetic field values are labeled on each scan for the beginning and end of the scan. (A) 34.78 GHz, (B) 9.376 GHz, (C) 2.39 GHz, (D) 1.39 GHz, (E) 560 MHz. From Belford et al. (1987).

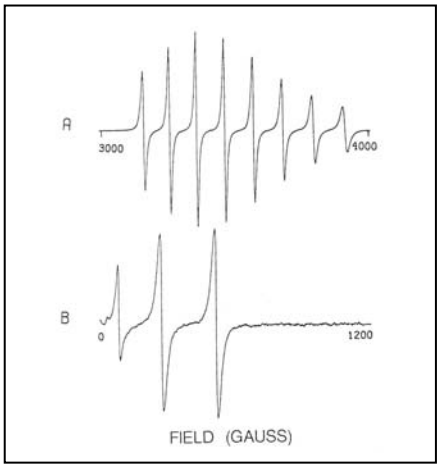

Figure 2-7 EPR spectrum of $VO(acac)_2$ in 1:1 toluene:chloroform solution at room temperature. Magnetic field values are labeled on each scan for the beginning and end of the scan. (A) 9.76 GHz, (B) 595 MHz. From Belford et al. (1987).

In addition to "missing" lines (e.g., the V spectrum in Figure 2-7), at low frequencies there may appear forbidden lines which become somewhat "allowed" due to mixing of states.

The importance of careful consideration of transition probabilities for comparison of EPR spectra when the sample and standard differ significantly was demonstrated by Siebert et al. (1994). Chromium in FeS_2 and in $AlCl_3{\cdot}6H_2O$ was measured by EPR and by ICPMS and AAS, with good agreement between methods.

As is well known, especially from recent demonstrations using high-field EPR, many EPR transitions are not observable at X-band (see the 2001 Multifrequency EPR Workshop). For $S > ½$ systems, if the ZFS $D > h\nu$ (≈ 0.33 cm^{-1} at X-band), some transitions cannot be observed. Similarly, as shown in Figure 2-7, some transitions that are easily observable at X-band are not observed at lower microwave frequencies. The field range limit of the spectrometer may also prevent observation of some transitions, even if in principle that could be observed at X-band. For example, Cordischi et al. (1999) pointed out that some Cr(III) transitions were beyond the 8000 G limit of the spectrometer used. A general discussion of transition probabilities is beyond the scope of this Workshop, but a general discussion in the context of quantitative EPR is provided by Siebert et al. (1994) and Nagy (1994), and more details can be found in standard texts.

When guidance is given here or elsewhere (e.g., Eaton and Eaton (1980)) to use a standard as similar as possible to the sample, the intent is to not only compare samples of the same size and solvent, but also standards for which the same type transitions are observed.

The introduction to what transitions one should expect to observe assumes that the relevant energy levels are thermally populated. All of pulsed EPR, ENDOR, and ELDOR depend on changing the population away from the equilibrium values.

2.7 Features of Transition Metal EPR

Transition metal ion electronic structures result in odd-electron ground states for many metals in common oxidation states, such as V^{4+}, Cr^{3+}, Mn^{2+}, Fe^{3+}, Co^{2+}, Ni^{3+}, and Cu^{2+}, and many clusters, such as iron-sulfur clusters in proteins. Whenever there is a possibility for a transition between +1/2 and -1/2 spin states, it is possible to observe an EPR spectrum at X-band. If there are closely-spaced excited states, or overlapping higher-spin states, then the relaxation time may be short, in which case cryogenic temperatures may be required to observe the EPR spectrum. Figure 2-8 shows the energy levels for a $S = ½$ ion in an octahedral field (the paper from which this figure was taken is about Sc^{2+}). This diagram applies to, for example, Ti^{3+}, V^{4+}, and Cu^{2+}. It is easy to observe the EPR spectra of Cu^{2+} and VO^{2+} complexes at room temperature, but low-spin Fe^{3+} and Co^{2+} have fast relaxation times at room temperature. For many Co^{2+} complexes, the relaxation time is so long near 4 K that passage effects occur, but the relaxation rate increases by about T^7 and becomes too short to observe the EPR signal above about 10-15 K. It is much more difficult to perform quantitative EPR of Co^{2+} than Cu^{2+} for this reason.

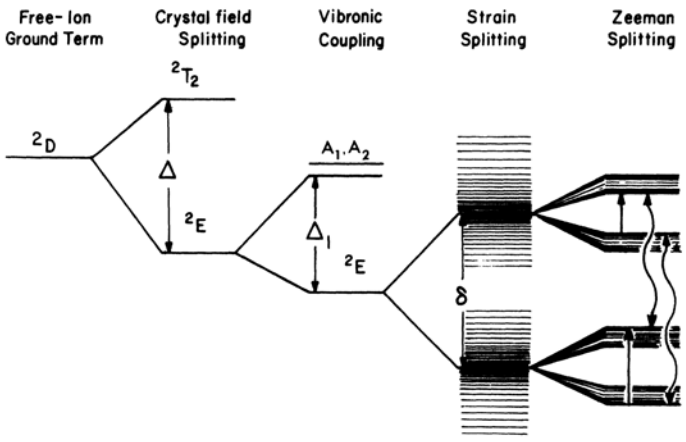

FIG. 11. Schematic energy-level diagram implied by the interpretation of the EPR parameters. The ^2D free-ion term is split by the cubic crystal field into ^2E and $^2T_2$ states with the ^2E state lowest. A weak-to-moderate vibronic interaction results in a series of vibronic states and the ground vibronic state is also a ^2E state. The first excited vibronic state is sufficiently far from the ground state to enable one to treat the ground state as an isolated ^2E state. This state is split by random internal strains into two Kramers doublets. The Kramers degeneracy is removed by an applied magnetic field and EPR transitions (represented by straight arrows) are induced by the microwave magnetic field. The wavy arrows represent vibronic relaxation processes which can produce an averaging of a portion of the anisotropic EPR pattern. This type of relaxation should not be confused with spin-lattice relaxation.

Figure 2-8 This figure, from Herrington et al. (1974) is also figure 8.4 in Weil et al. (1994, page 221).

2.8 Parallel and Perpendicular Transitions

Other paramagnetic metal ions, such as Fe^{2+} and Ni^{2+}, are missing from the list in the previous paragraph. In common ligand environments, these have even-spin states. Transitions that are forbidden because the spin has to change by more than ±1 are very weak in the normal EPR configuration. We strive hard to build resonators such that we observe with $B_1 \perp B_0$ for half-integer spin systems. However, the transitions in integer spin systems, such as triplets, transitions with nuclear spin flips $\Delta m_I = \pm 1$ (Anderson and Piette 1959), and the "half-field" transitions in interacting spin systems are enhanced with $B_1 \parallel B_0$. The Bruker ER4116DM "dual mode" cavity is designed for these studies. It is called dual mode because it operates in one mode with $B_1 \perp B_0$ at about 9.8 GHz, and in another mode with $B_1 \parallel B_0$ at ca. 9.3 GHz.

Hendrich and coworkers showed that the spectra of Mn(II) dimers can be interpreted with one set of parameters when both ⊥ and || mode spectra at X-band and Q-band as a function of temperature are simulated simultaneously (Golumbek and Hendrich 2003). In this spin system S = 0 (ground state), S =1, S = 2 *etc.* states contribute to different extents as the temperature is increased. This paper emphasizes the quantitative analysis of dinuclear Mn(II) complexes by using simulation of the spectra.

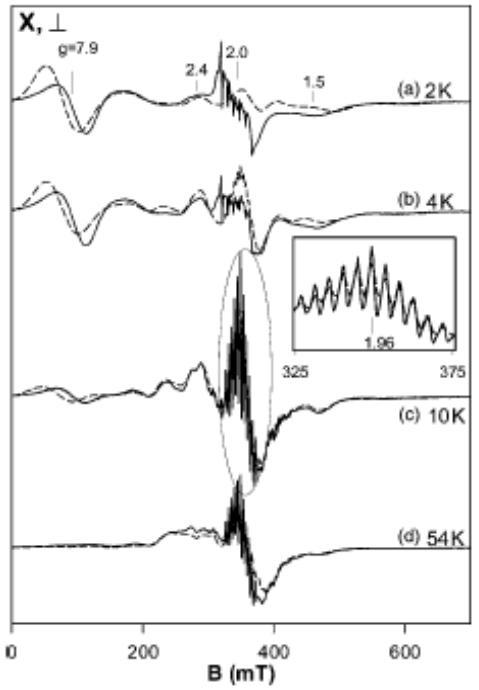

Fig. 7. Variable temperature, perpendicular mode, X-band EPR spectra (solid lines) and simulations (dashed lines) of an 11.5 mM sample of 1 in 50:50 CH_3CN:DMF. The simulation parameters are given in Table 1. Relative displayed intensities: (a, b) 1×, (c) 2×, (d) 3×; EPR conditions: temperatures as listed; frequency, 9.62 GHz; power, 0.02 mW (a,b); 0.2 mW (c); 2 mW (d); $B_{mod} = 0.6\,mT_{pp}$.

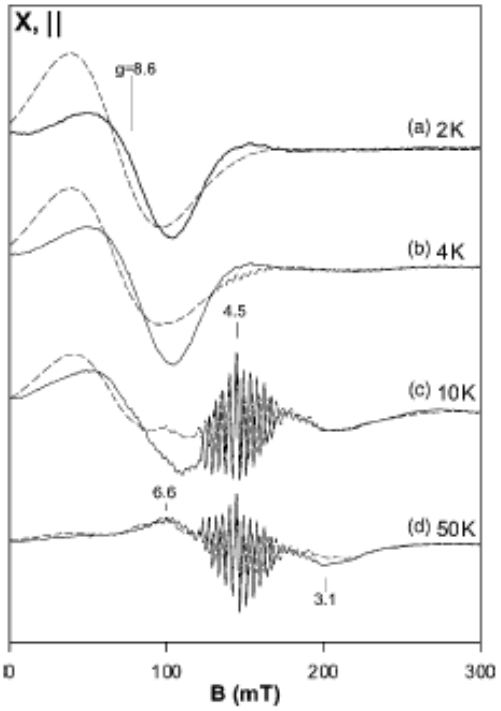

Fig. 8. Variable temperature, parallel mode, X-band EPR spectra (solid lines), and simulations (dashed lines) of an 11.5 mM sample of 1 in 50:50 CH_3CN:DMF. The simulation parameters are given in Table 1. Relative displayed intensities: (a–d) 1×; EPR conditions: temperatures as listed; frequency, 9.27 GHz; power, 0.002 mW (a–c); 0.2 mW (d); $B_{mod} = 0.6\,mT_{pp}$.

Figure 2-9 From Golumbek and Hendrich (2003). The spectra were obtained with an X-band Bruker ER 4116DM resonator in ⊥ and || mode as a function of temperature. The paper also reports ⊥ and || mode Q-band spectra.

The work of Hendricks and coworkers contains many important examples of spectra obtained with $B_1 \parallel B_0$. Quantitative analysis of integer spin systems was discussed in Juarez-Garcia et al. (1991). A coupled Fe(III)-Cu(II) complex was compared with simulations and with a standard consisting of a single crystal of Fe(II) doped zinc fluorosilicate. Hendrich and DeBrunner (1989) found that aquo Fe(II) was not a good reference standard for integer spin quantitation because the fraction of total spins observed is small, and the spectrum depends on sample preparation.

At low field/frequency even nitroxyl radicals exhibit transitions with $B_1 \parallel B_0$. (Lloyd and Pake 1954; Lurie et al. 1991; Guiberteau and Grucker 1993; 1996; Grucker et al. 1996), and (Sünnetçioğlu et al. 1991; Sünnetçioğlu and Bingöl 1993) have demonstrated the special features of spectra obtained at very low magnetic fields, where the usual "high-field approximation" does not hold. For example, normal nitroxyl radical spectra exhibit 3 transitions, one for each of the ^{14}N nuclear spin states. At low magnetic fields and low RF/microwave frequencies, forbidden transitions occur in addition to the familiar 3 lines for nitroxyls at high frequency. At very low magnetic fields, there are 10 transitions. Eight of the 10 transitions are called π transitions because they are allowed with $B_1 \perp B_0$ and 2 are called σ transitions because they are allowed when $B_1 \parallel B_0$ (see, for example, (Grucker et al. 1996)). The phenomena called the Breit-Rabi

effect on hyperfine separations is due to the same non-linear dependence of energy levels on magnetic field strength as results in the additional transitions at low field. See Figure 2-10

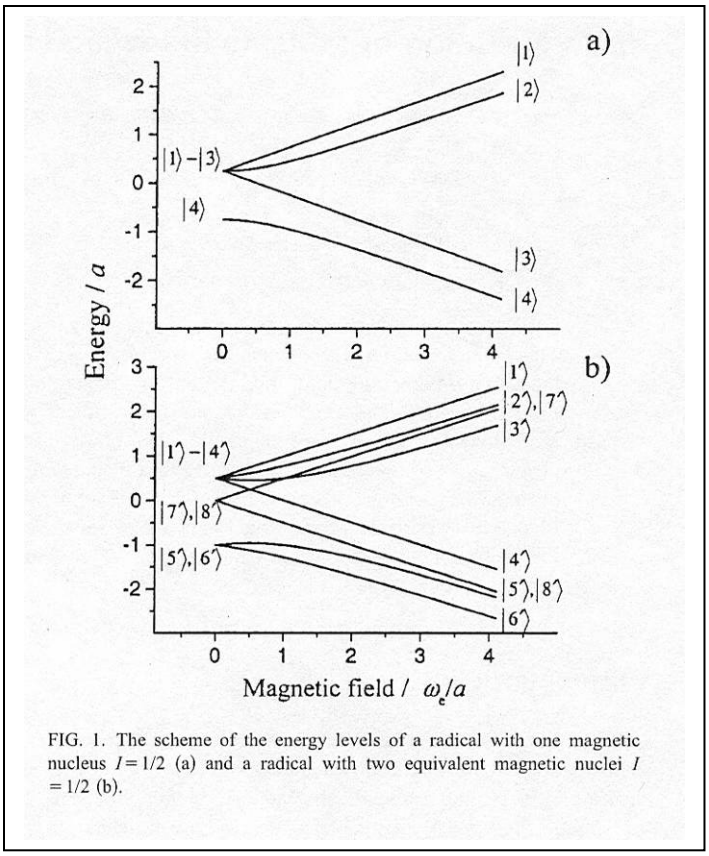

FIG. 1. The scheme of the energy levels of a radical with one magnetic nucleus $I = 1/2$ (a) and a radical with two equivalent magnetic nuclei $I = 1/2$ (b).

Figure 2-10 In the high-field limit the energy levels are parallel and increase directly proportional to magnetic field strength, but at the low magnetic field strengths in this plot, the energy level separations are not constant as the field changes. From Fedin et al. (2003a).

Guiberteau and Grucker (1993) provide similar plots for ^{14}N and ^{15}N nitroxides.

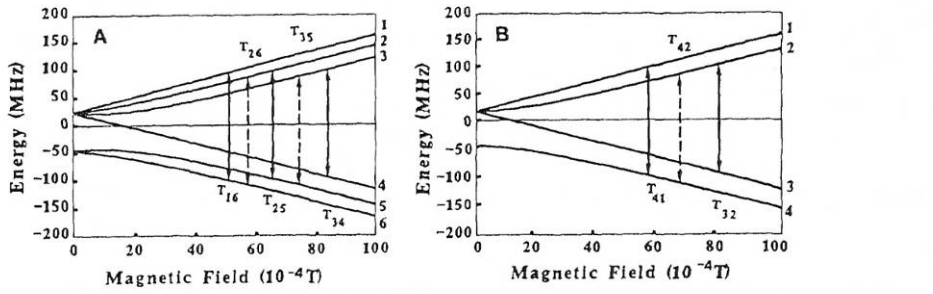

FIG. 1. Paramagnetic energy levels of nitroxides and allowed π (full arrows) and σ (dashed arrows) transitions in low magnetic fields for (A) the ^{14}N system and (B) the ^{15}N system. The length of the arrows corresponds to 199 MHz.

Figure 2-11 At high magnetic fields, such as the commonly-used X-band, only the π ($B_1 \perp B_0$) EPR transitions are allowed. In low magnetic fields, the σ ($B_1 \parallel B_0$) transitions become allowed. At low enough magnetic field the probabilities for σ transitions can become greater than the probabilities for π transitions. From Guiberteau and Grucker (1993).

The relative relaxation rates of transitions at low magnetic field are discussed by Fedin et al. (2003a; 2003b). They show that in the Redfield limit (fast motion) relaxation rates due to modulation of isotropic hyperfine interaction, anisotropic hyperfine, or spin-rotational interaction change for values of ω_e/a_N between about 1 and 10 for various transitions involving one or two I = ½ nuclei. Some transitions are predicted to increase in relaxation rate and some are predicted to decrease in relaxation rate as ω_e/a_N approaches zero. At 90 G (ca. 250 MHz), $\omega_e/a_N \approx 6$ for ^{14}N in nitroxyl radicals. Sünnetçioğlu and Bingöl (1993) calculated transition probabilities for nitroxyl radicals at low field and measured faster relaxation rates by CW progressive saturation at 10^{-3} than at 10^{-4} M, indicating that the relaxation rates were affected by electron-electron spin-spin interactions. When the EPR lines are detected by DNP at low magnetic fields, one of the lines has the opposite polarity from the others (Sünnetçioğlu and Bingöl 1993; Horasan et al. 1997; Sert et al. 2000).

Chapter 3 - Getting Started – Some Practical Matters

Each term in the expression for EPR signal voltage must be kept in mind during EPR measurements:

$$V_S = \chi'' \eta Q \sqrt{PZ_0}$$

Selecting reasonable values for each term will be discussed in this chapter, and then each term will be discussed in more detail in successive chapters.

3.1 Operating the Spectrometer – Words of Caution

Unlike many modern instruments, EPR spectrometers, having been built in a tradition of use primarily by specialists, are not designed to be fool-proof. Considerable care is required in using an EPR spectrometer to (a) prevent costly damage, and (b) obtain useful results. The new Bruker EMX-Plus is the first general purpose EPR spectrometer that is designed to be operated by someone focused on the applications rather than on the spectroscopy per se.

The guidance provided here is similar to that in several reviews of quantitative EPR. See for example (Randolph 1972; Eaton and Eaton 1980; Yordanov 1994; Czoch 1996; Mazúr 2006).

3.2 Sample Preparation

The sample is the χ'' term in the expression for V_s, and the sample also affects η and Q and determines the P used.

Quantitative EPR ultimately depends on use of an analytical balance and volumetric glassware. Since concentrations of samples are low, and samples are often limited so that only small volumes of solutions can be prepared, considerable care is needed to weigh and dissolve samples accurately so that this step does not limit the ultimate accuracy of the EPR measurement.

Solvent selection is critical for fluid solution studies, because of the effect of sample loss on resonator Q, as mentioned elsewhere in these notes. Once samples are frozen, the loss decreases substantially, because microwave loss is due to molecular motion. Hence, different frozen solutions do not have much differential effect on resonator Q. Note, for quantitative work, however, that sample volume changes when the temperature changes, so the concentration in terms of spins per cm^3 of sample changes upon freezing.

3.2.1 Capillary tube sealant

When aqueous solutions are studied using capillary tubing, there are tricks about how to seal the tubes. If the sample must be maintained under a defined atmosphere, then after preparation using standard techniques the sample tube would normally be flame sealed. If the goal is to maintain an atmosphere of defined composition, but the sample can be handled in air, then the sample can be put in a thin-wall Teflon tube or a machined TPX sample tube (fragile and expensive, but very effective). The Teflon tube can be "closed" at the bottom by simply folding it. If the sample is in glass or quartz capillary tubes, round or rectangular, the bottom of the tube can be closed with Critoseal, which is sold by major lab suppliers. However, Critoseal contains a clay material that has a fairly strong Mn(II) EPR signal. The Critoseal plug has to be outside

the active region of the resonator to avoid possible interference with the signal under study. The Bruker X-Sealant is a grease was developed specifically to avoid the Mn(II) contamination problem.

3.3 Don't Forget the Cooling Water!

Water cooling is needed for the microwave source and for the electromagnet. The recent Bruker spectrometers have interlocks to prevent damage to the source if you forget to turn the cooling water on, but you do not want to rely upon them.

3.4 Detector Current

The output of the crystal detector depends upon the magnitude of the bias current to the crystal detector. Each spectrometer should be checked to determine the range of detector current values within which the signal amplitude is independent of detector current. If the detector current drifts, as can happen with lossy solvents, or when the temperature is changed, significant errors in signal amplitude can result; S/N is degraded, and quantitative measurements are prevented. The output of the detector crystal is dependent on temperature. Since the bridge warms up during the first hour or so after power is turned on, the accuracy of quantitative spectra may change during this period. Similarly, the detector crystal itself changes temperature as a result of changes in incident power, so spectra run immediately after large power changes may not be equilibrium responses.

3.5 Searching for a Signal

While initially searching for a signal in a sample whose spectroscopic properties are not known, one can use relatively high spectrometer settings, such as 10 mW power, 1 Gauss modulation amplitude, a fast scan, and short filter time constant. This is likely to be adequate to at least detect a signal, if it is present, with reasonable S/N. Recognize, though, that such a cursory scan could miss samples at two extremes: (a) a signal with such long relaxation time and narrow line that it is saturated or filtered out, or (b) a broad signal in the presence of a more obvious sharp signal. Always look for spectra you do not expect. To obtain a quantitatively correct spectrum requires adjustment of microwave power, phase, modulation amplitude, gain, scan rate, and filter time constant. The criteria for selection of these settings are discussed in the following paragraphs.

3.6 Gain

The gain is adjusted to give the desired size of display and where possible should be increased to use the full range of the digitizer. The operator must always check for linearity if blessed with a signal strong enough to saturate some component in the detection system. One aspect of signal-averaging noisy spectra is sometimes overlooked: If the noise is being clipped then the signal is also being clipped. The maximum excursions of the noise must be within the range of the digitizer. In the EMX-Plus 24 bit digitizers are used, so that the detection has a very high dynamic range. For most purposes the routine operator can ignore gain settings in the EMX-Plus.

3.7 Effect of Scan Rates and Time Constants on S/N and Signal Fidelity

3.7.1 Bandwidth considerations

In a slow-scan CW measurement, in order to avoid distortion of the signal by the detection

system, the detection system bandwidth has to be large enough to permit about 10 time constants during the time a spectral line is traversed. Often, for scans that require several minutes, a time constant of ca. 0.1 s is used.

Noise in an EPR spectrometer may not be "white noise" (uniform noise amplitude over all frequencies). Non-white noise can occur due to various instabilities, ranging from electrical power instabilities to building vibrations. There usually is some 1/f noise (noise that is higher at lower frequency), so there is a tendency for better S/N at higher modulation frequencies. It is possible that particular modulation frequencies will give better S/N than other frequencies. White noise is also called random noise, and upon co-adding spectra, random noise will decrease relative to signal as the square root of the number of scans averaged. Some "noise" is determinant, that is, it always occurs at particular frequencies – it is unwanted signal due to something other than the EPR signal. Usually, these unwanted signals can be removed by subtracting a background. However, background subtraction also increases random noise by √2.

3.7.2 Scan Rate and Filter Time Constant

The operator has to choose a time constant. If the time constant is much longer than the conversion time (Xepr notation), the line position and shape will be distorted such that intensity is shifted toward later times in the scan (higher magnetic fields if the scan is from lower-field to higher-field). For example, a strong pitch sample was recorded with various time constants (Figure 3-1). On a Bruker spectrometer a BDPA sample was recorded with various time constants and conversion times. When the time constant was longer than the conversion time, the noise decreased but the line width increased. There is no advantage of selecting time constant less than the conversion time, so unless extreme noise filtering is needed and one is willing to accept the resultant line shape distortion, as a practical matter, time constant should be set equal to the conversion time.

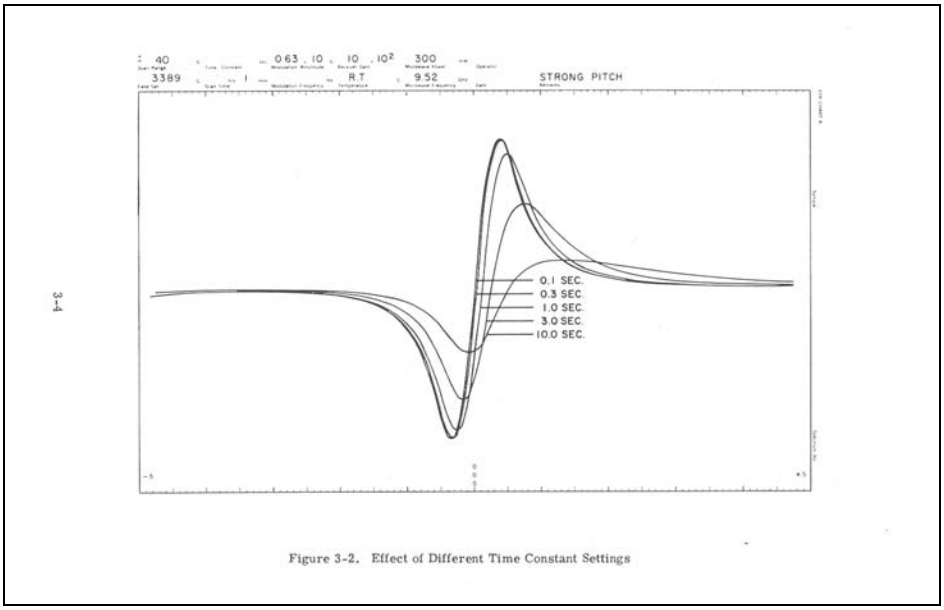

Figure 3-2. Effect of Different Time Constant Settings

Figure 3-1 This diagram from Varian E-4 Operating Techniques manual, 87-125-301, shows the qualitative effect of increasing the filter time constant while keeping other operating conditions constant.

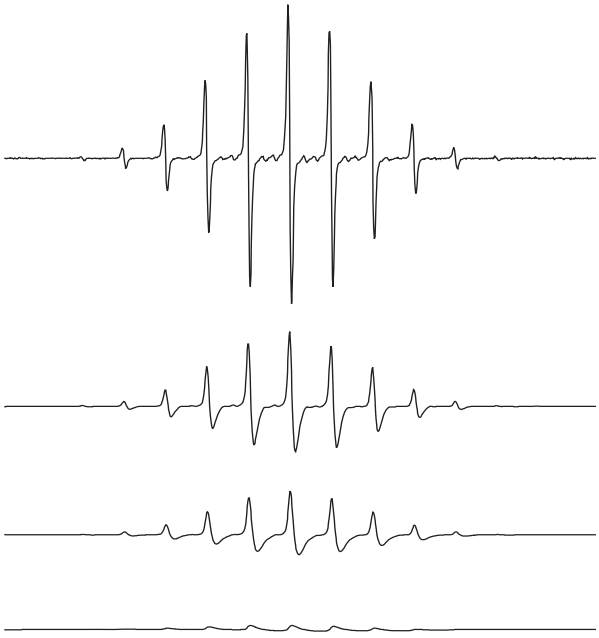

Figure 3-2 Successive scans show the decrease in resolution of the spectrum due to increased conversion time (effectively, increased filter time constant). If the conversion time is extremely long, the spectrum nearly disappears.

3.7.3 Selecting a non-distorting filter and scan rate

Although the S/N will increase when the time constant is greater than the conversion time, there will be distortion of the spectrum when the time constant is too long. As a good rule of thumb, the time constant should be chosen to be less than about 1/10 the time it takes to scan through the narrowest line in the spectrum. Consequently, scan rate and filter time constant are related to each other and to the CW line width in the following formula.

$$\frac{\text{(spectrum width in Gauss)}}{\text{(line width in Gauss)}} \times \frac{\text{(time constant in sec)}}{\text{(sweep time in sec)}} < 0.1$$

The inequality must be satisfied to obtain undistorted lines. A faster sweep or longer time constant does not give the system enough time to respond to changes in signal amplitude as the line is traversed.

Example: If you record a 20 G scan of a 0.1 G wide line in 84 s, the time constant should be less than 0.04 s; (20x0.04)/(0.1x84) = 0.095. If you use a 40.96 ms conversion time, the scan will be 84 s if you use 2048 steps. 1024 steps would result in a scan of 41 s, which would not be conservative with respect to line shape (and position) distortion.

The standard deviation of random (white) noise decreases proportional to the square root of the time constant of a filter applied to the noise. Thus, if the filter time constant is increased a factor of 4 from 20.48 ms to 81.92 ms, the noise will be reduced by a factor of 2. Actually, this needs to be qualified by saying that for this to be true, the filter time constant has to be longer than the A/D conversion time. In the Elexsys spectrometer, an integrating digitizer is used, and in Xepr,

the integration time of the digitizer is called the "conversion time." Effectively, the integration time is the time the ADC accumulates the signal and noise, which results in signal averaging that improves the S/N by the square root of the conversion time. The time for a magnetic field scan is the product of the conversion time (in seconds) and the number of data points to be acquired on the magnetic field axis. Thus, a conversion time of 81.92 ms for 2048 magnetic field steps results in a scan time of 167.8 s. A time constant longer than the conversion time will improve the S/N proportional to the square root of the filter time constant. A filter time constant much less than the conversion time will result in a noise level that is largely independent of the time constant, because the averaging determined by the conversion time will dominate the resultant noise level.

In the Bruker software one sets time constants in the way discussed above, but conversion times for the digitizer and number of points in the spectrum determine the scan time. The slower the scan the higher the resolution of the digitizer. The ranges are 0.33 seconds to 45 minutes and 9 bits to 22 bits.

Another feature of an integrating digitizer is that the signal level increases the longer the integration time (conversion time). Thus, if two spectra of the same sample are obtained with all parameters equal, but one with 10.24 ms conversion time and one with 81.92 ms conversion time, the numerical integral of the digitized spectrum will be 8 times larger for the 81.92 ms conversion time. These are the numbers that are displayed in the Xepr window, are saved as the amplitude of the spectrum, and will affect integrals of the area under the peaks, etc. Since this could cause undesirable confusion when comparing spectra, some users prefer to have spectra displayed and stored numerically normalized. This is an option in the Xepr menu.

Signal-to-noise can be improved by using a longer time constant and a slower scan. Why then, would one want to use an expensive computer system for S/N improvement, when the spectrometer is designed for extensive analog filtering? The answer is that with a perfectly stable sample and stable instrument, roughly equal time is involved in either method of S/N improvement. The problem is that perfect stability is not achieved, and the filtering discussion focuses on high frequency noise. Long-term spectrometer drift due to air temperature changes, drafts, vibration, line voltage fluctuations, etc., limit the practical lengths of a scan. Signal averaging will tend to average out baseline drift problems along with high frequency noise. Drifts in the magnetic field magnitude are not averaged out by filtering or slow scans, and always increase apparent line width. Ultimately, the resultant line broadening limits the spectral improvement possible with any averaging or filtering technique. In addition, computer collected spectra can subsequently be digitally filtered without changing the original data, whereas analog-filtered data is irreversibly modified.

If the sample decays with time, a separate set of problems emerges. Assume, for example, that you want to compare line shapes of two peaks in a noisy nitroxyl EPR spectrum, and that the amplitude of the spectrum is changing with time due to chemical reaction (shifting equilibria, decay, oxygen consumption or diffusion, etc.). In this case one wants to minimize the time spent scanning between points of interest. It would be wise to scan the narrowest portion of the spectrum that will give the information of interest. Then a numerical correction for the measured rate of change in the spectrum is the best way to handle the problem. The impact of the time

dependence can be minimized more effectively by averaging rapid scans than by filtering a slow scan.

3.7.4 A Note About Comparing Noise in CW and pulsed EPR

The signal-to-noise in a spectrum depends strongly on the bandwidth of the detection system. CW EPR typically uses a very narrow bandwidth via the 100 KHz phase-sensitive detector, and subsequently removes 1/f noise via a user-selectable filter time constant. Pulsed EPR has to use a much larger bandwidth to record the rapidly changing signals, so there is inherently poorer S/N in the recorded spectra. White noise increases linearly with the square root of the bandwidth.

3.8 Background Signals

"There are spins everywhere." (James Hyde, personal communication to almost everyone). There are EPR signals even if you do not put a sample into the resonator. Actually, the signal from O_2 in room air is easily measured at Q-band, and was used by Varian to calibrate sensitivity of Q-band spectrometers. There are signals from metal ions in both metallic and dielectric resonators. There are impurity and defect signals in quartz sample tubes and Dewar inserts, even when these are made of the highest purity quartz available. (Pyrex tubes yield an enormous iron signal – convenient for demonstrations.) Dirt transferred to the outside of sample tubes by routine handling will also yield EPR signals. Even some "pure" Teflon has a fairly strong EPR signal.

Caution – there is an iron background in glass wool, just as there is in Pyrex or Kimax glass tubing. Occasionally, it will be convenient to use fine "glass wool" to position a small sample, especially a "point" sample in a tube. One needs to use quartz wool, not glass wool, for this purpose.

The EPR signals that cannot be attributed to the sample of interest are generally called "background" signals, whether they are due to unwanted spins or to electro-mechanical effects on the resonator. Background signals should be recorded and subtracted from the spectrum of the sample of interest to obtain quantitative results.

3.9 Integration

Peak to peak amplitude is not sufficient to count spins. The area under the absorption curve is needed to quantitate the intensity. However, if the line shape is the same, regardless of what the shape is, it is valid to approximate the relative areas as width squared times height (Chesnut 1977).

The area under a derivative EPR signal can be obtained by digital double integration. It is now so routine to integrate spectra acquired into a computer, that the first and second integrals of an experimental derivative spectrum are commonly used to judge the quality (phasing, etc.) of the experimental data. Integration requires a constant baseline or a baseline correction after each integration, so there has to be good baseline on the low-field and high-field sides of the spectrum. One must use great care in evaluating the area under an absorption curve. Serious errors may result from failure to extend measurements sufficiently far from the center of the line. The percentage error resulting from finite truncation of the curve is especially large for Lorentzian lines because of their extensive wings.

Tails in a Lorentzian line have intensity extending out farther than they are usually recorded. See the plots and tables in (Poole 1967; 1983; Eaton et al. 1979; Weil et al. 1994). If the S/N is high and the background is negligible, integrating to a larger number of line widths will result in a larger integral. Czoch (1996) provided several plots of various truncation errors, including the following, which is based on the assumption that noise limits the allowable scan range to be integrated – i.e., that the signal disappears into the noise, so the effective number of line widths over which the integral can be calculated is decreased.

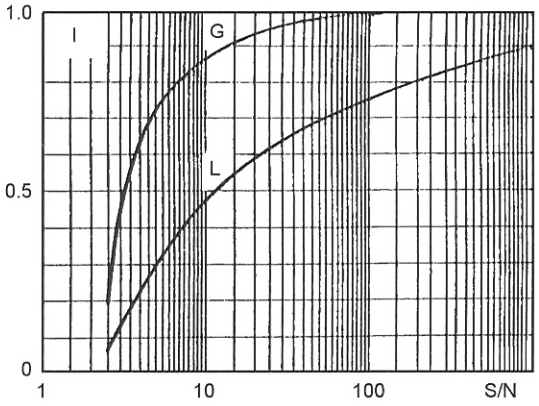

Fig. 14. Area under truncated Lorentzian (L) and Gaussian (G) as a function of signal-to-noise ratio.

Figure 3-3 from Czoch (1996).

Thus, it is important to obtain and subtract a background spectrum to get quantitatively useful integrations. The sample tube and solvent used for the background should be as close to that used for the spectrum of interest as possible. This is fairly straight-forward when spectra are being obtained with a TE_{102} cavity resonator at room temperature. For spectra obtained as a function of temperature, the background should be obtained at the same temperature. Performing these operations with the higher-filling factor dielectric and split ring resonators, such as in the FlexLine series requires considerable care. Inherently, the higher filling factor makes the frequency more sensitive to the position of the sample tube. Sometimes it is useful to rotate the tube in the resonator to better match the frequency of the background to the frequency that was found for the sample of interest. Slight differences in Q and coupling may make the appropriate fraction to subtract different from 1.

Beyond these matters, there are spectra that are inherently difficult to integrate, because they do not meet the ideal case described above of isolated lines with well-defined flat baselines on either side. The spectrum of interest might, for example, be a semiquinone radical superimposed on other unknown species, or the spectrum might be such that it is not possible to scan the field far enough to define the baseline. In these cases, it may be useful to combine simulation and integration. When the S/N is very low, if there is an overlapping spectrum from another species, and/or the background is large, it may be better to integrate simulated spectra fit to the experimental spectra than to integrate the experimental. For example, one could simulate the full

spectrum, matching it with the part that was actually measured, and then integrate the entire simulated spectrum. Gunter and co-workers (1975) discuss the sensitivity of double integration to background slope due to spectrometer drift, or the apparent slope that results from not recording far enough into the wings of the spectra. This discussion was in the context of integrating spectra to estimate the uptake of Mn by mitochondria.

Any time prior knowledge of the spectrum can be used, the accuracy of the results can be improved. For example, Halpern and coworkers have used spectral fitting to enhance quantitative EPR imaging (Halpern et al. 1993; 1994; Mailer et al. 2003).

Even for an inhomogeneously broadened line, signal is lost in the baseline if a wide enough scan is not used. For example, strong pitch was recorded with 60 and 100 G scan widths, and about 10% of the area found in a 100 G scan was lost in the 60 G scan.

The integral of a dispersion curve is infinite, but as an approximation over a finite scan width, the value can be taken as finite.

The magnetic field dependence of signal intensity was incorrect in some early literature, until Aasa and Vänagard pointed out the correct dependence on g, and not g^2 in 1975.

Some of the difficulties in integrating very wide spectra with significant background are illustrated by measurements of Fe^{3+} in kaolinite by Balan et al. (2000). Fe^{3+} is one of the more challenging species to measure quantitatively. They used Fe^{3+} in corundum (α-Al_2O_3) as a standard, but then since the spectra differed greatly, they simulated each spectrum to be able to compare the intensities. The Fe^{3+} occurred as "isolated" or dilute ions or as concentrated or strongly interacting ions. EPR was able to show that in these kaolinite samples about half of the Fe^{3+} was present as isolated ions.

3.10 Microwave Power

To obtain quantitative CW EPR spectra and to obtain undistorted EPR lineshapes, it is necessary to obtain spectra at microwave powers below those that cause significant saturation of the EPR spectrum. Most EPR samples can be saturated with the power levels available in commercial spectrometers. Thus, it is always important to check for saturation.

You can't just compare two spectra directly because they were acquired with the same microwave power. In the absence of saturation, the signal increase linearly with B_1. Therefore efficiency of resonator to convert microwave power to B_1 is important factor. Q is important. Filling factor is important. These depend on the type of resonator and the dielectric properties of the sample.

If there is no unresolved hyperfine splitting, the relationship between linewidth, B_1 and relaxation times is

$$\left(\Delta B_{pp}\right)^2 = \frac{4}{3\gamma^2 T_2^2}\left(1 + \gamma^2 B_1^2 T_1 T_2\right)$$

where ΔB_{pp} = peak-to-peak line width and γ = electron magnetogyric ratio (Schreurs and Fraenkel 1961; Eastman et al. 1969; Poole and Farach 1971). If B_1 is small enough that the

$\gamma^2 B_1^2 T_1 T_2$ product term is <<1, the signal is unsaturated. From the equations for EPR line shape one can extract a term that is commonly called the saturation factor:

$$s = \frac{1}{1 + \gamma^2 B_1^2 T_1 T_2}$$

In various contexts one can find the term 'saturation factor" used for the expression as written here, for just the denominator of this expression, and for just the $\gamma^2 B_1^2 T_1 T_2$ term.
Below microwave power saturation s = 1. As a practical matter one might set a limit of 0.98 or even 0.95 as an acceptable degree of saturation when obtaining CW or saturation recovery EPR spectra.

A practical matter for the operator is to know the relation between B_1 at the sample and the incident microwave power. The incident power can be fairly accurately calibrated on an X-band spectrometer with waveguide transmission line and critically-coupled cavity resonator.

One has to be careful comparing power saturation at different microwave frequencies (e.g., X-band vs. Q-band) because of the use of different resonators. For example, Froncisz et al. (1986) cite 4.8 G/√W for a Q-band TE_{011} cavity resonator. We will follow the tradition of using Λ ($=B/P^{1/2}$) to denote the B_1 per square root watt incident power.

The effect of a dielectric, such as a sample, sample tube, or especially a VT Dewar, on the distribution of B_1 in a resonator is sometimes called the "sucking in effect" in the EPR literature. Nagy (1994) makes a distinction between the "sucking in effect" of the sample itself and the "lens effect" of a Dewar or other dielectric surrounding the sample, and gives experimental results. Modern electromagnetic field calculations, such as with the Ansoft Corporation computer program HFSS (high frequency structure simulator) reveal the details of microwave field distributions, as shown by the recent papers from the Hyde laboratory about aqueous sample cells and uniform field resonators (Mett et al. 2001; Anderson et al. 2002; Hyde and Mett 2002; Hyde et al. 2002; Mett and Hyde 2003; Sidabras et al. 2005).

More et al. (1984) found $B_1 = 0.0159$ G/√W for a Varian E231 cavity. This value increased to 0.0267 with a VT Dewar in the cavity. The efficiency factor is affected by the sample, and the wall thickness of the Dewar insert, if one was used, so one has to be careful about how many significant figures should be cited, but these values give an indication of the range to be expected. Bales and Kevan (1970) and Rataiczak and Jones (1972) provide additional information on resonator efficiency factors. The Bruker ER4102ST standard TE_{102} cavity resonator, empty, achieves $\Lambda = 1.4$ (Workshop on Selecting an EPR Resonator, 2005, page 20), which is essentially the same as the older Varian resonator, as expected, since they are both TE_{102} X-band cavity resonators. The ER4118X-MD5 dielectric resonator in the FlexLine series has $\Lambda = 4.2$.

For an X-band rectangular (TE_{102}) cavity, the approximate formula $B_1 = 0.02\sqrt{QP}$ is handy for estimating the microwave B_1 in the resonator. In this expression, the resonator Q is commonly ca. 3000, and P is the power in watts. To get some practice in the use of these expressions, assume $T_1 = T_2$, and find the highest power at which one should operate an X-band EPR

spectrometer if the line width is 0.2 G, and is relaxation determined. From the formula for relaxation-determined line width,

$\Delta B = \frac{2}{\sqrt{3}\gamma T_2} = \frac{6.56 \times 10^{-8}}{T_2}$, 0.2 G corresponds to 3.28 x 10^{-7} s rad^{-1}.

Try P = 10 mW = 0.01 W. Then, $B_1 = 0.02\sqrt{QP} = 0.02\sqrt{3000 \times 0.01} = 0.11\,G$

Thus, the second term in the denominator for s is

$(0.11\ G)^2(1.7608 \times 10^7\ rad\ s^{-1}G^{-1})^2(3.28 \times 10^{-7} s\ rad^{-1})^2 = 0.4$

and s = 1/(1+0.4) = 0.71

so 10 mW is too much power.

At 2 mW, B_1 = 0.049 and s = 1/(1 + 0.08) = 0.93
This is still saturated enough that one ought to be able to detect the effect.

As a second example, consider typical X-band relaxation times for a nitroxyl radical at liquid nitrogen: T_1 = 200 μs, T_2 = 2 μs. With an attenuation of 40 dB below 200 mW, P = 0.02 mW. For an X-band rectangular resonator $B_1 \sim 2 \times 10^{-2} \sqrt{(QP)}$ with P in watts (Bales and Kevan 1970; More et al. 1984) and Q ~ 3500 so 40 dB produces $B_1 \sim 4.2 \times 10^{-3}$ gauss and $\gamma^2 B_1^2 T_1 T_2 \sim 1$, which indicates severe saturation. The fact that this power causes less saturation than calculated reflects the fact that spectral diffusion processes cause the effective relaxation times to be much shorter than the values measured by pulse methods (Eaton and Eaton 2000b). It is wise to check the power saturation experimentally.

A series of measurements at different power levels is called a progressive saturation study. A plot of such results will look like one of the lines in Figure 3-4.

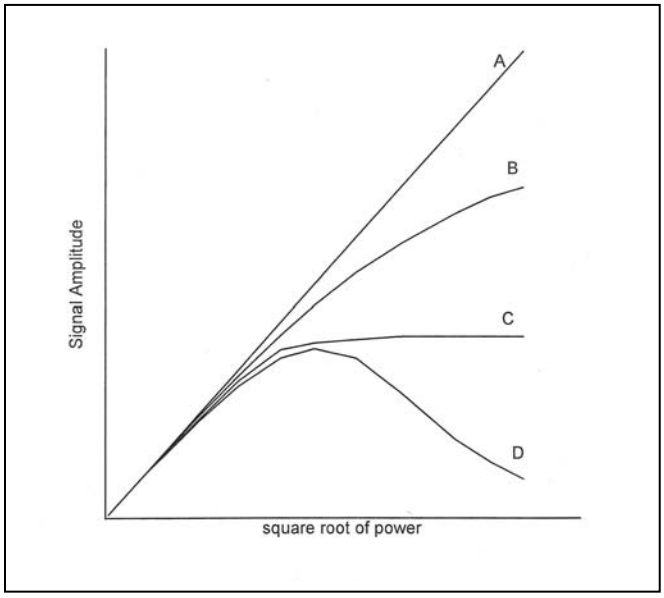

Figure 3-4. A plot of signal amplitude as a function of the square root of the microwave power incident on the cavity is called a power saturation curve. The plot would be linear if no saturation of the electron spin system occurred. To do quantitative EPR, it is necessary to operate at power levels below the power at which the curve becomes non-linear. The figure presents CW EPR power saturation curves for four cases: (A) no power saturation within the available microwave power of the spectrometer - short relaxation times; (B) a small degree of homogeneous saturation at the highest available power levels - intermediate relaxation times; (C) extensive inhomogeneous saturation, exhibiting a "leveling" of the saturation curve a relatively low power, but no subsequent decrease in amplitude of the EPR signal; (D) extensive homogeneous saturation, exhibiting a maximum in the saturation curve, due to long relaxation times.

The incident microwave power should be set to a value below that at which the power saturation curve deviates from linearity (Figure 3-4). To obtain quantitative EPR results you have to make sure you are measuring in the linear B_1 range. A quick way to check that you are operating in a range in which the signal intensity varies linearly with the square root of microwave power is to decrease the attenuation by 6 dB (a factor of 4 increase in power). The spectral amplitude should increase by a factor of 2; if it doesn't, reduce the power and try again. Since there is no strictly linear range, except for species with very short relaxation times, the operator has to make a judgment about how much deviation from linearity is acceptable. A good rule of thumb would be the noise level of the spectrum, because to use much lower power would result in additional uncertainties due to the lower S/N.

The power saturation plots of a crystalline BDPA sample is in Figure 3-5. It is similar to curve D in Figure 3-4. Direct (pulsed X-band) measurements of T_1 and T_2 of crystalline BDPA by Brändel et al. (1970) yielded $T_1 = T_2 = 2\text{x}10^{-7}$ s independent of temperature within experimental error (see their figure 7). The CW line width of ca. 0.7 G would correspond to $T_2 \approx 1\text{x}10^{-7}$s, so the line is relaxation determined. There may be slight purity differences between samples that would affect the extent of relaxation narrowing. We simulated the power saturation curve of crystalline BDPA in Figure 3-5 using the approach described in More et al. (1984), yielding $T_1 = 2.7\text{x}10^{-7}$ s and $T_2 = 1\text{x}10^{-7}$ s.

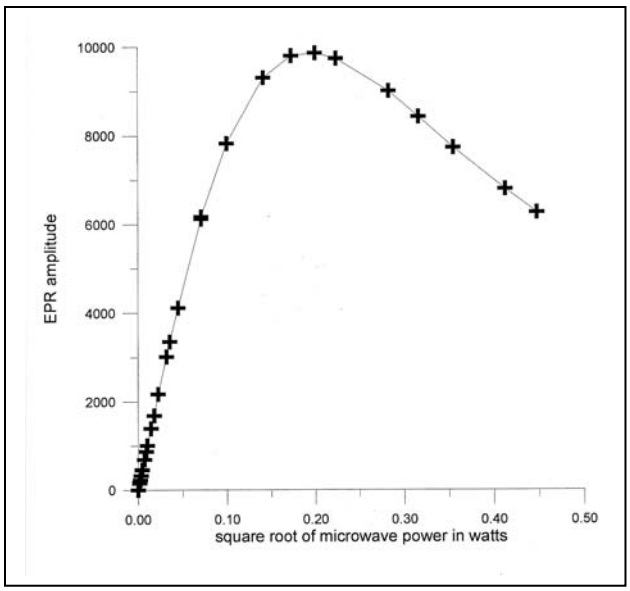

Figure 3-5 CW power saturation curve for BDPA.

Thus, BDPA is a reasonable sample to use to estimate B_1 in a resonator by CW EPR. Pulse methods are more accurate (see the Workshop on Selecting an EPR Resonator), but labs without pulse capability need an easy way to estimate B_1, which is important for quantitative comparisons of spectra. Knowing $B_1/\sqrt{W}$ incident power, and the hyperfine couplings, if they are not resolved, one can estimate relaxation times using the method outlined in More et al. (1984). Note that to get a good estimate of B_1 it is necessary to be able to go past the maximum in the intensity as a function of microwave power saturation curve. This was an important criterion in selecting the BDPA sample. If one uses too much power, the EPR lines are broadened, as shown in Figure 3-6.

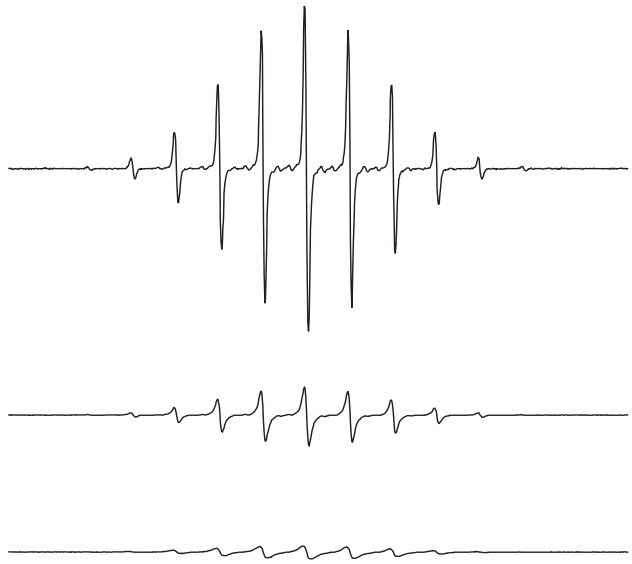

Figure 3-6. Increasing microwave power (top to bottom in this figure) broadens the EPR lines.

Even as pulsed EPR spectrometers become more common, CW continuous saturation characterization of spin relaxation will remain important. Faster relaxation times can be better characterized by CW methods than by pulse methods. In addition, the methods are

complementary in the information they provide. In the literature $P_{1/2}$ is commonly used as a saturation parameter (Mailer et al. 1977). $P_{1/2}$ is the incident microwave power at which the EPR signal has half the amplitude it would have in the absence of saturation.

Several papers have been published proposing standards for calibration of B_1 in a resonator by power saturation methods. For example, Copeland (1973) suggested using the CW power saturation of the radical induced by γ-irradiation of glycylglycine, for which he obtained a value of $(T_1T_2)^{1/2} = 4.0x10^{-7}$. Harbridge et al. (1998; 2003) confirmed that CW power saturation yields this value, but showed by direct pulsed EPR that at room temperature T_1 is ca. 50 μs and T_2 = 0.32 μs. These values yield $(T_1T_2)^{1/2} = 4.0x10^{-6}$. However, pulsed ELDOR measurements showed that there were also competing nuclear spin relaxation (T_{1n}) and spin diffusion mechanisms. Thus, the assumption of the CW power saturation method that the saturation is proportional to $B_1^2T_1T_2$ is not valid, and the actual T_1 and T_2 cannot be used in the B_1 determination proposed by Copeland.

3.11 Modulation Amplitude

If a sample is strong enough, and the detection system is set up for direct detection of the output of the crystal detector or double-balanced mixer detector, an absorption signal as sketched in Figure 2-2 could be recorded. However, most of the time, the S/N would not be adequate for this to be a useful method of detection. As we will show in a later section, the EPR signal intensity is rarely larger than the noise until some method is used to separate the signal from the noise. In CW EPR, as in many other fields of science, the S/N is increased by using a method of encoding the desired signal by modulating some parameter that affects the signal, and then separating the desired signal from noise or other incoherent undesired signals by phase-sensitive detection at the modulation frequency in a lock-in amplifier. The lock-in amplifier selects the signal at the modulation frequency with a high selectivity, and filters the signal with a selectable time constant, with the result that noise is suppressed and S/N is increased. See the separate section about filter time constant. More details about how a lock-in amplifier works is given in Poole (1967, p.452) and (Conradi 1977; Ashton et al. 1980) for those who want to dig further.

The following figure (see similar figure in (Weil et al. 1994, page 482)) shows that the principle of magnetic field modulation and phase sensitive detection at the modulation frequency involves using a modulation amplitude small enough that it samples an approximately linear segment of the EPR absorption signal. Of course, no portion of the absorption signal is actually linear, and the importance of the degree of distortion from a true derivative is a matter of operator judgment. This explanation is about how the EPR signal is recovered from noise. In this Workshop, however, we need to go somewhat further, because with regard to quantitative EPR, there are several critical aspects of the choice of modulation frequency and modulation amplitude. As we emphasize repeatedly, the operator has to decide what information about the spin system is desired, and control the appropriate parameter. If the details of line shape are important, then the spectrum has to be obtained under conditions that distort the spectrum as little as possible.

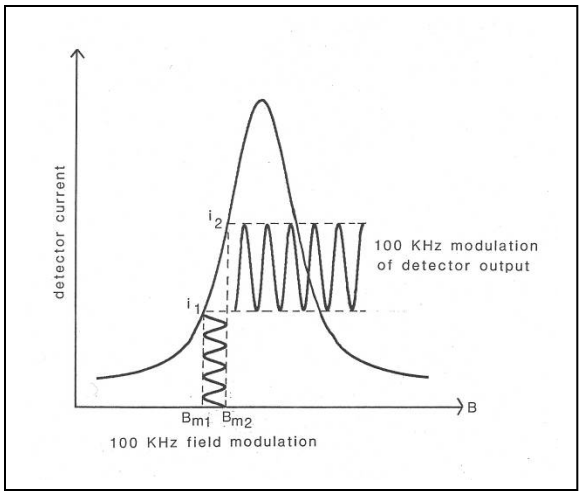

Figure 3-7 (same as Figure 2-4) The principle of magnetic field modulation and phase-sensitive detection at the modulation frequency is illustrated by this sketch. The EPR absorption curve is traced out as the magnetic field is swept at constant microwave frequency (Eaton and Eaton 2005).

Wilson (1963) calculated the effect of modulation on the shape and area of Lorentzian and Gaussian lines, and showed that derivative line shapes occur when the modulation is sufficiently small. See also the papers by (Burgess and Brown 1952; Wahlquist 1961; Smith 1964) and the extensive discussion in Poole (1967; 1983). Figure 3-7 shows how the derivative line shape occurs in the phase-sensitive detection when the modulation is small. Small, in this case, means that the amplitude of the modulation in the magnetic field direction samples a portion of the absorption curve that is locally linear. The amplitude and the phase of the detected signal (labeled as at the common modulation frequency of 100 kHz in the figure) is positive on the low-field side of the line, is zero at the peak of the line, and then is negative on the high-field side of the line. The magnitude of the EPR signal is related to the amplitude of the magnetic field modulation. To the extent that the portion of the line sampled is nearly linear, the amplitude of the signal increases with increase in the modulation amplitude. However, this linear response disappears when the amplitude becomes large enough that the curvature of the Lorentzian or Gaussian (or more complicated) line becomes significant.

The distortion of the derivative line shape that occurs as the modulation amplitude becomes significant relative to line width is shown in Figure 3-8 from Smith (1964). Although the data in this figure are NMR spectra, the conclusions are general and transfer to EPR without change.

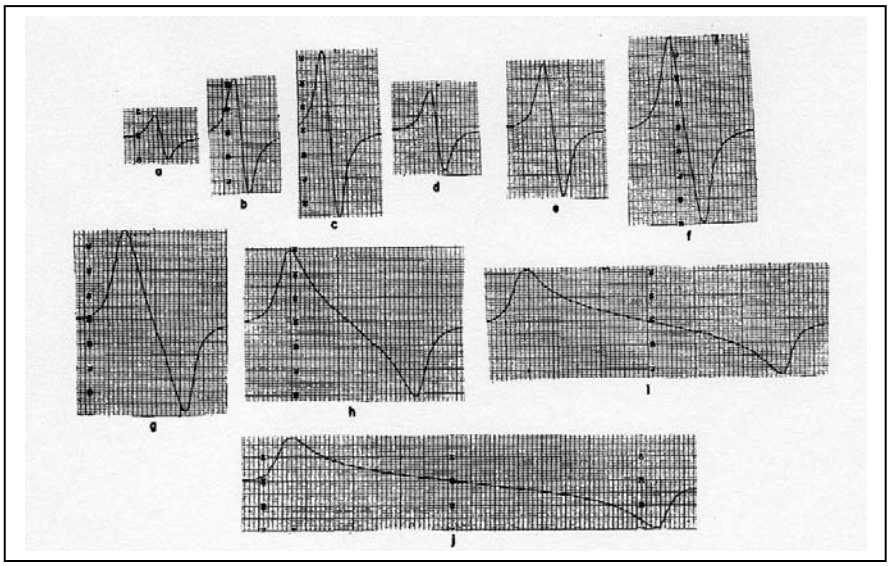

Figure 3-8 In part a the modulation is small relative to line width. In e the modulation amplitude is about equal to the derivative peak-to-peak line width. In g-j the modulation is increasingly large relative to the line width. The gain is the same in parts a-c, and then reduced by a factor of 2 in d-j. From Smith (1964).

When the modulation amplitude ($B_{m2} - B_{m1}$ in Figure 3-7) is less than about 1/10 of the derivative peak-to-peak line width, ΔB_{pp}, the distortion of the signal is only a few percent. Increased signal amplitude comes at the cost of increasing distortion of the EPR line shape. However, modulation amplitudes up to about 1/3 of ΔB_{pp} cause relatively little distortion. For the most accurate lineshapes you should always scan the spectrum with a very small modulation amplitude, determine the narrowest linewidth, and set the modulation amplitude to 1/10 of that linewidth. If you were using too large a modulation amplitude during the initial scan, repeat the measurement of the linewidth, and adjust the modulation amplitude again if necessary. For small modulation amplitudes the S/N increases linearly with modulation amplitude. It may happen that the S/N is too low to obtain a spectrum with the modulation amplitude meeting the above criteria. In this case, one has to go back to the basic question - what information do you want from the sample? If lineshape is the crucial information, then signal averaging will be needed to improve the S/N. If subtleties of lineshape are of less significance, it may be acceptable to increase the modulation amplitude up to roughly 1/2 of the linewidth. If the area under the peak is the information desired, overmodulation is acceptable, since the area is linearly proportional to modulation amplitude, even when the modulation is so large as to cause distortion of the lineshape. Computational approaches have been developed to correct for the lineshape distortion due to overmodulation (Robinson et al. 1999a; 1999b).

Although the example presented here is for a single line, it should be evident that in complicated, possibly overlapping, envelope of lines, the arguments apply to the narrowest feature. Hyperfine structure can be obscured by using excess modulation amplitude. A discussion of how to calculate the undistorted line from the over-modulated line is in the appendix by Mailer and Robinson.

For wide EPR lines, as occur for many metals, especially in rigid lattice, it often is not possible to use modulation amplitude as large as 1/0 of the line width. The modulated magnetic field produces eddy currents in metallic parts of the resonator, and since this is in a magnetic field, vibrations can be set up. For each resonator there will be a modulation amplitude above which microphonics will add noise and hence, even though there might be increased signal amplitude with increased modulation amplitude, there might be decrease in S/N. Furthermore, eddy currents result in heating of the resonator, which is also undesirable. Bruker specifies a maximum modulation amplitude to be used with each type resonator.

3.11.1 Modulation Amplitude Calibration

To perform quantitative EPR that validly compares samples run in different laboratories or even in different resonators in the same lab, it is necessary to calibrate the modulation amplitude. This involves making sure that the modulation amplitude selected in the software (or selected by a front panel switch in older spectrometers) actually results in the listed value at the sample. The distortion of the EPR line by modulation amplitude that is large relative to line width (Figure 3-8) can be used to calibrate the modulation field. As shown in Poole (1967, page 398-413) and (Weil et al. 1994, page 554-556), when the modulation amplitude is about 1/3 of the line width, a Lorentzian spectral line is broadened by about 3%, and when the modulation is ca. 2/3 of the line width, the line is broadened by about 11%. How important this broadening is depends on the information one desires from the spectrum. Many tables and plots of the effects of modulation

on line widths, shapes, and areas are given in Poole (1967, Chapter 10). These effects are incorporated into the automatic modulation calibration routine in Xepr, which also automatically adjusts modulation phase for optimum signal. If you perform the calibration manually, it will be handy to have a plot of Table 10-1 from Poole (1967). This tabular data reveals, for example, that if a line is 1 G wide and the modulation amplitude is 4 G, the observed over-modulated line will be ca. 3.5 G wide.

Figure 3-9 shows the broadening of a BDPA sample. There was no observable broadening when the modulation amplitude was less than half of the line width (top spectrum). Increasing the modulation amplitude to 1 G resulted in observable broadening (middle spectrum) and 2 G modulation amplitude (substantially larger than the line width) started to split the signal.

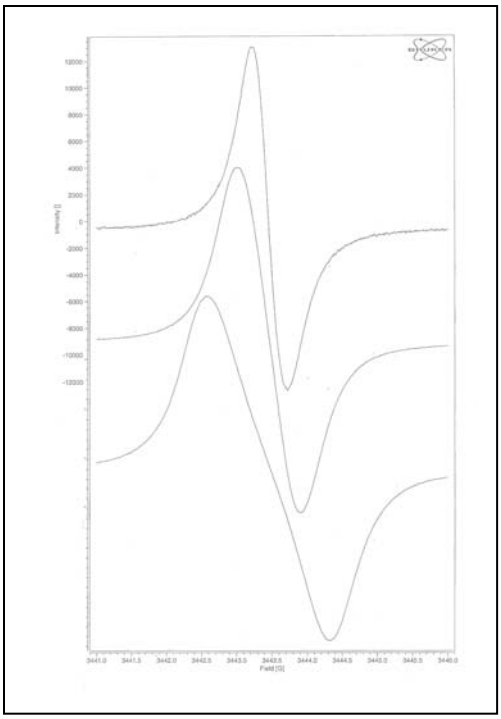

Figure 3-9 Effect of magnetic field modulation amplitude on a narrow-line BDPA spectrum. These spectra were recorded at X-band using 100 kHz modulation. The top spectrum was recorded with modulation less than about half the line width. The middle spectrum is broadened to about the 1 G modulation amplitude, and the bottom spectrum, recorded with 2 G modulation is beginning to split into two lines. The scan width for these spectra was 5 G. The receiver gain for the top spectrum (low modulation amplitude) was 6 dB higher than for the other two spectra.

Bruker provides a DPPH sample to use for the calibration of the modulation field. BDPA, which is commercially available, also is a convenient material to use. A tiny spec gives a strong EPR signal with a line width of less than 1 G. Note that you should not use a sample with a long relaxation time, such as irradiated quartz or trityl radicals for this modulation calibration, because passage effects will result in an erroneous calibration.

Caution: If you perform the Bruker automatic modulation calibration when the resonator is in a cryostat, use a gas flow to remove heat and monitor the temperature of the resonator. The cryostat is very effective, and it is easy to increase the temperature of the resonator above its design limit. Do only a few modulation frequencies at a time and give the resonator time to cool between calibration steps.

The modulation distribution is independent of the quartz Dewar insert, although the B_1 distribution is strongly affected by the quartz of the Dewar insert (and these inserts are not all the same). Calibrations are specific to a particular Dewar and resonator combination.

3.11.2 How to Select Modulation Frequency

100 kHz corresponds to 10 μs. Many free radicals have relaxation times this long, especially in rigid solids or at temperatures below ambient.

100 kHz modulation also corresponds to 35 mG. When two frequencies are present, there are always sums and difference frequencies. Consequently, 100 kHz magnetic field modulation puts 35 mG sidebands on each EPR transition. For lines that are hundreds of mG wide, these sidebands are a negligible contribution to the line shape. However, for a narrow line such as an organic radical for which all hyperfine splittings are resolved and hence lines have relaxation-determined line widths, and for species such as trityl and LiPc which have line widths as small as ca. 22-30 mG, the line shape can be distorted by the modulation sidebands (Figure 3-10).

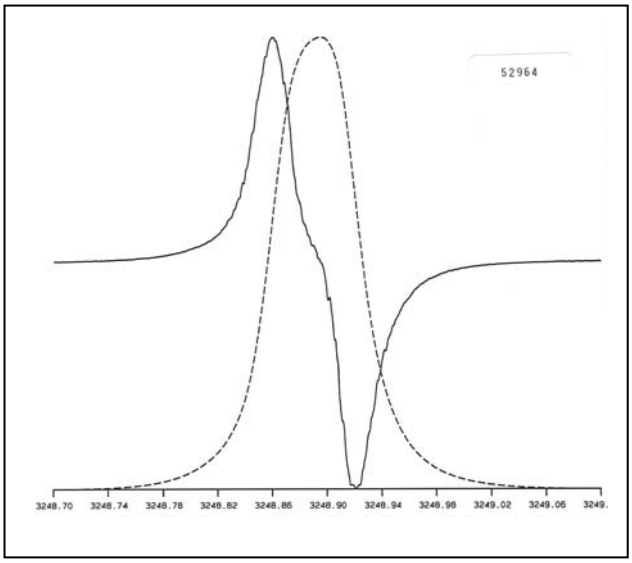

Figure 3-10 X-band EPR spectrum of lithium phthalocyanine (LiPc) in the absence of O_2, recorded with 100 kHz magnetic field modulation. The derivative peak-to-peak line width of this sample was about 23 mG when recorded with low-frequency modulation. The 100 kHz modulation sidebands broaden the line.

In such cases, much lower modulation frequency is needed to get true line shapes. Halpern and coworkers routinely use 5 kHz modulation for CW EPR of trityl radicals (Mailer et al. 2003).

3.11.3 Modulation Sidebands

In the above trityl spectrum one can see the distortion of the EPR line due to the use of 100 kHz modulation. The sidebands themselves were demonstrated using the very narrow lines of the TCNE anion radical, which are relaxation-determined, with no unresolved nuclear hyperfine coupling. The spectrum of a single line, obtained with 10 kHz modulation so that the sidebands are within the EPR line, is shown in Figure 3-11.

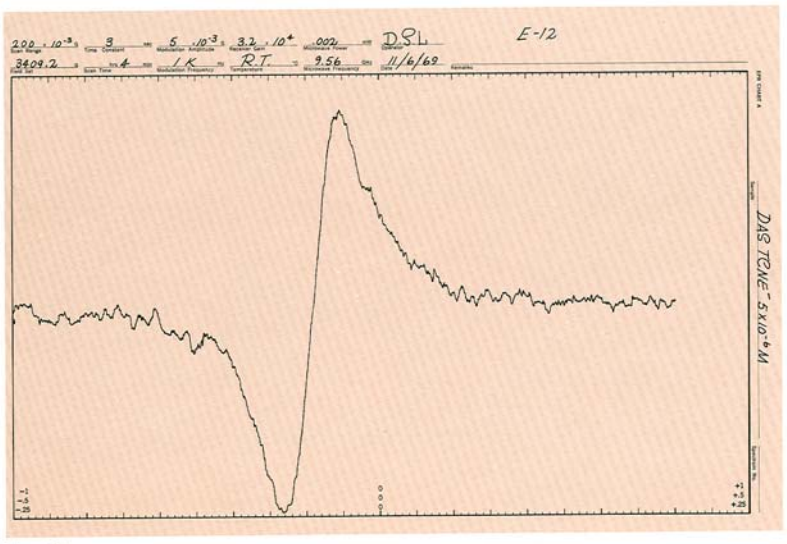

Figure 11

Figure 3-11 A single line of the 9-line TCNE anion radical, obtained with 10 kHz modulation and 5 mG modulation amplitude in order to avoid distorting the line. From a 1970 Varian brochure titled "EPR with Varian E-line Spectrometers."

By using a small modulation amplitude (20 mG), which in electrical engineering would be called a low index of modulation, and by exactly adjusting the phase of the phase-sensitive detector, the sidebands, but no centerband, are detected. The spectrum exhibits the lower and upper 100 kHz sidebands separated by about 72 mG.

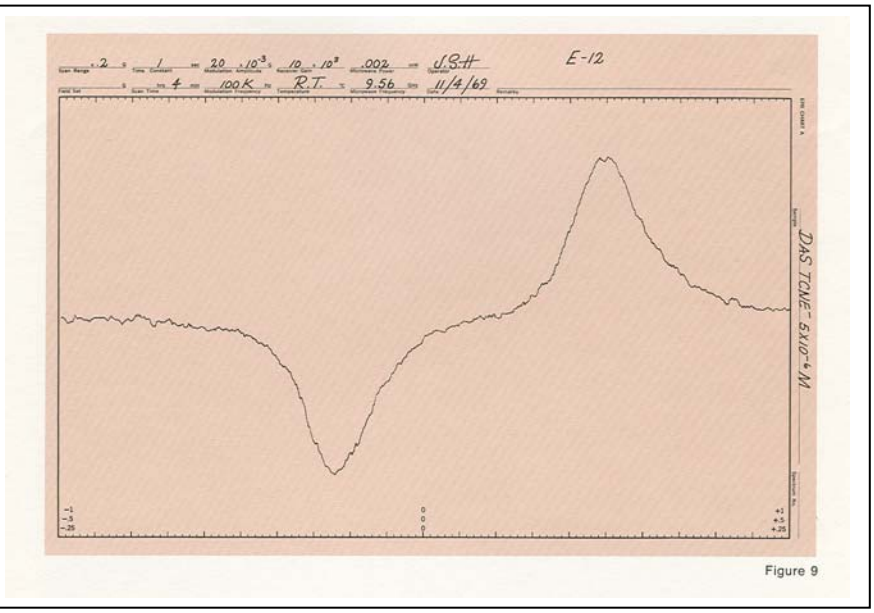

Figure 9

Figure 3-12 A single line of the 9-line TCNE anion radical, obtained with 100 kHz modulation and 20 mG modulation amplitude in order to exhibit the modulation sidebands. From a 1970 Varian brochure titled "EPR with Varian E-line Spectrometers." Note that the spectrum was obtained by James S.Hyde, and the sample was prepared by Dr. M. R. Das in the laboratory of Jack Freed.

When the same spectrum was repeated with a high index of modulation, the first, second, and third sidebands were all observed:

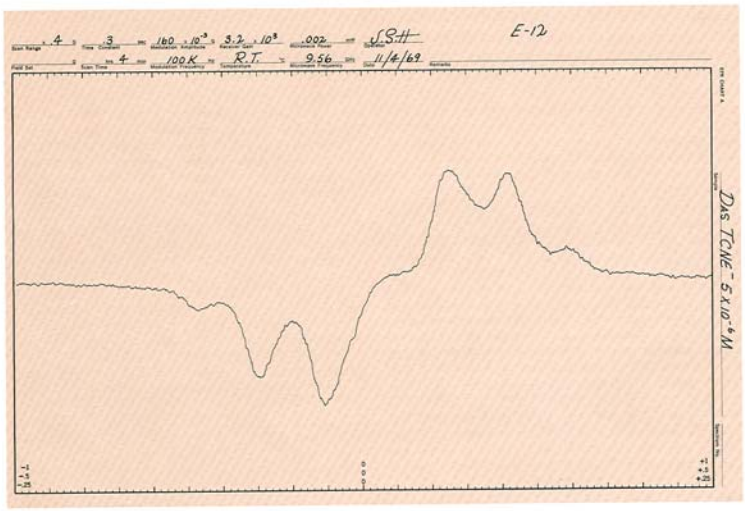

Figure 3-13 A single line of the 9-line TCNE anion radical, obtained with 100 kHz modulation and 160 mG modulation amplitude in order to exhibit multiple modulation sidebands. From a 1970 Varian brochure titled "EPR with Varian E-line Spectrometers."

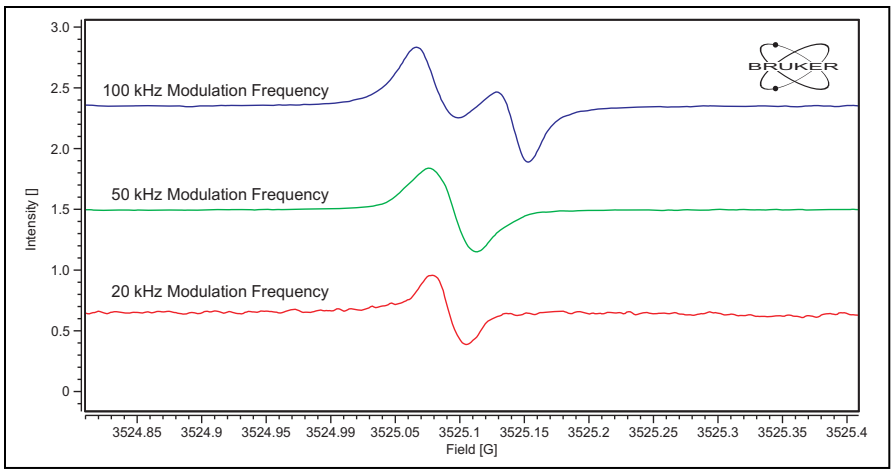

Figure 3-14 N@C_{60} has a very narrow line. Modulation sidebands are observed when 100 kHz magnetic field modulation is used.

Furthermore, with both high modulation frequency and high modulation amplitude, the rate of passage through a line may be of the order of or faster than relaxation rates, resulting in passage effects. This is the rapid scan EPR regime. For example, 1 G sinusoidal modulation at 100 kHz is a magnetic field scan of $2\pi x10^5$ G/s at the point of maximum scan rate as shown in recent papers from the Eaton lab (Stoner et al. 2004; Joshi et al. 2005b; Tseitlin et al. 2006). Passage effects are not as unusual a phenomenon as might be expected. It is easily demonstrated by the standard irradiated quartz sample, and other narrow-line samples with long relaxation times.

As a tradeoff between low frequency noise and distortion by modulation sidebands, most CW EPR spectra are obtained using 100 kHz modulation. However for samples with narrow-line spectra such as deuterated triaryl methyl radicals, lower modulation frequencies are required to avoid broadening of the ca. 30 mG linewidths (Mailer et al. 2003). ST-EPR spectra are usually obtained with modulation at a lower frequency and detection at the second harmonic - e.g., 50

and 100 kHz. For slow-passage EPR, it is necessary to have the reciprocal of the modulation frequency much greater than T_1.

$$\nu_m^{-1} >> T_1$$

This criterion is not met as often as it is assumed to be. Some samples at liquid nitrogen temperature, and many samples at liquid helium temperature, have T_1 that is too long to permit use of 100 kHz modulation. Passage effects, recognizable as distortions of line shapes, or even inversion of signals upon reversal of the field scan direction, alert you to the need to use a lower modulation frequency. On older instruments, such as the Varian E-line and Century series spectrometers, there was a large degradation in S/N at lower modulation frequencies. In the current Bruker spectrometers there is very little increase in noise at low modulation frequencies. The increase in electron spin relaxation times with decrease in temperature often forces one to use the lowest modulation frequency available on the spectrometer. Bruker spectrometers have modulation frequencies between 1 and 100 kHz.

Kälin et al. (2003) describe modulation sidebands from the perspective that they are actually multiple photon transitions, and that the shape of the lines in field-modulated CW EPR is due to the unresolved sideband pattern of these lines.

3.12 Illustration of the Effect of Modulation Amplitude, Modulation Frequency, and Microwave Power on the Spectra of Free Radicals

In addition to the distortion of the line shape illustrated above for trityl, accidental equivalence of hyperfine splitting and modulation sidebands can cause confusion about the number of hyperfine lines. This was illustrated by the change in apparent hyperfine in galvinoxyl radical (also called Coppinger's radical).

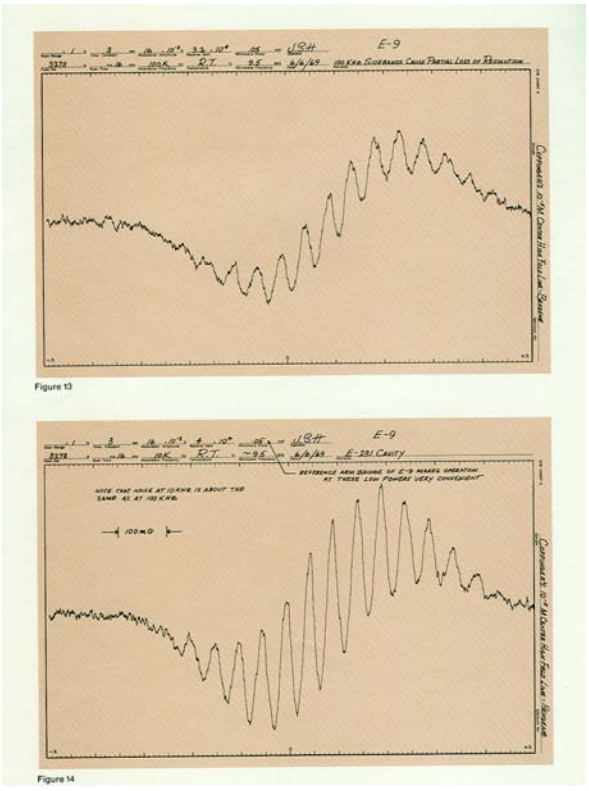

Figure 3-15 A single line of the galvinoxyl radical, obtained with 100 and 10 kHz modulation and 16 mG modulation amplitude. Note that the spectrum is much better resolved when 10 kHz modulation is used than when 100 kHz modulation is used. The apparent hyperfine splitting is ca. 45 mG, which is close to the 36 mG 100 kHz sidebands. Based on careful count of the hyperfine pattern, and especially the symmetry of the pattern, the 100 kHz spectrum looks like there is an odd number of t-butyl protons, whereas the radical has 36 t-butyl protons, as is consistent with the 10 kHz spectrum. From a 1970 Varian brochure titled "EPR with Varian E-line Spectrometers."

The following figure presents two lessons. First, the resolution is better with 10 kHz

modulation than with 100 kHz, as was also shown in Figure 3-15. The new lesson here is that increasing microwave power broadens the EPR lines due to saturation. If one were to perform an exploratory search for the spectrum with 1.0 mW and 100 kHz modulation, which are good general parameters with which to search for a spectrum, the additional hyperfine due to the t-butyl protons would not be observed. Although it is difficult to see from the selection of spectra presented here, it also turns out that the maximum spectral intensity occurs at 0.7 mW when 100 kHz modulation is used, but at 0.1 mW when 10 kHz modulation is used. Thus, the CW power saturation behavior is obscured by use of 100 kHz modulation when the lines are so narrow as in galvinoxyl.

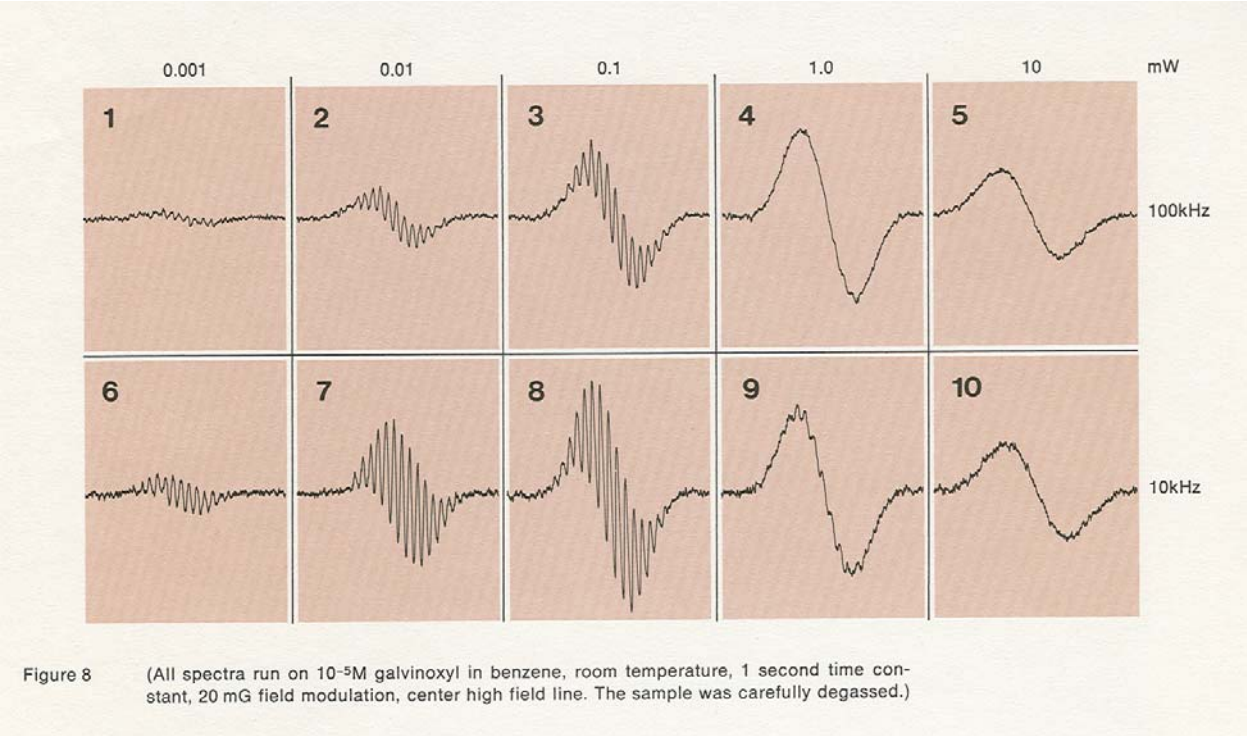

Figure 8 (All spectra run on 10^{-5}M galvinoxyl in benzene, room temperature, 1 second time constant, 20 mG field modulation, center high field line. The sample was carefully degassed.)

Figure 3-16 The galvinoxyl transition pictured is the same as in the previous figure, where the incident microwave power was 0.05 mW, half of that in panel 3 in this figure. The modulation amplitude is 20 mG, a little larger than the 16 mG in the previous figure. From a 1970 Varian brochure titled "EPR with Varian E-line Spectrometers."

3.13 Phase

There are two phase settings in the normal CW spectrometer, the reference arm phase and the phase of the phase-sensitive detector operating at the field modulation frequency (often 100 kHz). If the reference arm phase is wrong the signal amplitude will be low, and dispersion will be mixed with absorption. This phase setting is adjusted to maximize the detector current at high microwave power. If the 100 kHz detector phase is wrong the signal amplitude will be low. Since a null is easier to see than a maximum, the best approach is to set the phase for null signal, and then change phase by 90°. For saturation transfer spectroscopy this setting is very critical, and a substantial literature has been devoted to it (Hyde 1978; Hyde and Thomas 1980; Watanabe et al. 1982; Beth et al. 1983). It is also important to adjust the phase of the AFC

system (normally 70 or 77 kHz), but there is no user control of this phase in commercial instruments.

3.14 Automatic Frequency Control and Microwave Phase

The automatic frequency control (AFC) circuit is designed to keep the microwave source (klystron or Gunn diode) frequency locked to the resonant frequency of the sample cavity (resonator), as that changes due to temperature changes, changes in the sample, etc. The amplitude of the EPR signal has a cosinusoidal dependence on the frequency match, so it generally is not strongly affected by a slight change in the AFC correction signal. However, the AFC correction mixes in some dispersion signal with the absorption signal. If the sample is somewhat saturated, this mixing can be important, because the dispersion signal does not saturate as readily as does the absorption signal. The standard irradiated fused silica sample (Eaton and Eaton 1993) sold by Wilmad as WGSR-01-4 has a long electron spin relaxation time T_1 and spin-spin relaxation time (see below), and the CW absorption spectrum mixes with the dispersion spectrum unless the frequency is very carefully set and controlled. Hence, this sample is a good monitor of the functioning of the automatic frequency control (AFC) circuit of the spectrometer (Ludowise et al. 1991).

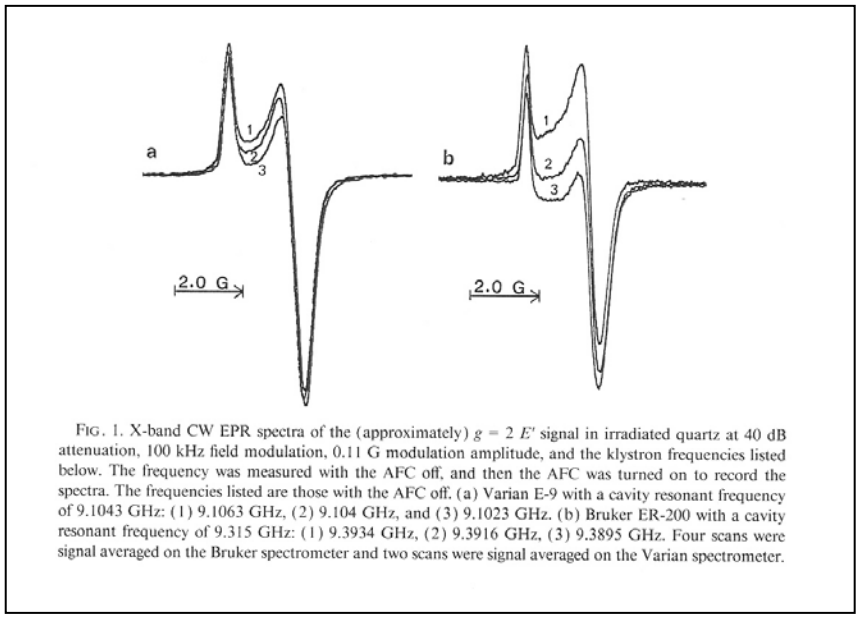

FIG. 1. X-band CW EPR spectra of the (approximately) $g = 2$ E' signal in irradiated quartz at 40 dB attenuation, 100 kHz field modulation, 0.11 G modulation amplitude, and the klystron frequencies listed below. The frequency was measured with the AFC off, and then the AFC was turned on to record the spectra. The frequencies listed are those with the AFC off. (a) Varian E-9 with a cavity resonant frequency of 9.1043 GHz: (1) 9.1063 GHz, (2) 9.104 GHz, and (3) 9.1023 GHz. (b) Bruker ER-200 with a cavity resonant frequency of 9.315 GHz: (1) 9.3934 GHz, (2) 9.3916 GHz, (3) 9.3895 GHz. Four scans were signal averaged on the Bruker spectrometer and two scans were signal averaged on the Varian spectrometer.

Figure 3-17 Dispersion and absorption spectra mix when the AFC correction signal is large. The effect of this mixing can be seen sensitively when the electron spin relaxation time is so long that the absorption signal is partially saturated. From Ludowise et al. (1991).

When the power incident on the resonator is very low, there is not enough reflected power to make the AFC circuit function properly. For example, Calvo et al. (2000) found that at temperatures below 4.2 K, incident powers of 0.2 to 1 nW were required in a study of the photosynthetic reaction center, and manual tuning was required to achieve a pure absorption EPR signal. The Q-band spectrometer used was locally built and used a TE_{011} brass cavity.

The latest Bruker spectrometers incorporate a DC AFC circuit to provide better stability at low incident powers and under some pulsed EPR conditions.

EPR signal amplitude can be increased, but at cost of losing information about the number of

spins and the linewidth. For example, a spectrum that exhibits well-resolved hyperfine at low power and modulation amplitude, will exhibit poorer resolution, but better S/N, at higher power and higher modulation amplitude.

3.15 Sample Considerations

All of this discussion is sample dependent. The amount of sample that can be put in a single-mode resonator is limited by the wavelength of the RF/microwaves. One can increase sample size with minimal effect on Q for a non-lossy sample, and one can increase Q substantially via resonator design, but Q will be sample-limited for a lossy sample of finite dimensions.
What is the ultimate Q? The resonator Q cannot usefully be increased without limit, e.g., by using superconducting resonators, because source noise will dominate and the S/N will not increase. Thus, for a non-lossy sample the ultimate S/N limit is the source noise. All of these considerations lead to the conclusion that the best S/N for a given sample will be achieved by designing a resonator for the sample. This is why there is such a wide array of resonators available.

3.16 Passage Effects

So far we have emphasized being careful to avoid saturating the CW EPR spectrum. There are easily accessible experimental situations, especially at cryogenic temperatures, at which one observes extreme relaxation-dependent phenomena, called passage effects (Weger 1960). One such example is in Figure 3-18. These phenomena are readily observed at room temperature using the irradiated quartz pulsed EPR standard sample, which is available from Wilmad.

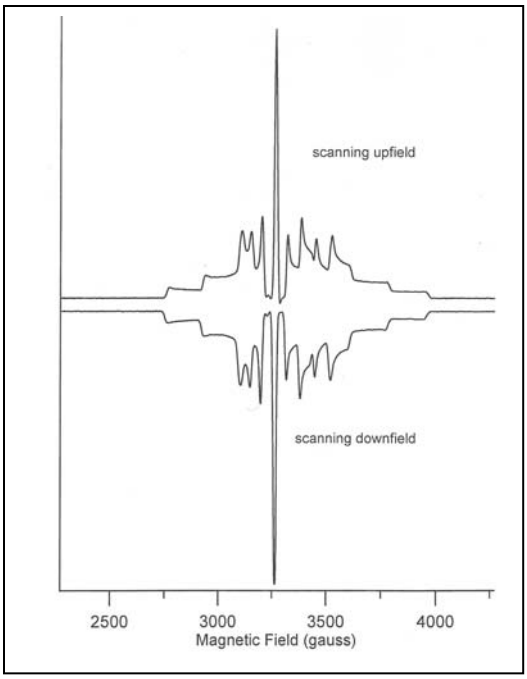

Figure 3-18 X-band CW derivative EPR spectra of vanadyl porphyrin in frozen solution at ca. 5K. When an EPR spectrum is scanned too fast to allow the spins to be at thermal equilibrium, passage effects occur. In extreme cases the first-derivative spectrum looks like an absorption spectrum, and the spectrum turns upside down when the field-scan direction is reversed. For less extreme cases of passage effects, distorted spectra are observed, which are best identified by recording spectra with both increasing and decreasing magnetic field scan rates, and by changing modulation amplitude and microwave power. In the absence of passage effects the scans should be superimposable (after scaling), assuming that the correct filter time constant has been selected.

3.17 Software

The era when one twisted knobs on the front panel of the spectrometer bridge and console is largely past. Modern spectrometers are software controlled, and contain multiple microprocessors to store calibration data and operate modules of the spectrometer under

command from the main software program, which in Bruker Elexsys spectrometers is Xepr The program used in the EMX is called WinAcquisit.

The operator interacts with the spectrometer via the keyboard of a PC. For normal CW EPR, even the adjustment of the TE_{102} cavity coupling iris is controlled by keyboard and mouse commands. (In pulsed EPR spectrometers, one still adjusts the coupling of a split-ring resonator with fingers.)

Xepr now has capability for quantitative comparison of spectra. This will be introduced at the 2008 EPR Symposium.

3.18 Summary Guidance for the Operator

3.18.1 Scaling Results for Quantitative Comparisons

Unless the spectra to be compared are obtained under exactly the same conditions, it will be necessary to scale the area (double integral of the first-derivative signal) obtained for the unknown to compare it with the standard. This involves:

(i) subtract the background spectrum

(ii) correct for modulation amplitude. Area scales linearly with modulation amplitude, even when spectra are overmodulated.

(iii) correct for gain. Area scales linearly with gain settings of the detector amplifier. However, note that in the current Bruker software gain is reported in units of dB with the relationship gain = 20 log(signal amplitude).

(iv) correct for microwave power. Be sure to obtain spectra at power levels below saturation. Under these conditions, area scales as the square root of the incident microwave power.

(v) correct for Q differences. Area scales linearly with Q.

(vi) correct for temperature differences. Note that EPR is a measurement of bulk spin magnetic susceptibility. Thus, the area scales with the population difference of the ground and excited states. For isolated $S = 1/2$, the temperature dependence typically obeys a simple Boltzmann behavior. Interacting spin systems, and cases of $S > 1/2$, can result in complicated temperature dependences. In this regard, note that most solid reference materials are not magnetically dilute, so their temperature dependence does not obey a simple Curie law (Molin et al. 1966; Slangen 1970; Goldberg et al. 1977). A paper on chromic oxide is illustrative of the efforts needed in these types of cases (Goldberg et al. 1977). Also note that the density of solutions, and hence the number of spins at a given position in the B_1 field varies with temperature. In addition, solvent loss tangent varies with temperature. The temperature dependence of the sample and reference have to be the same, or known and the differences mathematically compensated for.

(vii) correct for spin differences. The transition probability, and hence the area, scales as $S(S+1)$. For example, comparing $S = 1/2$ and $S = 3/2$, assuming all transitions are observed, the relative areas are in the ratio 3/4 to 15/4 from this effect. If one observes only part of the transitions, which is common for $S > 1/2$, it is also necessary to correct for the relative multiplicities, which go as $(2S+1)$. In some cases simulation of the spectra may be required.

(viii) correct for g-value differences. Area scales as g. Note that papers and books published prior to Aasa and Vanngard (1975) paper state incorrectly that area scales as g^2.

(ix) correct for field scan width. For first derivative spectra, the scan width correction factor is $(1/\text{sweep width})^2$.

(x) When an integrating digitizer is used, as in the Bruker E500 series spectrometers, the recorded signal area varies with scan time. This is taken into account in the "normalized acquisition" option of Xepr.

If the software includes a "normalization" option it is important to know which parameters are included. It is also important to ensure that the signal plus noise nearly fills the full scale of the digitizer as much as possible.

All of these general considerations (except modulation amplitude) apply to both CW and time-domain spectra. In the case of time-domain spectra there are two other major considerations. First, the spectrum can depend very sensitively and very strongly on the microwave pulse conditions and the observation conditions. For example, a magnetic field-swept, spin echo-detected spectrum depends on the interpulse time τ at which the echo is recorded. Most ESE spectrometers use boxcar detection of the echo amplitude. The shape of the field-swept spectrum depends on the portion of the echo that is sampled by the boxcar averager and the digitizer.

3.18.2 Signal Averaging

As noted above, the noise in a spectrum will decrease, and the S/N will increase, proportional to the square root of the number of scans averaged, proportional to the filter time constant, and proportional to the conversion time. Note the discussion of the interactions among these parameters, and their effect on line shape fidelity, in the previous section. The challenge for the operator is to choose the method of S/N improvement that is best for the sample and the environment. If the noise were white (i.e., truly random) all methods should give the same result. However, the real environment of a laboratory includes building vibrations, which are often of the order of a fraction of a Hz to a few Hz, sample temperature variations, power line variations, etc. The room temperature variations can be extreme if the ventilation system directs air currents into the magnet gap. The weak pitch standard S/N test conditions are designed to reveal some of these problems, and in many cases the operator will observe that the limiting noise is a “baseline wander” within a small factor of a Hz. Even if a sample is largely immune from room temperature variations, such as when it is in a cryostat, there can be slow drifts in the temperature of the cooling gas (He or N_2). The result of these considerations is that it is usually better to perform signal averaging of multiple magnetic field scans at the fastest rate consistent with line widths than to perform a single slow scan with a long filter time constant.

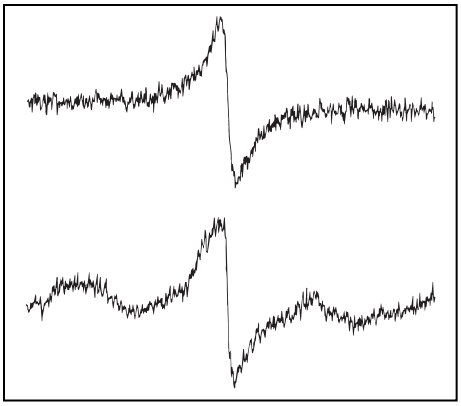

Figure 3-19 The upper spectrum was acquired with short time constant and multiple-scan signal averaging. The lower spectrum was acquired with a long sweep time and long time constant.

Signal averaging reduces the effective noise bandwidth proportional to the square root of the number of scans averaged.

3.18.3 Number of data points

One of the ironies of using the power of computers to enhance EPR is that the early computers were so limited in speed and memory that there was actually a reduction in the number of magnetic field axis data points acquired by most systems. For example, the recorder stepping motors used prior to computers often had 9600 steps across the spectrum. Initial computer-interface spectrometers used only 1024 magnetic field steps. Xepr supports 8192 magnetic field steps (13 bits), and the EMX-Plus defines the magnetic field axis in 24 bits. The calculation of how many data points you need is essentially the same as the calculation for time constant – there should be at least 10 magnetic field samples over the narrowest line in the spectrum. Thus, if the line is 0.1 G wide, magnetic field steps should be no larger than 0.01 G, which with 8192 magnetic field steps limits the spectral scan width to ca. 80 G.

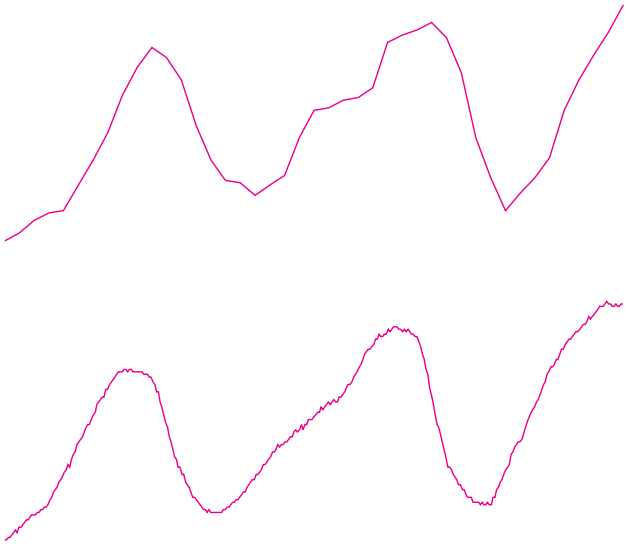

Figure 3-20 An expanded view of an EPR spectrum using 1024 data points (upper trace) or 8192 data points (lower trace).

Note that specific values used in this section are among those selectable via the Xepr software on the Elexsys spectrometers.

3.18.4 Cleanliness

Spins are everywhere. Most dirt, and tobacco smoke!, has an EPR signal. Some materials used for suspended ceilings contain significant amounts of Mn(II). The cavity must be protected from dirt. It is good practice to prohibit smoking in the spectrometer room, and to clean the outside of all sample tubes just prior to inserting them into the cavity. A tissue such as 'Kimwipe' and a cleaner such as a residue-free electronic contact spray cleaner is handy for this purpose. Fingerprints will transfer dirt to the cavity.

Inevitably, the cavity will become contaminated, possibly from a broken sample tube, causing significant background signals. The mildest cleaning that will remove the known or suspected contaminant should be used. Check the manufacturer's guidance on solvent compatibility. For

the rectangular resonator Bruker suggests ethanol, hexanes, toluene, and/or 0.1 molar EDTA followed by methanol. Some people use an ultrasonic cleaner, but this is not wise - it may loosen critically torqued parts of the cavity. After cleaning, purge the cavity and waveguide with clean dry nitrogen gas to remove the last traces of solvent. Some resonators may need to be returned to the vendor for cleaning.

3.18.5 Changing Samples

Always attenuate the power to ca. 40 dB below full power before changing samples when doing CW EPR, to avoid unnecessary spike of power to the detector crystal.

3.18.6 NMR Gaussmeter Interference

Another, perhaps surprising, problem that can occur when one "tries too hard" is that if the NMR gaussmeter probe is very close to the EPR cavity, in an attempt to minimize the magnetic field offset between the NMR probe and the EPR sample, the modulation used in the NMR probe can broaden the EPR signal. In one case where we tested this with a trityl sample, the line width increased from 26 mG to 64 mG.

Chapter 4 - What Matters, and What Can You Control?

4.1 Crucial Parameters and How They Affect EPR Signal Intensity

We present the expression for the EPR signal again as a reminder:

$$V_S = \chi'' \eta Q \sqrt{PZ_0}$$

Many spectrometer and sample parameters and interactions between the sample and the spectrometer affect the quantitative accuracy. Some of them can be controlled by the operator. Others cannot be controlled by the operator, but need to be known to accurately perform quantitative measurements. For example,

- The operator can control the preparation of the sample.
- The operator can select a sample and a resonator (see 2005 Workshop on Selecting an EPR Resonator) such that there is minimum perturbation of the microwave fields in the resonator. However, the resonator Q must be measured for accurate comparisons. See Chapter 6 for more about Q.
- The operator can make the calibration standard such that its width, intensity, and dielectric loss are similar to the unknown.
- The operator rarely can control the relaxation properties of the sample, but has to be sure that the sample is not power-saturated when making quantitative comparisons, or is saturated to the same extent as the standard.

The list of variables to consider is long, but the operator must always keep these in mind, and control or measure as many as possible.

- Microwave power and B_1 at the sample
- Modulation amplitude
- Gain
- Scan time and detector time constant
- Magnetic field scan width
- Type of cavity
- Properties of any Dewar insert in the cavity (B_1 depends on the Dewar wall thickness)
- Physical size of sample
- Sample position in the cavity
- Dimensions and uniformity of the sample tube
- Dielectric properties of the solvent at the microwave frequency (see 2002 Workshop)
- Detector current
- AFC offset
- Temperature of the sample and its effect on sample concentration, species dissociation, paramagnetism, and dielectric loss.
- Microwave frequency (and magnetic field)

Some of these variables, and some EPR spectrometer operating aspects relevant to quantitative EPR are discussed in (Wertz and Bolton 1972, Appendix D) and (Weil et al. 1994, Appendix E). Also valuable are the chapters: Bolton et al. (1972) and Randolph (1972). Many of the "string and sealing wax" aspects of EPR are recorded in the book by Alger (1968). These serve mostly to alert the operator to the kinds of things that have to be considered in performing quantitative

EPR, but do not tell how to do it. In fact at the time of Alger's book, EPR was considered to be rather non-quantitative. A comparison study of standard samples was judged to exhibit errors of as much as 50% (Alger 1968, page 205). Some of the factors affecting signal intensity were discussed by Bryson et al. (1975). In retrospect, it is likely that a large source of uncertainty was lack of measures of resonator Q and possibly some other parameters. Dalal et al. (1981a) emphasized the importance of measuring Q, especially when using lossy solvents. Blakley et al. (2001) discussed the importance of matching the resonator Q for standard and sample. Fairly extensive reviews by (Eaton and Eaton 1980; 1990; 1997; 2005) provide additional references. As an example of the effect of lossy solvent on resonator Q, a 1 mm diameter capillary tube containing water reduced the Q of a rectangular cavity from ca. 3000 to ca. 500-600. Since the EPR signal is proportional to resonator Q, an attempt to make a quantitative measurement of a 1 mm aqueous sample relative to a non-lossy standard could introduce an error of a factor of 5 or so. There is also a lens effect of the dielectric sample, and quartz Dewar insert, increasing the microwave B_1 at the sample relative to that of an empty cavity. Dalal et al. (1981a) give many details.

One has to be careful to consider the age of the EPR spectrometer. In the early days of EPR there was little focus on quantitative accuracy of spin concentrations. Goldberg (1978) documented the uncertainties in settings on older Varian spectrometers and their effect on signal levels. Better results were obtained by Yordanov and Ivanova (1994b). The rather discouraging view of intra- and inter-laboratory comparisons presented in these older papers have been relieved substantially by the attention paid to resonator Q, sample positioning (see the papers cited in table 5-1), reference standards, and dramatic improvements in EPR spectrometers, including special purpose Bruker spectrometers dedicated to alanine dosimetry, beer stability, etc.

4.2 What Accuracy Can One Aspire To?

With modern spectrometers, and careful attention to experimental conditions, inter-laboratory comparisons have achieved 3% standard deviation on samples with internal standards (Gancheva et al. 2008). Alanine dosimeters containing Mn^{2+}/MgO as an internal standard were measured on 12 instruments of 6 different models by three manufacturers, run by 10 operators. This 3% standard deviation was obtained only after a preliminary comparison showed the need to use a procedure that involved low power and modulation amplitude, and a combination of sweep time and time constant that gives a distortion-free spectrum.

Yordanov et al. (1999) report that the same operator on the same instrument can achieve about ±2% reproducibility on the same sample. However, if the measurement was made relative to an internal standard, the standard deviation reduced to 0.5%.

Statistical studies of gain, power, and modulation amplitude, and repeated insertion of the same sample, on a Bruker ER 200D were reported by Yordanov and Ivanova (1994b). The largest variations were in microwave power attenuation and sample positioning.

Even with modern instruments, however, some cautions have to be observed. For example, incident microwave power attenuation uses a rotary vane attenuator. In older instruments the attenuation was set manually by rotating a knob. In modern X-band spectrometers the same type

rotary vane attenuator is under motor control. However, ultimately, the attenuation is dependent on some small backlash in the gears, and for the most accurate work it is important to approach the attenuation setting from the same direction each time to obtain reproducible attenuations. Microwave sources have finite lifetimes, and the power output could change with time, so calibration either with a calibrated power meter or with a standard sample from time to time is a good idea. The lore of the field is that one should let the system "warm up" a while before recording spectra. Although this guidance is a residue from the vacuum tube era, it actually retains some validity for different reasons. The sensitivity of a crystal detector is temperature dependent, so for the most accurate quantitation, the crystal should be at the same temperature in compared measurements. In fact, the Bruker spectrometers designed for quantitative EPR have provision for temperature control of the detector. Microwave detectors can fail quickly due to high power burnout, but more commonly, the sensitivity slowly degrades over time due to occasional, non-lethal, excess incident power. Calibration with a standard sample is also useful to monitor this aspect of spectrometer performance. These problems should be small and uncommon on modern instruments, but cannot be ignored for the most accurate work.

Quantitative EPR depends, ultimately, on the analytical balance and on volumetric techniques such as calibrating glassware, some of which is an art disappearing from standard college curricula. Unless precision quartz sample tubes are purchased, for accurate work the sample tubes need to be calibrated just like any other piece of analytical glassware. For example, one can weigh a measured length of solvent in the tube at a known temperature to measure the internal volume of the tube. There are uncertainties due to the rounded bottom of the tube and meniscus at the top of the column of fluid, however, these approximately compensate for one another. Thus, weighing the empty tube, then adding liquid and weighing again, yields the mass of a measured length of fluid. Tables of density vs. temperature in the Handbook of Chemistry and Physics can be used to derive the volume of the tube. It is a bit more difficult to reproducibly put powdered or microcrystalline material in a tube. The main concern is reproducibility, so each operator has to develop a procedure. For example, add a couple mm of loose powder at a time, followed by tapping in a routine way on a hard rubber stopper, then add more powder and repeat until the column of material is as long as desired. The packing density, measured by weighing the tube before and after filling, is strongly dependent on the method of packing the powder.

As discussed in this Workshop, some parameters can be controlled by the operator to optimize for one aspect of the information content of the EPR signal, but optimizing for one observable may negatively impact another. For example, when performing the normal field-modulation, phase sensitive detection method, and applying a filter to the signal before recording it, the signal-to-noise (S/N) could be expressed as:

$$S/N \propto (\chi'')(Q)(B_1)(\text{modulation amplitude})(\text{filter time constant})$$

Although S/N is proportional to the filter time constant, enhancing the S/N may degrade the line shape.

4.3 Detector Current – Adjusting the Coupling to the Resonator

Adjusting the coupling to the resonator can be one of the most time-consuming aspects of preparing to obtain an EPR spectrum. To the novice operator it may seem like a mysterious ritual. In this section we attempt to remove part of the mystery. The goal stated in most operating instructions is to have the resonator "critically coupled" to the transmission line. The iris coupling assembly of a cavity, or the antenna coupling assembly of the Bruker X-band FlexLine dielectric and split ring resonators, can be viewed as transformers that transform the impedance of the resonator to the impedance of the transmission line (waveguide or coaxial line). At "critical coupling" (i.e., when the impedance is properly matched) the microwave power incident on the resonator is all absorbed in the resonator, and none of the power is reflected. The tuning "dip" is a plot of reflected power vs. microwave frequency. Ideally, zero power is reflected at critical coupling, so the dip should be as deep as it will go.

At EPR resonance, the impedance of the resonator changes, so some of the incident power is reflected, and this power is detected as the EPR signal. This simple picture is complicated by the fact that the EPR bridge is based on an imperfect circulator. Although most of the microwave power follows the circular route from source to resonator to detector (ports 1, 2, and 3 in the usual diagram), about 1% of the power incident on port 1 goes directly to port 3 (detector) instead of to port 2 (resonator). Thus, the power reaching the detector is the sum of the ideal EPR signal model for a critically coupled resonator and the microwave power that goes through this direct (leakage) path. The leakage power increases linearly with increase in the power incident on the resonator, since they are both affected by the same attenuator between the source and the circulator. The power through the reference arm together with the leakage and reflected power biases the detector crystal to an optimally sensitive region of its response curve. For the crystals used in EPR spectrometers, this occurs at ca. 200 μA current through the detector. The spectrometer functions best for quantitative EPR when there is only a very small change in detector current as the spectrometer goes through EPR resonance. If you can see a change in the detector current, the EPR signal is much too strong to get quantitative results. From an engineering perspective, the operator is really adjusting the resonator, circulator, and transmission line between them to critical coupling as a unit. The resonator itself may be slightly away from critical coupling. The phase of the resonator reflection coefficient can be anywhere from zero to 360 degrees relative to the incident microwave phase as the resonator coupling is adjusted near critical coupling. Slight mismatch of the resonator at some position of the coupling device will cause the reflected power to cancel the leakage through the circulator, with the result that the detector current will stay almost constant as the power incident on the resonator is changed by changing the attenuation. This is what the operator is actually doing when adjusting to "critical coupling."

Some of the source power is taken around the circulator in the reference arm, where the attenuation and phase are adjusted to properly bias the crystal detector. The reference arm microwave phase adjustment has the purpose of making the reference arm power in phase with the EPR signal. Since the proper phase is that for which there is constructive interference between the microwave paths, the final phase adjustment seeks to maximize the detector output, and hence maximize the EPR signal.

There are two different methods for adjusting coupling. It can be done with the reference arm off, in which case the adjustments are to minimize the detector current. Alternatively, the adjustment can be done with the reference arm on, in which the goal is to keep the detector current at 200 μA (centered in the Xepr display). Step-by-step operating procedures for a Bruker spectrometer are given by Jeschke (2007).

Chapter 5 – A Deeper Look at B_1 and Modulation Field Distribution in a Resonator

Since the square root of power in the expression

$$V_S = \chi'' \eta Q \sqrt{PZ_0}$$

is proportional to the B_1 at the sample, V_s is proportional to B_1 at the sample. Consequently, it is important to examine the details of the distribution of B_1 over a sample of finite size, such as the standard liquid or powdered sample in a 4 mm o.d. quartz sample tube. In the usual magnetic field modulation, phase-sensitive detection CW EPR experiment, the signal area is proportional to the modulation amplitude at the sample. Consequently, it is also important to consider the distribution of modulation amplitude over the sample. These are discussed in the following paragraphs.

5.1 Separation of B_1 and E_1

It is the microwave magnetic field, B_1, that induces the EPR transitions detected in EPR spectroscopy. Also associated with B_1 is the microwave electric field, E_1. The E_1 can induce rotational transitions in the sample, thereby generating heat in the sample. This phenomenon should be familiar to you from the effects of a microwave oven on your food. This microwave absorption contributes to the dissipation per cycle and thereby reduces the resonator Q. It is therefore important to position the sample in a region with high B_1 and low E_1.

For cavities, there is a natural separation between B_1 and E_1 because upon resonance, a standing wave is excited within the cavity. Standing electromagnetic waves have their electric and magnetic field components exactly out of phase, *i.e.* where the magnetic field is maximum, the electric field is minimum and *vice versa*. The spatial distribution of the electric and magnetic field amplitudes in a commonly used EPR cavity (TE_{102} rectangular mode) is shown below.

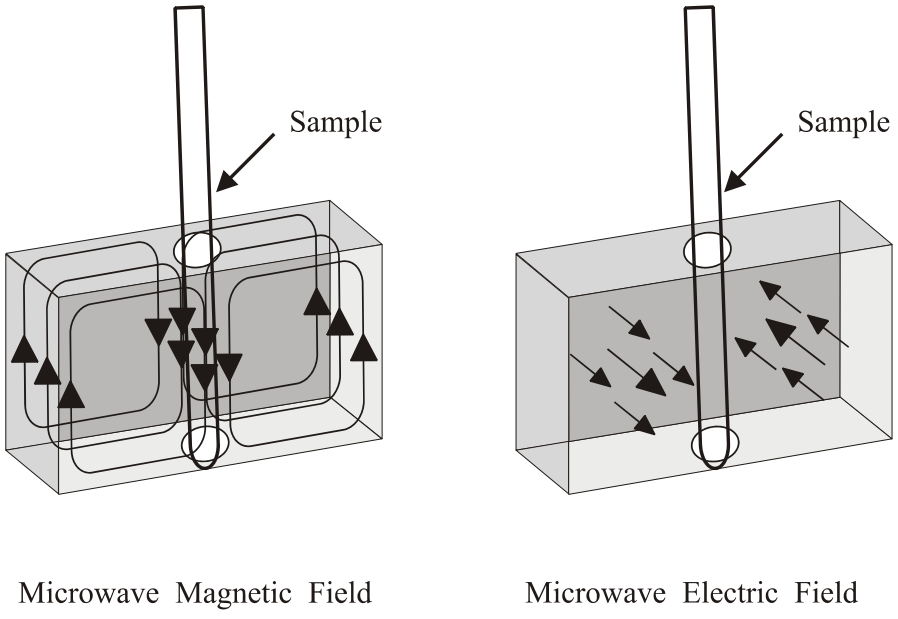

Figure 5-1 Placement of the EPR sample in a TE_{102} rectangular cavity for the maximum B_1 and minimum E_1.

Here we use the spatial separation of the electric and magnetic fields in a cavity to great advantage. If we place our sample in the electric field minimum and the magnetic field maximum, we obtain the biggest signals and the highest Q. Cavities are designed for optimal placement of the sample.

5.2 Inhomogeneity of B_1 and Modulation Amplitude.

The microwave B_1 field is inherently non-uniform in a microwave cavity, because the resonant condition necessitates standing waves, which have to have zeros and maxima. Modulation amplitude (MA) also is not homogeneous in the resonator. There have been many studies of the B_1 and modulation distributions in resonators. Early studies that informed operators of the major considerations were performed on the Varian E231 cavity. The early literature is summarized in Eaton and Eaton (1980) and experimental guidance is given in Eaton and Eaton (2005). Dalal et al. (1981a) describes the effects of lossy solvents. More et al. (1984) describe the simulation of power saturation curves of line samples considering B_1 and modulation distributions. Additional information is given in (Schreurs et al. 1960; Kooser et al. 1969; Mailer et al. 1977). More recent studies have examined the Bruker TE_{102} cavity resonator (Mazúr et al. 2004; 2005; Mazúr 2006; Yordanov and Slavov 1996; Yordanov and Christova 1997; Yordanov and Genova 1997; Yordanov et al. 1999 and references cited therein).

The nonuniformity in B_1 and modulation amplitude have resulted in many papers describing mechanical devices intended to precisely and reproducibly position samples in the resonator (see, for example, Chang (1974)). The sample also affects the microwave field (Rages and Sawyer 1973; Dalal et al. 1981a).

Nonuniformity of B_1 and modulation amplitude also affect measurements of microwave power saturation (Mailer et al. 1977). Comparison between labs will not agree unless attention is paid to variations in B_1 and modulation amplitude over the sample.

Different types of resonators have different distributions of B_1 and modulation field over the sample. Refer to the 2005 Workshop on Selecting an EPR Resonator for details.

Recently, the Hyde lab has described “uniform field” resonators, in which there is a sample region in which the B_1 field is uniform over a larger fraction of the resonator than in standard cavity or loop gap resonators. These are designed especially for aqueous samples (Mett et al. 2001; Anderson et al. 2002; Hyde and Mett 2002; Hyde et al. 2002; Mett and Hyde 2003; Sidabras et al. 2005).

Mazur and coworkers and Yordanov and coworkers have characterized the Bruker TE_{102} rectangular “ST” resonator and the TE_{104} double resonator from the viewpoint of quantitative CW EPR. The effect of distribution of B_1 and modulation amplitude on quantitative EPR was measured for 14 commercial cavities (Yordanov et al. 2002). Due to differences in construction, the B_1 and modulation distributions along the length of a sample could be similar, or one could be longer than the other. In table 5-1 we list a major topic for each of the papers. The papers contain more detail than is indicated in the table.

As an example of the type of measurement that has been made to monitor the dependence of signal intensity on sample position in the resonator, thus measuring the product of B_1 and magnetic field modulation amplitude, see Figure 5-2.

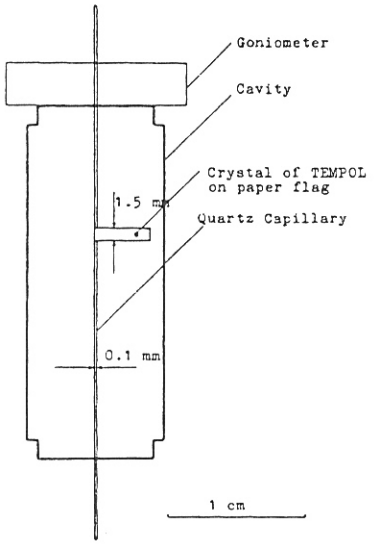

Figure 5-2 Device to position a sample to measure signal amplitude as a function of position in the cavity from (Nagy 1994).

Table 5-1 Characterization of TE_{102} and TE_{104} Cavity Resonators

Topic	**Reference**
Effect of shape of sample and sample position	(Nagy and Placek 1992)
Alignment procedure for sample in TE_{104} cavity	(Mazúr et al. 1996a)
Movement of line samples into TE_{104} cavity	(Mazúr et al. 1996b)
TE_{104} rectangular double resonator; differences in sample shape	(Mazúr et al. 1997c)
TE_{104} and TE_{102}; line sample moved along axis	(Mazúr et al. 1997a)
Alignment procedure for sample in TE_{104} cavity	(Mazúr et al. 1997b)
Line sample in TE_{102} or TE_{104} cavity	(Mazúr et al. 1998)
Radial and angular dependence in TE_{102} cavity	(Mazúr and Valko 1999)
Radial and longitudinal dependence in TE_{102} and TE_{104}	(Mazúr et al. 2000)
Large cylindrical samples with variable internal diameter and lengths of sample in TE_{102} and TE_{104}	(Mazúr et al. 2001)
A dozen useful tips – sample positioning etc.	(Mazúr 2006)
Effect of quartz insert in TE_{102}	(Yordanov and Slavov 1996)
TE_{102} and TM_{110}; length and diameter of samples	(Yordanov and Genova 1997)
Distribution of modulation and microwave B_1	(Yordanov et al. 2002)

There are cases where quantitative EPR is used in industrial QA/QC applications and very stringent demands are placed on the quantitation. If you have many samples with all the same size, properties, etc., commercial solutions are available. The Bruker BioSpin e-scan benchtop units have been tailored for specific applications. The development of these systems also follows

what is outlined in this section and keep application scientists and development engineers very busy.

The effect of distribution of B_1 and modulation on the EPR signal in a Bruker ER4119HS resonator is shown in Figure 5-3.

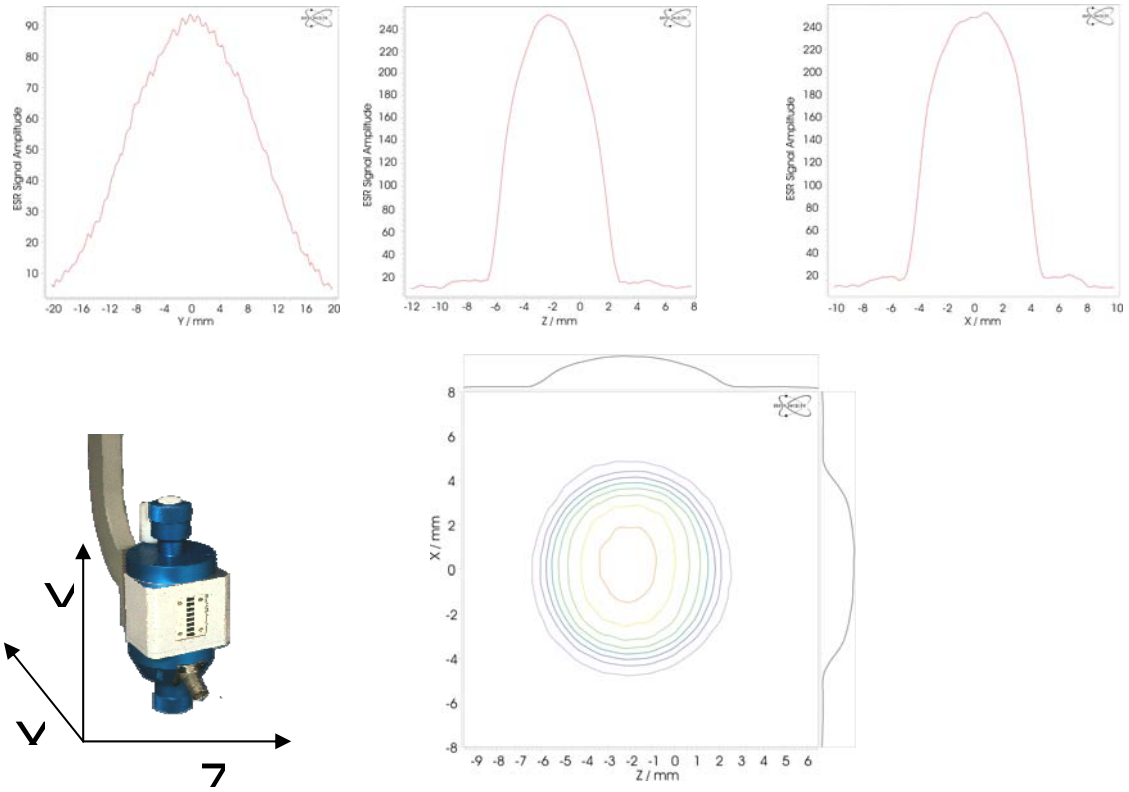

Figure 5-3 Signal intensity distribution for a Bruker ER4119HS resonator.

The B_1 distribution in the resonator affects the size, shape, and placement of the sample in the resonator. Ideally, one wants a uniform B_1 field over the sample. In addition, if the sample is lossy, one wants negligible E field in the sample. In a TE_{102} cavity resonator there is a nodal plane at which B is maximum and E is minimum. This is the normal sample location. In cylindrical resonators, the node is the center axis of the cylinder. Split ring, loop-gap, and other such lumped circuit resonators approximately separate the B and E fields, but have a capacitive gap that results in a fringing E field near the sample. Various bridged loop gap resonators are designed to minimize the fringe E field. This E field is why frequency and Q are so strongly dependent on sample placement in these type resonators.

5.3 Sample Size

A sample that is too small can be difficult to quantitate because of low S/N and because resonator background signals and slopes can become a significant part of the apparent EPR signal. However, a larger sample is not always better. A sample can be too large, as shown in papers by Vigouroux et al. (1973) and by Goldberg and Crowe (1977). Vigouroux et al. (1973)

showed broadening of the line when a TE_{011} cylindrical cavity with Q = 1500 contained more than about 10^{19} spins of DPPH and more than about $3x10^{20}$ spins of Mn(II). Proportionately more spins are acceptable for hyperfine-split samples such as Mn^{2+}. Goldberg and Crowe (1977) made more precise measurements of widths and amplitudes and found nonlinearities of the order of 1% when samples of ca. $3.4x10^{18}$ spins of $MnSO_4 \cdot H_2O$ or ca. $3.6x10^{17}$ spins of DPPH were used in a TE_{102} cavity with loaded Q of about 3000. Although not tested by Goldberg and Crowe, proportionately fewer spins will cause problems with extremely narrow-line samples, such as lithium phthalocyanine (Smirnov et al. 1994; Ilangovan et al. 2004) and triarylmethyl radicals (Ardenkjaer-Larsen et al. 1998).

Large samples. If unknown and known sample are the same size and long (> 2 cm for X-band) positioning is not as great an issue.

5.4 AFC Considerations

For substances with many spins per gram, such as solid DPPH, BDPA, LiPc, etc. a barely visible sample can easily overload the spectrometer. In extreme cases the operator can see changes in the detector current and AFC offset voltage as the field is swept through resonance. Any noticeable effect is much too large for proper quantitative EPR spectroscopy. Quantitative EPR assumes that the microwave absorption in the sample is a small perturbation on the resonator Q. See the equations for Q given in Chapter 6. Microwave absorption by the sample is a change in the resistance term in the denominator. This is what results in the EPR signal, but it has to be very small. If one does have to measure a sample that has too many spins per G – i.e., an extremely narrow line can cause disturbance of the AFC, which will look like an even narrower line. Figure 5-5 is an example. Turning off the AFC requires very careful phasing, but gives a truer line shape. Operating with a field/frequency lock has been the preferred way to stabilize magnetic field/frequency for recording narrow lines. However, if the signal is strong and narrow, some rather bizarre spectra can be recorded. Such as Figure 5-4, which was obtained with the same trityl sample as were the spectra in Figure 5-6. The hypothesis is that the intense narrow signal causes the F/F lock to oscillate when it searches for a proper match. When using an external resonator to lock the microwave source, the shape of the spectrum will depend strongly on the exact frequency of the external stabilizer resonator.

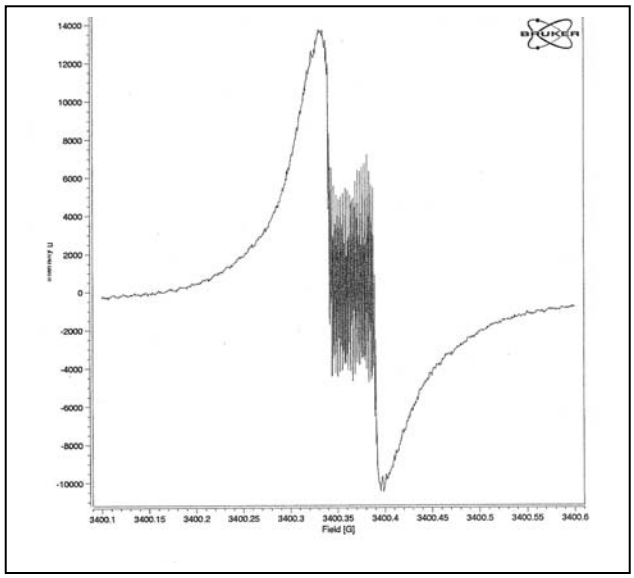

Figure 5-4 This strange X-band spectrum was obtained while attempting to use the field/frequency lock to record a narrow-line 0.2 mM deuterated symmetric trityl spectrum. The rapid oscillations are attributed to the effect of the very strong narrow signal on the ability of the F/F lock to find the proper match.

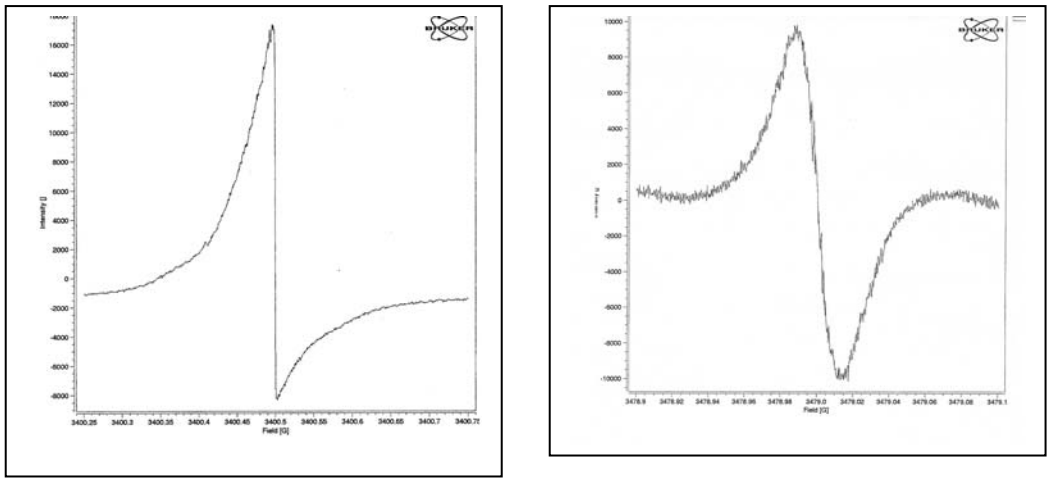

Figure 5-5 The two spectra in this figure are of the same sample of 0.2 mM trityl (Nycomed deuterated symmetric trityl) in a Teflon tube inside a 4 mm quartz tube, degassed by passing gaseous N_2 over the Teflon tube. The spectrum on the right hand side matches expectations for this species, which has a line width of ca. 26 mG and ^{13}C hyperfine lines close to the center line. This shape could be obtained without AFC lock, or with the AFC locked to an external cavity (the external stabilizer cavity used for pulsed EPR in an E580 bridge was used in this case). 10 mG 7 kHz magnetic field modulation was used, and the microwave power was attenuated 56 dB from 200 mW (0.5 μW). Note that the total scan width is 200 mG. The spectrum on the left hand side was obtained with normal AFC lock, but no F/F lock, and 500 mG scan width, and shows a distorted lineshape.

We have observed these phenomena with many very-narrow-line EPR spectra. Great effort is required to avoid power saturation, modulation broadening, AFC effects, field-frequency lock distortions, and to get proper phase. Spectra similar to that in Figure 5-5 have been published and attributed to spin systems with very narrow lines. This problem is inherent in AFC systems, including the new d.c. AFC systems.

AFC offset can cause mixing of absorption and dispersion. This phenomenon is easily demonstrated with the irradiated quartz sample (Wilmad Glass WGSR-01-4) See (Ludowise et al. 1991).

5.5 Flat cells

Since improved S/N is a constant goal in EPR, the operator wants to put as large an aqueous sample in the resonator as possible. Long ago it was shown that this could be achieved by using a flat cell with dimensions empirically determined. The ER 4103TM (TM_{110}) with a large, specially designed flat cell gives a sensitivity about a factor of 4 higher than an ER 4102ST (TE_{102}) cavity. With the optimized flat cell and positioning devices the largest lossy samples can be studied with this cavity. It was observed empirically by Hyde (1972) and by Eaton and Eaton (1977) that rotating the flat cell 90^o - perpendicular to the nodal plane – also yielded high quality results. The perpendicular orientation of the flat cell was originally observed in a Varian cavity, but has been found to often be the preferable orientation for a flat cell in the Bruker ER 4102 ST

cavity. In addition, sandwiches of flat cells worked better than single flat cells. The general principle that breaking up the aqueous sample into smaller portions gives better spectra than one large water sample has been routinely used in our lab since then, and forms the basis for the Bruker "aqua-X" sample holder that consists of many small diameter tubes. Precise positioning of flat cells is facilitated by spring-loaded fine screw sample tube positioning devices sold by Varian and Bruker that screw onto the top and bottom of a cavity resonator.

The expense (and fragility) of commercial quartz flat cells cause many investigators to use capillary tubes for routine studies of aqueous samples at X-band. The rectangular glass capillary tubing we found useful is now available from VitroCom (New Jersey) as "large ratio rectangle tubing" in borosilicate or clear fused quartz. The 0.4 by 8 mm i.d. size is convenient.

5.6 Double-Cavity Simultaneous Reference and Unknown

The use of a double-cavity resonator, made by joining two TE_{102} cavities together might seem to solve some of the problems outlined here, since the frequency will be the same, and if the magnetic field is sufficiently homogeneous over the larger double cavity, the magnetic field will be the same. These features make a double-cavity handy for measuring relative g-values when it is more convenient to have separate reference and unknown samples rather than using concentric or internal standards. However, the perturbation of the microwave field by the sample can result in different magnitude of B_1 at the standard and the unknown. This effect is sketched in the Figure 5-6, which is from Casteleijn et al. (1968). When a Dewar was inserted in one sample port, the field in the other sample port shifted by 1-2 mm. Mazúr et al. (2003) showed that a Dewar in one cavity could reduce the signal from a sample in the other cavity.

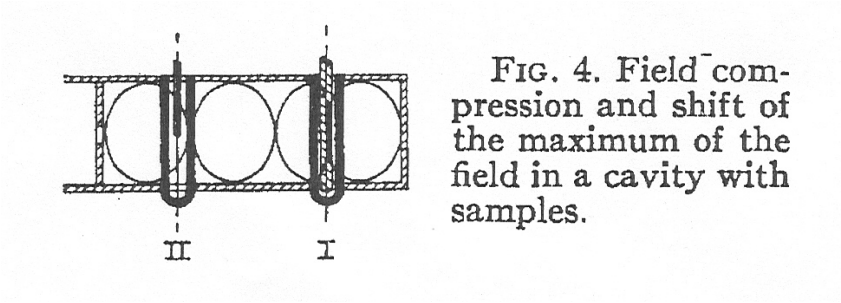

FIG. 4. Field compression and shift of the maximum of the field in a cavity with samples.

Figure 5-6 from Casteleijn et al. (1968).

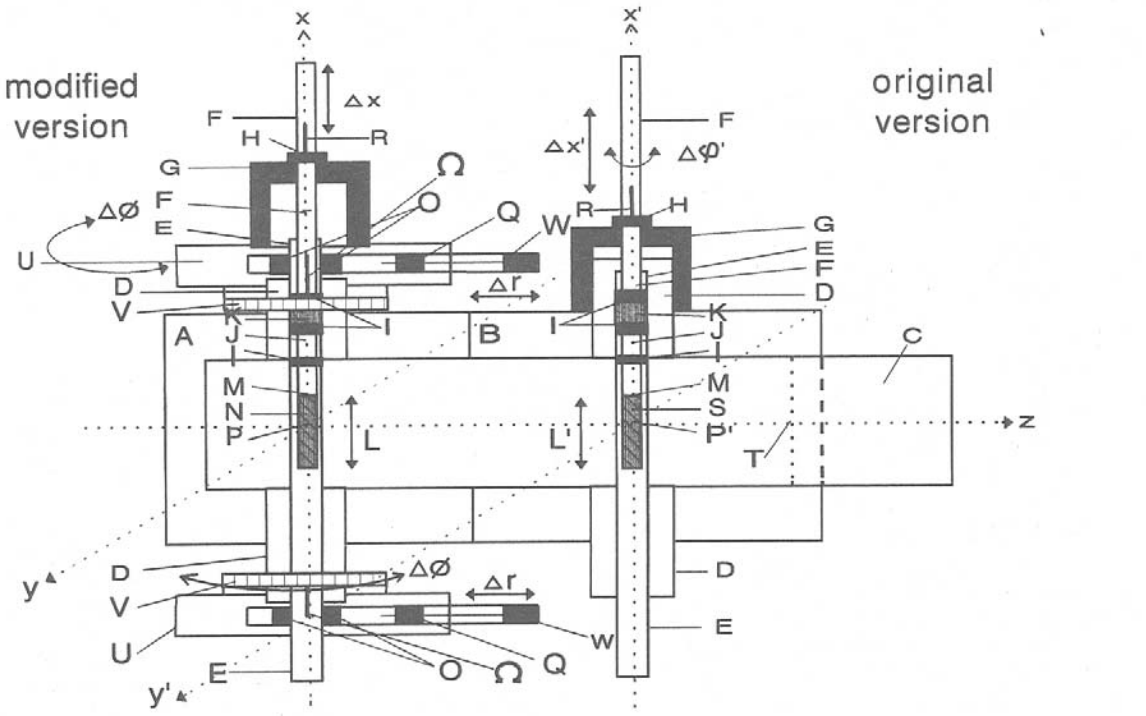

FIG. 1. Schematic diagram of the cross section of the double TE_{104} rectangular cavity with both the new and previous sample tools for quantitative EPR measurements. The modified tool with the ability for precise positioning of the cylindrical sample at various points of the intracavity space is shown in the first cavity (A). The previous sample tool is shown in the second cavity (B), for comparison.

Figure 5-7, from Mazúr et al. (1997b).

5.7 Summary

Absolute determination of the number of spins in a sample has been described as one of the most difficult EPR measurements. (Actually, the same is true of visible spectroscopy. The extinction coefficient reported for DPPH varies by as much as 10%.) Our experience is that very careful end-to-end measurements have to be made of the gain of the spectrometer, and the resonator has to be very carefully characterized (Rinard et al. 2002a; 2002b; 2002c; 2004). The good agreement between calculated and measured signal intensities reported in these papers was the result of an enormous number of measurements characterizing every feature of the spectrometer. Note, for example, that it is difficult to measure gains and losses of many microwave components to better than 1 dB without a very carefully calibrated test bench, but 1 dB error in power ratio has 12% effect on the EPR signal (see Chapter 11 for further discussion of these matters). Consequently, as a practical matter, one compares an "unknown" sample with a "known" sample. The latter should have been prepared using the quantitative methods of an analytical chemistry laboratory. Further, to compare the signals from two samples the equation for the EPR signal tells us that it is essential to know the filling factor, η, the Q, and the power incident on the sample to within the accuracy of the desired result. Because B_1 varies through the resonator, and the magnetic field modulation varies over the resonator, reproducible positioning of the sample in exactly the same size tube is essential. Unless the sample is in the same solvent, in the same size tube, in the same position in the resonator, the Q is not likely to be the same, and would have to be measured by one of the methods given in the 2005 Workshop booklet and discussed in Ch. 6. The equation assumes that both samples are in the linear

response region – that is, that the signal response is strictly linear with B_1 and does not exhibit any microwave power saturation – so it is desirable that the power saturation behavior be characterized for both samples. Although not explicitly stated in the equation, the microwave frequency would have to be the same also. Many of these conditions are difficult to achieve with a high-filling-factor resonator, because in such a resonator the sample has a large effect on the frequency and Q. Therefore, most quantitative EPR studies have been done in cavity resonators, and most carefully characterized of these have been the standard TE_{102} rectangular resonator.

Chapter 6 – Resonator Q

The quality factor, Q, of a resonator has central importance in EPR. Many problems with irreproducibility in EPR intensities within a lab, or among labs, are due to different values of the resonator Q. To perform quantitative comparisons of EPR signals, it is necessary to either measure Q or perform the comparison in such a way that Q is kept substantially constant (same size sample, same dielectric loss properties, same coupling of the resonator).

The standard formula shows that the signal voltage is directly proportional to Q.

$$V_S = \chi'' \eta Q \sqrt{PZ_0}$$

Resonance means that the resonator stores the microwave energy; therefore, at the resonator's resonant frequency, no microwaves will be reflected back for "perfect" coupling of the resonator (called critical coupling). A small amount of microwave power is stored in the resonator. Most of the incident microwave power is dissipated in the resistance of the resonator. Resonators are characterized by their Q, or quality, factor which indicates how efficiently the cavity stores microwave energy. The Q, is defined as:

$$Q = \frac{2\pi \times (\text{Energy Stored})}{\text{Energy Dissipated per Cycle}}$$

where the energy dissipated per cycle is the amount of energy lost during one microwave period. Energy can be lost because the microwaves generate electrical currents in the resonator which in turn generate heat. As Q increases, the sensitivity of the spectrometer increases. We can measure Q factors easily because there is another way of expressing Q:

$$Q = \frac{\nu_{res}}{\Delta\nu}$$

where ν_{res} is the resonant frequency of the cavity and $\Delta\nu$ is the difference in frequency between the two points at which half of the power incident on the resonator is reflected. Broad dips correspond to low Q and narrow dips correspond to high Q.

EPR spectrometers have a mode called "Tune" in which the microwave frequency is swept (abscissa) and the reflected microwaves are detected (ordinate) in order to find the resonant frequency. At the resonant frequency, a "dip" is observed. When a "lossy" sample is inserted into a resonator, the Q decreases. The EPR spectrometer operator will see this effect in the "resonator dip" display on the console as a sample is inserted into the resonator. The dip becomes much broader as a lossy sample (such as an aqueous sample) is inserted. If the sample loss is too high, it will not be possible to critically couple the resonator, and a smaller sample will be required.

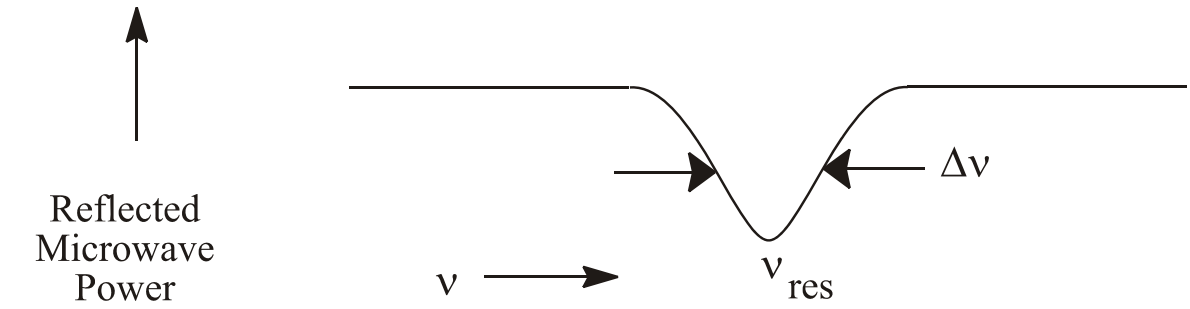

Figure 6-1 Reflected Microwave power from an EPR resonator.

The effect on resonator Q of inserting a lossy sample is shown in the series of snapshots of the tuning mode of the spectrometer.

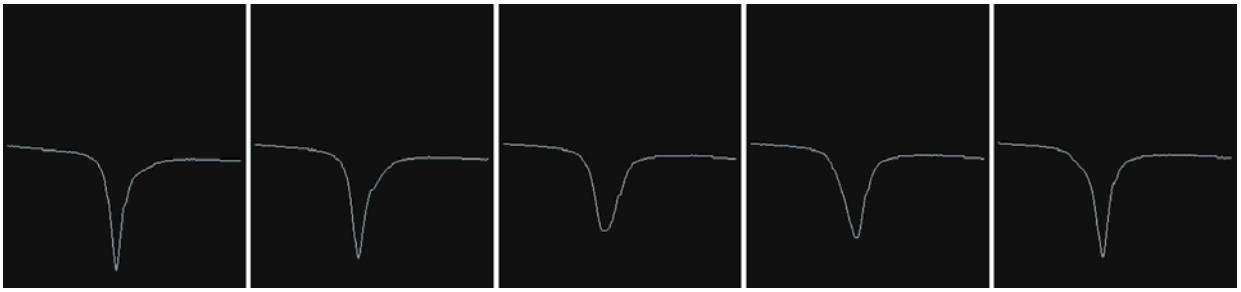

Figure 6-2 Changes in the resonator "dip" due to inserting a lossy sample.

6.1 Conversion Efficiency, C'

It is the B_1 that drives the EPR transition. The EPR intensity grows linearly with B_1 if the spectrum is not saturated (see Figure 3-4). What you can control on your EPR spectrometer is the microwave power. How are these two parameters related?

$$B_1[G] = \frac{C' \cdot \sqrt{P[W]}}{\sqrt{\Delta\nu[MHz]}}$$

P is the microwave power in Watts. Δν is the resonator bandwidth in MHz which has already been mentioned in the discussion of Q. C' is the conversion efficiency. Expressing the conversion efficiency this way, instead of the more common Λ, helps to see the relation to resonator bandwidth.

Increases in the microwave power are costly and contribute only very slowly owing to the square root relationship. Decreasing the bandwidth (increasing the Q) helps, but may have consequences for certain types of experiments or may be dependent on your sample's dielectric properties. The conversion efficiency is the most crucial parameter. It depends on many complicated factors. Optimization of this parameter is one of the most difficult challenges in designing resonators.

A consequence of an electrical engineering principle called "reciprocity" is that the EPR signal detected for a given B_1 is proportional to the conversion efficiency. Since B_1 is also proportional to the conversion efficiency, for a given incident microwave power the EPR signal is proportional to the conversion efficiency squared.

One general rule of thumb is that C' increases as the resonator size decreases. In essence, you are concentrating and focusing more of the microwave power on the sample. For a loop-gap resonator, B_1 is proportional to $1/\sqrt{}$(length times diameter).

It is important in quantitative EPR that B_1 and not the microwave power is the important parameter to use when comparing results from two samples. Just because you have used the same power in the same resonator does not mean B_1 is identical because of the effect of the sample's dielectric properties on the B_1 distribution and on the Q.

For EPR the most useful expression is for what is called the "loaded Q" of a resonator. This term is sometimes used incorrectly in the magnetic resonance literature to mean the Q of a resonator "loaded" with a lossy sample, such as an animal. The electrical engineering definition of 'loaded Q' is the Q of a resonator coupled to a transmission line. The "unloaded Q" – i.e., for the resonator not coupled to a transmission line is twice the loaded Q when the resonator is matched, i.e., critically coupled. Some papers report the unloaded Q, but the loaded Q of the resonator will be one-half of the reported unloaded Q. Sometimes subscripts L and U are used to denote the loaded and unloaded Q values, but since the loaded Q is so commonly used, the L subscript is often omitted. Caution should be exercised in citing Q values unless they are clearly defined.

There are many ways to express the Q of a resonator. Each provides useful insight, so several expressions are provided here (without derivation, which would distract from the primary discussion).

In terms of an RLC circuit, the resonator Q is given by:

$$Q = \frac{\omega_0 L}{R}$$

This is the unloaded Q. The loaded Q will be half of this value when the resonator is critically coupled. Rewriting this equation with the denominator equal to the sum of the resistance of the resonator itself and of the sample, we get:

$$Q = \frac{\omega_0 L}{R + r_{sample}}$$

This equation nicely shows that the lower the resistance of the resonator and of the materials in it (e.g., less lossy sample) the higher the Q. The inductance of a cylindrical resonator is related to the length, z, and the cross sectional area, $A_R = \pi d^2/4$ (d is the diameter of the loop)

$$L = \mu_0 \frac{A_R}{z}$$

Skin depth is $\delta = \sqrt{\frac{\omega \mu_0 \sigma}{2}}$

where σ is the conductivity of the material of the resonator and $\mu_0 = 4\pi x10^{-7}\ T^2J^{-1}m^3$ is the permeability of vacuum

The resistance, including skin effect, of the resonator loop is

$$R = \frac{\pi d}{z}\sqrt{\omega\frac{\mu_0}{2\sigma}}$$

Capacitance can be calculated using:

$$C = \frac{A\varepsilon}{d}$$

A is the area of the plate of the capacitor
d is the distance between plates
ε is the permittivity of the material between the plates of the capacitor. Permittivity is the dielectric constant x ε_0 ($\varepsilon_0 = 8.854 \times 10^{-12}$ F m^{-1})

In EPR resonators, the dielectric in the gap is usually air (or N_2 or He gas during low temperature operation), but it is common to use Teflon in the gap to increase the capacitance and thus lower the frequency of a lumped circuit resonator. The main problem with using a dielectric such as Teflon in the capacitive gap is that its dielectric constant is very temperature dependent.

In actual resonator design one would use modifications of the above formulae that account for edge effects of finite length inductors and finite area capacitors, but the formulae given here give a good approximation,. It is much harder to estimate the capacitance of narrow gaps and specially shaped gaps such as in the Bruker split ring resonator.

Thus, knowing the properties of the materials of the resonator and the size, one can calculate Q (see Poole, 1st edition, page 266). However, it is easier and more accurate to measure Q than to calculate it from first principles. Bruker Xepr measures Q using the bandwidth as shown in the above figure.

6.2 Relation of Q to the EPR Signal

From a classical viewpoint, the EPR signal is a voltage that is generated by spins that are in the xy plane of the resonator (the static magnetic field is in the z direction). For CW EPR, this is often viewed as absorption of microwave energy at resonance increasing the effective resistance in the denominator of the equation for Q given above. This change in resonator Q results in a change in microwave power reflected from the resonator to the detection system, since the resonator is no longer exactly critically coupled. This description reinforces the concept of equivalent resistance in the denominator of the equation for Q, but one should keep in mind that the EPR signal is actually a voltage induced into the resonator by the magnetization of the spin system. This change in reflected power is what is converted into the "EPR spectrum" interpreted by the spectroscopist. Similarly, absorption of microwaves by the "lossy" sample, independent of EPR absorption, is an increase in the resistance term in the denominator of the equation for Q, lowering the Q and hence lowering the EPR signal intensity. For an alternative picture of where the EPR signal comes from, we take a small digression at this point. The picture just given is in terms of "resistive loss" in the sample and resultant change in Q. The microwave power absorbed by the sample creates a net magnetic vector rotating at the Larmor frequency. The magnetic field of the precessing spins produces a voltage in the resonator, and the resultant voltage couples into the transmission line reciprocally to the way the microwaves got to the resonator. Since the fields due to the electron spins are encoded by the field/frequency resonance, the resultant microwave signal at the detector is the EPR signal. Sometimes one speaks in terms

of the currents induced in the conductors of the resonator by the spin magnetic field, but the more general discussion in terms of the fields themselves works for both metallic and dielectric resonators.

6.3 Contributions to Q

There are many contributions to the measured loaded Q, Q_L, of an EPR resonator. They add as reciprocals (Dalal et al. 1981a).

$$\frac{1}{Q_L} = \frac{1}{Q_U} + \frac{1}{Q_\varepsilon} + \frac{1}{Q_r} + \frac{1}{Q_\chi} + \frac{1}{Q_\mu}$$

The contributions to Q include:
Q_U is the unloaded Q, with loss attributable only to the resistance of the walls of the resonator.
Q_ε is the effect of dielectric losses on Q
Q_r is the effect of energy lost through the cavity coupling holes or due to conducting walls less than many skin depths. Q_r is also called the radiation quality factor.
Q_χ is the effect of power absorbed by the sample at resonance (i.e, the EPR signal).
Q_μ is the effect that arises from surface currents in high-conductivity samples, and is proportional to B^2.

For a critically coupled resonator, i.e, one that is perfectly matched to the transmission line, Q_r equals the Q effects of all features internal to the resonator and $1/Q_r$ equals the sum of all other terms on the right hand side of this equation, so we rewrite it as:

$$\frac{0.5}{Q_L} = \frac{1}{Q_U} + \frac{1}{Q_\varepsilon} + \frac{1}{Q_\chi} + \frac{1}{Q_\mu}$$

For low conductivity samples Q_μ can be ignored, and for small samples Q_χ can be ignored, and the equation can be rewritten as

$$\frac{0.5}{Q_L} = \frac{1}{Q_U} + \frac{1}{Q_\varepsilon}$$

which states that the two main effects on Q are the materials of construction of the resonator and dielectric loss in samples placed in the resonator. For the empty resonator, $Q_U = 2Q_L$.

Using the equations for inductance, L, and resistance, R, in the first equation for Q, the equation for loaded Q becomes (Rinard et al.,1999a):

$$Q_L = \frac{d}{8}\sqrt{2\omega_0\mu_0\sigma}$$

from which it is seen that the frequency dependence of Q is proportional to the diameter of the resonator and to the square root of its resonant frequency.

A larger resonator has a higher Q, other things being equal. If the length of the resonator is not changed, the resistance of the walls of the resonator will increase linearly with increase in radius, but L will increase as the square of the radius. Recall that this equation for Q is applicable to a series resonant circuit.

An approximate expression, which has heuristic value, is in terms of resonator volume and surface area times the skin depth, δ, (Alger 1968, page 109):

$$Q \approx \frac{\text{volume of the cavity}}{\delta(\text{surface area of the cavity})}$$

Since dissipation of energy occurs in the surface of the cavity, and more energy can be stored in a larger resonator, this expression makes sense. From this expression it is easy to see that a resonator made of a poorer conductor (e.g., brass or aluminum instead of silver or copper) will have a lower Q.

6.4 Measurement of Resonator Q

Since the measurement of resonator Q is crucial to many EPR studies, we present here some guidance on making such measurements. Different instrumentation and electrical engineering test and measurement support will be available in various laboratories, so we present several options and comment on their use.

The Bruker Xepr and Win Acquisition software provides an estimate of the resonator Q, using the definition in terms of half-power bandwidth. If the Q is very low, or if the off-resonance baseline (full-reflection) is not flat, the computer algorithm will not return as accurate an estimate of Q as for the high-Q case, because the full reflection level is not well-defined. Nevertheless, it is a very useful measure of similarity of samples for quantitative EPR and can be performed conveniently under the exact same conditions as the EPR acquisition.

The following illustration is from the Bruker E500 operator manual. This is a section of the Xepr main window.

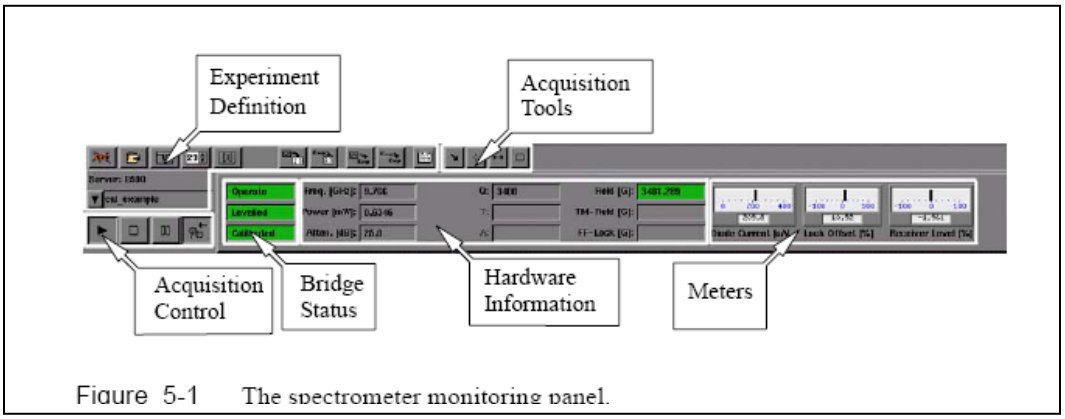

Figure 5-1 The spectrometer monitoring panel.

Q: This displays the approximate Q factor value of the cavity. You need to switch to tune mode and set the Attenuation to 30 dB to read the Q value properly. It is not meant to be an accurate measurement of the Q factor but an estimate.

6.4.1 Measurement of Δω

Varian E-line spectrometers are still being used in some labs, so we tell how fairly accurate measurements of Q can be performed on the E-line bridge.

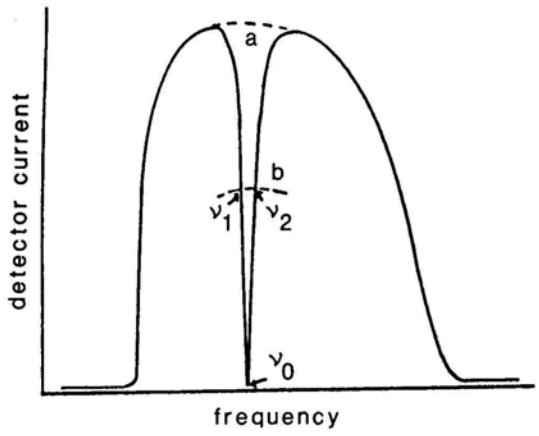

Figure 10. Klystron power mode, showing the "dip" due to cavity absorption. The vertical axis is power (detector current), and the horizontal axis is frequency; a is the detector current off resonance, b is the detector current at half-power, ν_0 is the resonant frequency of the cavity, and $\nu_2 - \nu_1$ is the half-power bandwidth of the cavity. The width of the dip is a measure of cavity Q. The dip should be in the moddle of the power mode to get maximum power from the spectrometer. When the reference arm power is turned on, the display increases in amplitude and the dip does not touch the baseline, since in this case the power from the reference arm adds to the power reflected from the cavity. When the reference arm is on, the symmetry of the power mode with respect to the dip is a measure of the relative phases of the reference arm and the signal arm.

Figure 6-3 is from Dalal et al. (1981a), which presents more details, and Eaton and Eaton (1997). In the Varian spectrometer one can attach a voltmeter to the detector current meter in the bridge to obtain digital readout of the voltages corresponding to the half-power points. A frequency counter is needed to obtain sufficiently accurate $\Delta\omega$ for the calculation of Q.

These measurements are made in the "tune" mode of the spectrometer, with the reference arm off. When the resonator is critically coupled, only a very small amount (essentially negligible) power is reflected at the resonant frequency, ν_0. Thus, this reflected power can be taken as zero, and the half-power points are the half-height frequencies on the power reflection vs. frequency plot shown in the first figure in this section. For a critically coupled resonator, this remains true even if the Q is low. However, if the power measurement is done relative to the off-resonance value, e.g., by moving the resonant frequency by inserting a wire into the resonator and calibrating the voltage detector in terms of power, as in the manual method described above, there can be problems measuring a low-Q resonator. This is because the resonant curve may affect the klystron or Gunn diode power output plot far enough away from resonance that the "baseline, off-resonance" reflected power cannot be measured accurately. The method described here is thus better for higher Q values, for which the accuracy is limited by the accuracy of the half-power frequency measurements.

6.4.2 Q Measurement Using a Network Analyzer – by George A. Rinard

If a network analyzer, such as a HP8753D, is available the resonator Q can be measured accurately. Modern network analyzers have ways to null out the effect of transmission lines to

the resonator. This may result in a measure of Q that is different from that measured for the resonator in a spectrometer. The reason for this is that when a resonator is "critically coupled" in a spectrometer, the operator really is coupling the resonator a bit away from critical coupling. The coupling and the frequency of the resonator are not those for minimum reflection from the resonator, but is offset slightly in frequency and coupling in order to provide a reflection from the resonator to null out leakage through the circulator. In essence, the circulator, transmission line, and resonator are being adjusted as a unit to minimize power at the detector at resonance.

When a resonator is critically coupled, negligible power is reflected at the resonant frequency, but when the resonator is overcoupled (or undercoupled) the power reflected at resonance is appreciable and another method is required to measure the loaded Q for these conditions. The following examples are intended to clarify the method of measuring Q for the case of overcoupled resonators. The problem is that with a strongly overcoupled resonator, the "baseline" of no power absorbed in the resonator may be rather far from the resonant frequency. The solution is to (1) measure the power reflected at resonance, (2) from this determine the input power to the resonator at resonance, (3) divide the resonator input power at resonance by 2, (4) determine what the reflected power will be if half of the input power is reflected, and then (5) measure the (half-power) frequencies at which the reflected power is that calculated in step (4).

For any degree of under or over coupling the Q is still defined by

$$Q = \frac{\nu_0}{\nu_2 - \nu_1}$$

ν_0 is the resonant frequency and ν_1 and ν_2 are the lower and upper half-power frequencies. The network analyzer will probably display frequencies in Hz so we use ν rather than $2\pi\nu$ in this section. Power will also usually be easiest to read in dB, so we use dB in this section.

The above 5 steps can be summarized in a single formula. If the reflected power in dB at resonance is dB_0, then the frequencies ν_1 and ν_2 will be those at which the reflected power in dB is:

$$dB_{hp} = 10\log\left(1 - \frac{1 - 10^{\frac{dB_0}{10}}}{2}\right)$$

It is convenient to calculate expected power levels with a programmable calculator or Mathcad or some other program. Example results are tabulated:

Reflected power at resonance, dB_0	Reflected power at ν_1 and ν_2
-2 dB	-0.886 dB
-20 dB	-2.967 dB
-40 dB	-3.01 dB

As expected, if the coupling results in -20 to -40 or more dB reflected at resonance, then the resonance curve is sharp enough that ν_1 and ν_2 are at 3 dB below the off-resonance reflected power.

6.4.3 Q by Ring Down Following a Pulse

Q can be measured on a pulsed EPR spectrometer. The power ring down following a pulse is a direct measure of resonator Q. This method works better the higher the Q, because for very low Q one usually observes reflections and switching transients interfering with the exponential ring down of the resonator.

Following a pulse, the power delivered by a cavity rings down exponentially:

$$U = U_0 e^{-\omega t / Q}$$

The higher the Q is, the longer the ring down time becomes. This is why resonators are overcoupled to decrease the Q in order to minimize dead time in pulsed EPR experiments. Measuring Q of a very-low-Q resonator or of a strongly overcoupled resonator is a bit more involved. When using ring down after a pulse, miscellaneous reflections in the system may distort the measured power from a pure exponential decay.
Measuring Q of a very-low-Q resonator or of a strongly overcoupled resonator is a bit more involved. When using ring down after a pulse, miscellaneous reflections in the system may distort the measured power from a pure exponential decay.

In this method, set up the spectrometer for a pulsed EPR measurement, which almost always involves overcoupling the resonator. Use a pulse long enough that the transient from the rising edge of the pulse has fully recovered before the end of the pulse. For example, at X-band a pulse length of 80-100 ns is adequate. Using a digital oscilloscope record the shape of the reflected pulse, and fit the recovery following the end of the pulse to a single exponential. For example, on the Bruker E580, use a LeCroy oscilloscope as the transient recorder to record the shape using "random interleaved sampling (RIS). Use Xepr to fit the exponential decay. The time constant for the decay is denoted here as τ. At X-band τ will be of the order of 2-4 ns for a strongly overcoupled resonator.

For a double-balanced mixer (DBM) biased on the LO side to, e.g., ca. 10 mW (+10dBm), as in the Bruker pulse bridge, the output signals are linear in voltage, not power. Some mixers use different power levels, but the key point is that the LO power fully saturates the mixer diodes. For this case, the measurement of Q is:

$$Q_L = \pi\nu\tau$$

where τ is the ring down time constant and ν is the resonator frequency. The ns and GHz cancel conveniently, so it is easy to keep track of orders of magnitude, and for the case of τ = 4 ns at 9.5 GHz, Q = 120.

Home-built pulsed spectrometers often have a crystal to detect reflected pulse shape. For a crystal detector, with the power in the range where the output voltage is less than ca. 15-20 mV, the voltage output is linear in microwave power incident on the crystal.

$$Q_L = 2\pi\nu\tau$$

For background explanation of this method, sometimes called the decrement method, see the text by Ginzton (1957) pages 428-429.

Chapter 7 – Filling Factor

Another factor that is a linear contributor to the EPR signal voltage is the filling factor, η.

$$V_S = \chi'' \eta Q \sqrt{PZ_0}$$

In order to detect an EPR signal, the sample must make a significant perturbation on the properties of the EPR resonator upon fulfilling the conditions for EPR resonance. One simple measure of perturbation size is the ratio of the volume of the sample to the volume of the resonator. Filling factor is actually a bit more complicated than a simple volume ratio. B_1 is not homogeneous in a resonator. The essential factor is the ratio of B_1 squared integrated over the sample volume to B_1 squared integrated over the resonator volume. In non-mathematical terms, B_1 must be large where the sample is. A compromise, however, is to minimize E_1 over the sample.

Abragam (1961, page 83) defines the filling factor as $\eta = V_S/V_C$, the volumes of the sample and coil, and uses this in an expression for the "voltage available at the terminals of the coil."

The concept of filling factor was originated by Bloembergen et al. (1948), and a form of the filling factor for application to pulsed NMR was presented by Bloembergen and Pound (1954). Bloembergen et al. (1948) stated that "The quantity ζ is a filling factor for the circuit determined by the fraction of total r-f magnetic energy that is actually stored in the space occupied by the sample." The filling factor is a correction to account for the fact that only part of the B_1 in the resonator interacts with the sample. The magnetic moment per unit volume is proportional to B_1 in the CW case, so the integral is of B_1^2 over the sample in the CW case, as described in Poole (1967, page 291):

$$\eta = \frac{\int_{\text{sample}} B_1^2 dV}{\int_{\text{cavity}} B_1^2 dV}$$

With fairly uniform B_1 and small samples, this is consistent with Abragam's definition. Bloembergen and Pound (1954) gave an expression for the voltage generated in a resonator, which included a filling factor. Rewriting their expression for signal voltage in SI units for a resonator with one turn (e.g., a LGR) gives the equation:

$$\text{Voltage} = \mu_0 \omega_0 M_0 \eta A$$

where A is the cross section of the resonator.
In this equation the voltage is the maximum value of the sinusoidal FID or ESE signal voltage. M_0 is the magnitude of the spin magnetization. The filling factor, η, was defined by Bloembergen and Pound as

$$\eta = \frac{\int_{\text{sample}} M \cdot \frac{B_1}{i} dV}{M_0 \cdot \int_{\text{resonator}} \frac{B_1}{i} dV}$$

i is the current in the resonator. M and B_1 are not necessarily uniform.

The numerator in the Bloembergen and Pound equation can be related to that in the Poole equation by recognizing that for the small turning angle ($\theta < \pi/2$) appropriate to the CW case, the magnetization in the xy plane is $\propto \sin\theta \propto \theta \propto B_1$, so the integrand in the numerator involves B_1^2. Since M_0 is outside the integral in the denominator in the Bloembergen and Pound equation, the denominator appears to be quite different fromthat in the Poole equation. The denominator of the Bloembergen and Pound equation is the magnetic flux that would link the resonator if the resonator were completely filled with the magnetization M_0. The term $\mu_0 M_0 \eta A$ then represents the magnetic flux that links the resonator if the magnetization over the resonator is as implied by the denominator of the Bloembergen and Pound equation. This would be strictly true only if

$$\mu_0 M_0 \eta A = \int_{\text{sample}} M \cdot \frac{B_1}{i} dV$$

Thus, the use of the filling factor η is an approximation intended to avoid integrating over the sample. The approximation has to be defined for each case consistent with the experiment.

The original source for this concept is the NMR paper by Bloembergen et al. (1948). Another definition, in the context of pulsed NMR, is that the filling factor accounts for the fact that not all B field coming from the sample (e.g., in an FID or echo) will pass through the detection coil. This was presented in many texts only qualitatively, with inhomogeneous B_1 over the sample ignored. Hill and Richards (1968) in the context of pulsed NMR give a voltage S/N in terms of a filling factor η "a measure of the fraction of the coil volume occupied by the sample". They then define η as the ratio of integrals of B_1 squared, as in Poole (1967), although they do not give a reference for the formula. "The factors affecting η are somewhat different for a coil and a cavity. For a sample filling a coil this may be written approximately as

$$\eta = \frac{1}{2}\frac{V_S}{V_C}$$

The factor ½ appears since about half the energy is stored outside the coil." "For a cavity, the filling factor will be about 1 when the cavity is completely filled with sample."

Note that if the B_1 is assumed to be constant over the sample, there is no difference between the integration over B_1 and over B_1^2, and the volume ratio often given for η does not imply one or the other.

In the literature about filling factors, the formulae do not include the fact that only half of the B_1 in the sample is effective in producing an EPR signal. Note that the B_1 calculated from fundamental principles, involving inductance and power, in a conventional resonator is linearly polarized. That is, B_1 fluctuates sinusoidal with stationary components. On the other hand, the magnetization from the spin system is circularly polarized. One can visualize the linearly polarized B_1 as being composed of two circularly polarized components rotating in opposite directions, one in the same direction as the spins and one in the opposite direction. It is easy to see that each one of the circularly polarized components of B_1 has half the intensity as the linearly polarized B_1. Only the component of B_1 rotating in the direction of the spins is effective in producing an EPR signal. Following convention, we use the linearly polarized B_1 in the filling factor calculation, and include the factor of ½ in the calculation of the signal voltage to account for the effect of the circularly polarized B_1 (Chapter 11)

Calculation of the filling factor is complicated because of the variation of the microwave B_1 over the sample. Modern finite element calculations, such as with the Ansoft HFSS software, are required for accurate estimates of the filling factor for a sample and resonator combination.

Table 7-1 presents some approximate calculations of filling factors, some of them performed with Ansoft HFSS. These values are intended to give the operator a rough idea of the magnitudes of filling factors for samples and resonators that approximate common experimental situations.

Table 7-1 Calculated Filling factors

X-band resonator	sample in 4 mm o.d. tube	filling factor
Bruker dielectric	2 mm o.d. by 10 mm long quartz rod	6.2%
Bruker split ring	same	9.5%
Bruker rectangular cavity	same	0.57%

A good rule of thumb is that a standard 4 mm o.d. quartz EPR tube, filled with a low-dielectric constant sample has roughly a 1% filling factor in an X-band TE_{102} cavity resonator, and that a LGR, split ring, or dielectric resonator sized for such a tube will have about an order of magnitude larger filling factor.

Less total sample will be in the LGR, split ring or dielectric resonator, because they are usually not as long as the sensitive volume of the TE_{102} cavity, but the magnetic field modulation over the sample will be more uniform in the smaller resonators. Detailed comparison of the net result on S/N requires finite element calculation of both the B_1 field and the modulation field.

The filling factor for a sample with significant dielectric constant is increased by the effect of the dielectric in the microwave distribution. See Dalal et al. (1981a) and the 2002 Workshop booklet for a discussion of lossy solvents.

As is discussed above, one must also consider the distribution of magnetic field modulation over the sample. Nagy (1994) gave the following formula for the filling factor for a small spherical sample in a rectangular cavity.

$$\eta(\varepsilon', R) = \frac{16\pi R^3}{3V_{cavity}}\left(1 - \frac{k^2R^2}{5}\varepsilon'\right)$$

where R is the radius of the sample, and ε' is the dielectric constant of the sample.
Note that this formula predicts a decrease in η with an increase in either the radius or the dielectric constant, ε'. This is in contrast to the well-known increase in B_1 in a long cylindrical or flat sample in a TE_{102} cavity. Nagy (1994) presented experimental data consistent with the prediction for a spherical sample. Subsequently, Yordanov and Slavov (1996) showed that the intensity of a point sample increases with increase in the wall thickness of a long cylindrical quartz tube.

Attempting to achieve a high filling factor for a particular type of sample is a major incentive for creation of new types of resonators. Much of resonator design is concentrated on optimizing this ratio, the conversion efficiency and minimizing the dielectric losses.

Chapter 8 - Temperature

For many studies it is essential to vary the temperature of the sample. Often, cryogenic temperatures are needed. For example, for pulsed DEER measurements the sample must be rigid. The relaxation times of many metal ions are so fast that the lines are T_1-broadened and it is necessary to lower the temperature to observe narrower line spectra.

8.1 Intensity vs. Temperature

For substances that obey the Curie law, the susceptibility is proportional to 1/T with T in K. This will include almost all species studied by EPR except those that have strong ferromagnetic or antiferromagnetic coupling, or thermally accessible excited states. The relative population of two energy levels, such as the two energy levels of an electron spin in a magnetic field, is given by the Boltzmann distribution function. As is shown in standard texts, the ratio of spins in the high-energy state to those in the low-energy state is:

$$\frac{N_\alpha}{N_\beta} = e^{-\frac{g\beta B}{kT}}$$

Since the population difference is very small, above a few K the difference in populations, which is what we measure in EPR, is $\frac{g\beta B}{2kT}$. Since the energy level differences are very small, at X-band and above 4 K it is a reasonable approximation to say that the spin magnetic moment is

$$M = N\frac{g^2\beta^2 B}{4kT}$$

Hence, relative intensities of signals that are not power saturated can be corrected for the Boltzmann population effect by multiplying by the ratio of the temperatures. The importance of this for quantitative EPR is that in variable temperature studies if all changes in Q, etc., have been accounted for, the EPR integrated intensity multiplied by the absolute temperature should be constant. This is a good check to perform on VT EPR studies. Deviations could be due to violation of the assumption of independent spin behavior, or to partial saturation of some of the spectra.

Large changes in temperature also result in changes in the bulk magnetization. Crippa et al. (1971) reported the temperature dependence of the integrated EPR intensity for DPPH, Varian pitch, and lignite. The ratio of the areas depends on the temperature, because they exhibit different magnetic behaviors.

8.2 Practical Example

A bimodal resonator was used to record the EPR of a dimetal cluster in ribonucleotide reductase with B_1 parallel and perpendicular to the Zeeman field (Pierce et al. 2003). With CuEDTA as a standard to relate spin concentration to intensity of spectra, three species were followed quantitatively during titration with Mn(II). Simulations of X-band and Q-band spectra in perpendicular and parallel modes were used to quantitatively estimate concentrations of metal species in this protein. Since these samples involved cases of spin-spin interaction, the signal intensities did not all follow the Curie law. For a signal that follows the Curie law, the product of temperature times signal intensity will be constant. Figure 8-1 shows that the g = 11.7 and g = 4.6 signals in the $Mn_2^{II}R2$ samples have different temperature dependences, showing that they come from different spin manifolds.

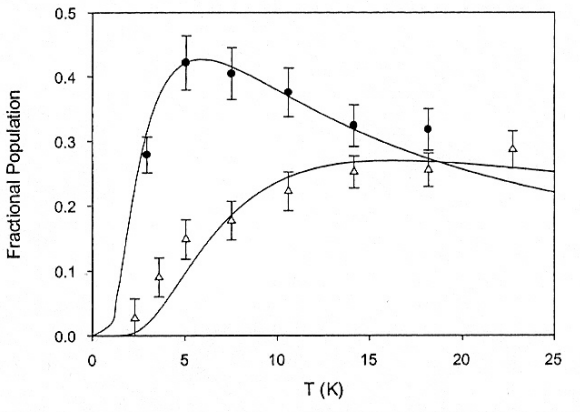

Figure 6. Signal times temperature versus temperature dependence of the $g = 11.7$ (●) and $g = 4.6$ (△) signals. The theoretical curves are the fractional populations of the $S = 1$ and $S = 2$ manifolds for $J = -1.8 \pm 0.3$ cm^{-1} from eq 2.

Figure 8-1 This plot of signal intensities times temperature (T) would be constant (horizontal lines) if the spin system followed the Curie law (intensity proportional to 1/T). The shapes indicate that the signal come from different spin manifolds of the $Mn_2^{II}R2$ site, and that the two Mn(II) are antiferromagnetically coupled. Figure from (Pierce et al. 2003).

Another quantitative EPR study of a high-spin system provided the full energy matrix for S = 7/2 and showed excited state spectra that had maximum amplitude in the 20-50 K range (Hagen et al. 1987).

8.3 Glass-Forming Solvents

Quantitative results cannot be obtained unless the sample does not precipitate or aggregate upon changing the sample temperature. Formation of regions with locally high concentrations can be avoided by using solvents that form glasses rather than crystallizing. It may take some experimentation to find a solvent (usually a mixture) in which the radical remains dissolved and which forms a glass upon cooling. Although there are many reports in the literature of spectra obtained in frozen pure solvents, many such solvents such as toluene and chloroform crystallize. We have seen toluene appear to form a good glass upon initial rapid freezing, but then crystallize during a series of variable temperature spectra. Many mixtures of common solvents reproducibly form glasses. Some convenient (and maybe non-obvious) solvent mixtures are listed in (Drago 1977, page 318) (included in the appendix), and in Zecevic et al. (1998). Solvents in the following list are from (Zecevic et al. 1998) or from unpublished results in our lab, unless otherwise noted.

Various mixtures of alcohols, branched-chain hydrocarbons tend to form glasses when cooled.
Halocarbon oil (-(CF_2-$CFCl)_n$-
o-terphenyl
1,3-bis-(1-naphthyl)-5-(2-napthyl)benzene (Swallen et al. 2006)
19:1 o-terphenyl:decalin
3:1 o-terphenyl:decalin
1:1 o-terphenyl:decalin
9:1 CF_3CH_2OH:ethylene glycol
1:1 cyclotridecanone:cyclooctanone
1:1 water:glycerol
Glycerol

Triethanolamine
Decalin
3:1 iso-octane:$tBuNH_2$
9:1 iPrOH:MeOH
9:1 nPrOH:MeOH
4:1 EtOH:MeOH
95:5 CH_2Cl_2:MeOH (Wada et al. 2006)
2-Me-THF
2,5-Me_2THF
$(nPr)_2O$
6:1 to 1:3 glycerol:nPrOH
1:1 nBuOH:nPrOH
6:1 to 1:3 decalin:3-Me-pentane
3-Me-pentane
Nujol
1:1 anisole:3,4-di-methoxy-benzene
1:1:1 anisole: 3,4-di-methoxy-benzene: 2,5-di-methoxy-benzene
9:1 toluene:THF
2:1 toluene:$CHCl_3$
Xylene:decalin (any ratio)
Mixed tri-methylbenzenes

Various sugars and their derivatives form room-temperature glasses.
Sucrose octaacetate
Trehalose:sucrose (Dashnau et al. 2005)

Ethanol undergoes some change at ca. -150 ^oC that changes relaxation times.
Some solvents tend to break EPR tubes upon temperature changes. Water, of course, is extremely difficult to freeze and thaw in EPR tubes. 4:1 ethanol:glycerol often breaks tubes at about -120 ^oC. Even 1:1 water:glycerol can be a problem because it undergoes a phase transition at about -100 to -90 ^oC, and can break the sample tube if it is warmed slowly through this temperature. We always use medium-wall tubes for solvent mixtures that have a tendency to undergo phase transitions.

Triethanolamine (mp. 21.57 ^oC) forms good glasses when rapidly frozen, but if it is held at ca. 10 ^oC the solution becomes cloudy.

8.4 Practical Aspects of Controlling and Measuring Sample Temperature

The operator needs to be aware that the temperature of the sample is not necessarily the temperature shown on the readout device. In gas-flow systems, there is a temperature gradient over the sample. Consider, for example, that just below the resonator the temperature is, say, 4.2 K or 77K, and a few cm above the resonator the top of the sample tube is at room temperature.

A measurement of the temperature gradient for two cases, -160^oC and 300^oC, when using a nitrogen gas flow over the sample was published in Varian 87-125-514 and is reproduced in Figure 8-2. The gradients shown in the figure are exemplary only, and the actual gradient will

depend on the gas flow rate, the absolute temperature, the sample tube diameter and the Dewar inner diameter. For critical measurements, one should replace the sample tube with another tube of the same diameter that contains a thermocouple at the position of interest, in effect making the calibration of Figure 8-2 for the resonator and gas flow system of interest.

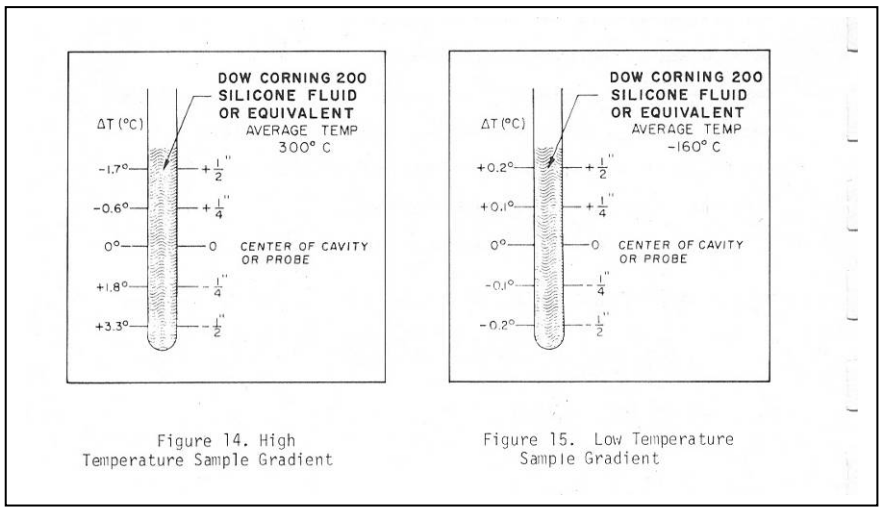

Figure 8-2 Example of the temperature gradient for two cases, -160°C and 300°C, when using a nitrogen gas flow over the sample in a TE_{102} cavity with a quartz Dewar insert. The figure is from the documentation for the E-257/WL-257 variable temperature accessory. Varian 87-125-514 B671.

Some EPR measurements, such as of spin labels in membranes, require much more uniform temperature over the sample. For this, the temperature of the resonator, and not just the sample, has to be controlled. Alaouie and Smirnov (2006) published a method combining fluid-exchange temperature blocks mounted on the walls of a cavity and insulated from the magnet (see Figure 8-3), with which they demonstrated ± 0.033K temperature variation over the sample length.

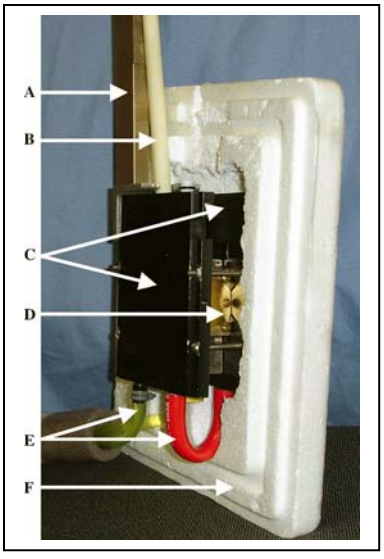

Figure 8-3. Photograph of the NCSU VT probehead assembly for a Varian Xband
TE102-type resonator with a half of the Styrofoam_ insulation removed: (A) X-band waveguide, (B) iris tuning rod, (C) aluminum radiators, (D) front plate of the EPR resonator, (E) connecting tubing for heating/cooling fluid, (F) one of the two Styrofoam_ insulating enclosures. From Alaouie and Smirnov (2006).

Cooling with liquid nitrogen or liquid helium is performed with two very different types of temperature control systems. They are available from various vendors, but for purposes of specificity the Oxford and Bruker products will be mentioned here. The ESR900 style He gas continuous flow system cools the sample, analogous to the nitrogen flow systems used above 77 K. The temperature gradient across the sample can be rather large when using the ESR900. The

temperature increases from ca. 4.2 K to room temperature in a distance of about 30 cm. Our experience is that the actual temperature at the sample depends strongly on He gas flow (more sensitively than can be estimated from the flow meter) and on heater power. Thus, the temperature depends on exact dimensions of the sample tube, other things being constant. The temperature is also sensitive to the pressure in the liquid He Dewar, so it is a good idea to use the bladder provided by Oxford and a Bunsen valve to maintain constant Dewar pressure.

Figure 8-4 Picture of ESR900 cryostat from the Oxford Instruments web site http://www.oxford-instruments.co.uk/wps/wcm/connect/Oxford-+Instruments/Products/Low+Temp+%26+-Magnetic+Sample+Environment/ESR+-Cryostats/ESR+cryostats
The brass spacer in this picture is where the EPR cavity is when the cryostat is installed in the cavity.

Newer ESR900 cryostats contain a thermal ballast (a metal block) that provides a somewhat longer time constant for temperature changes than in the older cryostats that did not have the thermal ballast. Some of the newer transfer lines have larger diameter capillary tubes, which facilitate using N_2 as well as He, since N_2 is more viscous.

The CF935 cryostat is designed for smaller resonators, such as Q-band cavities or dielectric or split-ring FlexLine resonators at X-band and lower frequencies. In these cases, the cold gas can cool the resonator and the sample. There is an OFHP Cu region in the cryostat to create a uniform temperature region, and the temperature gradient over the sample can be negligibly small. However, it may take ca. 15 minutes for the sample temperature to become the same as the temperature of the sensor used in the feedback control circuit for the heater. Ideally, one would have a second temperature sensor very close to or slightly above the sample, and wait until the two sensors agree before taking EPR spectra. We use a Cernox sensor at the position of the resonator. With two calibrated sensors, one near and one below the sample, the temperature uncertainty is reduced to the calibration errors of the sensor when using the CF935. This is a large improvement over the ESR900. However, for X-band cavities it is necessary to use the ESR900, and be aware that temperature may be the limiting uncertainty in your quantitative EPR.

A fundamental difference between these two cryostats is that the ESR900 cools the sample, leaving the cavity at room temperature, and the CF935 cools both the sample and the resonator. Cooling a metal resonator to 77 K decreases the resistance of the metal, and increases the Q of the resonator a factor of 2-3 (Wright et al. 2000, and our observations).

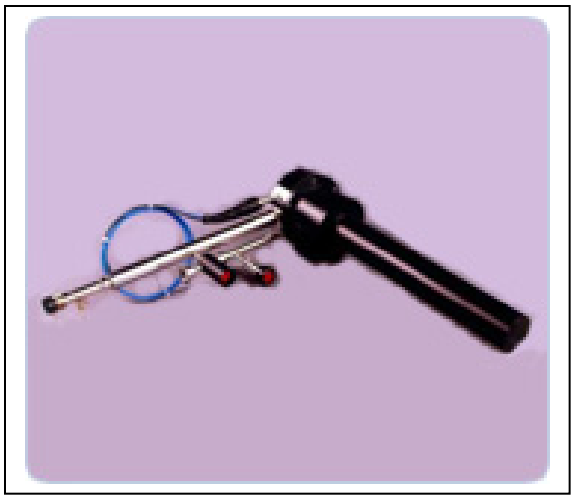

Figure 8-5 Bruker/Oxford CF935 continuous flow cryostat for liquid He and liquid N_2 operation. Picture taken from the Oxford web site.

In addition to the two types of cryostats shown, the full system consists of the storage Dewar (usually a 100-liter Dewar for liquid He), a high-efficiency transfer line, a gas-flow monitor, and a diaphragm pump to pull the gas from the system and expel it either to a recovery system or to the atmosphere. The transfer line and ESR900 or CF935 Dewar have to be evacuated before each use. In labs near sea level, it is usually adequate to pump with a diffusion pump or a turbomolecular pump and close the evacuation port valve prior to use. Because of the construction of the valves, it has been found necessary at high altitude (such as Denver and Colorado Springs!) to continuously pump the cryostat during operation. Bruker has integrated a roughing pump and a turbomolecular pump into a convenient unit for evacuating transfer lines and cryostats (ER4112HV-PMT).

There are many tricks for achieving cryogenic temperatures for EPR measurements. How important some steps are depends on the humidity and altitude of the laboratory. The cryogen flows through a very fine capillary in the transfer line. Humid air in the lab could condense in the capillary and block gas flow. Thus, purge the transfer line and the cryostat with dry gas (He gas is convenient) for a few minutes before inserting the transfer line into the cryogen storage Dewar or the EPR cryostat.

It is extremely easy to set up oscillations in He vapor, resulting in large temperature control oscillations. Mechanical vibrations, such as someone bumping into the storage Dewar or the transfer line can start the oscillations, as can a too-rapid change in a flow-valve setting. When using He, it is best to throttle liquid flow at the storage Dewar rather than gas flow at the input to the diaphragm pump. To stop the oscillations, temporarily cut back on the He flow and/or place the heater in manual mode rather than automatic control mode.

Cooling with liquid N_2 is actually more difficult than cooling with liquid He. Liquid He is cold enough to cryopump imperfectly evacuated transfer lines, but with liquid N_2 residual gases in the vacuum shield can cause substantial heat transfer to the outer walls, resulting in very inefficient cryogen transfer. If the outside of the transfer line gets cold, reevacuate it. Another problem is that N_2 freezes at slightly reduced pressure, so it is easy to block the capillary with frozen N_2 if the differential pressure to too large. Thus, for cooling with N_2, one throttles the flow before the diaphragm pump, rather than at the liquid storage tank, the opposite of the best practice for liquid He.

When performing CW (or pulse) EPR measurements as a function of temperature, close attention should be paid to the changes in T_1 and T_2 as a function of temperature (Eaton and Eaton (2000b)). As a guide, remember that T_1 of a nitroxyl radical is ca. 200 μs at 100 K. T_1 varies roughly as T^2 in the temperature range commonly studied by chemists.

8.5 Operation above room temperature

Operation above ca. 300K requires special attention to the materials of construction of the resonator. The Bruker FlexLine resonator assemblies are designed for low-temperature operation, but not operation above ca. 320 K. Operation with sample temperature controlled up to about 400 K can be performed with cavity resonators with internal Dewar inserts and heated N_2 gas. Higher temperatures require special resonators, such as the Bruker TE_{011} ER4114HT high temperature resonator for 400 -1200 K.

Chapter 9 - Magnetic Field and Microwave Frequency

9.1 g-values

To measure g values you have to know the microwave frequency and the magnetic field well, or make the measurement relative to a standard that is close enough in field that there is little error in the field offset.

Calculation of spin Hamiltonian parameters (refer to the 2006 Workshop on Computation of EPR Parameters and Spectra) results in quantitative comparison of calculated and experimental g values. For example, Drew et al. (2007) used DFT to calculate g values of thiomolybdenyl complexes. The importance of accurate experimental values was highlighted in Drew et al. in the discussion of the results for one compound for which the experimental g values were higher than both the calculated values and the experimental values for similar compounds. Maybe the calculations were more accurate than the experiment.

Stesmans and VanGorp (1989) used an EPR to NMR frequency ratio method to measure the g value of Li-doped LiF as 2.002293 ± 0.000002.

9.2 Microwave Frequency

Get a frequency counter. With a well-calibrated counter, the largest source of error in g-value measurements is the magnetic field measurement. Be sure to note the aging specifications on a frequency counter, and for the most accurate measurements of g values, use a recently calibrated frequency counter. For example, a high-quality commercial frequency counter has a time base aging rate of about 1 ppm per year. Some papers report g values to precisions that may approach the accuracy of the microwave counter.

The resonant microwave frequency usually is changed by inserting the sample in the resonator. This is caused by the dielectric constant (also called the relative permittivity) of the sample. The dielectric properties of the sample are usually higher than that of air, so the frequency decreases upon inserting the sample. One way to understand this effect is to consider the formula for capacitance: $C = \varepsilon_r \varepsilon_0 A/d$ where A is the area of the capacitor and d is the distance between the plates of the capacitor. Clearly, if the dimensions remain the same, the capacitance increases as the dielectric constant (ε_r) increases. Now, combine this with an expression for the frequency of a resonator, $\omega = 1/\sqrt{(LC)}$ where L is the inductance and C is the capacitance of the circuit (the cavity or LGR in this case). Inserting the sample increased C so it decreased the frequency.

9.3 Magnetic Field

The Bruker Hall probe is sufficiently accurate that it can be used as the standard for measurement of the magnetic field at X-band. However, the Hall probe and sample are not in the same place in the magnetic field. The operator needs to calibrate of this offset. The cryostat affects the field offset between the sample position and the Hall probe position, so you have to do the correction with the cryostat in place. The offset can be several gauss. Bruker Xepr includes a function for calibrating this offset so that accurate fields and g values can be read from the spectra. For this purpose it is convenient to use solid DPPH, whose g value is generally quoted as 2.0036 or 2.0037± 0.002 (Wertz and Bolton 1972, page 465) (Weil et al. 1994, page 558). One can also use a sample of known precision g-value such as perylene radical cation. At

other microwave frequencies, a Mn(II) sample is often used, but it is difficult to prepare well-defined and reproducible solid samples with known hyperfine splittings. There have been many attempts to reproducibly prepare a Mn(II) sample with well-defined hyperfine splitting to use as a magnetic field scan standard. However, the Mn(II) hyperfine is so exquisitely sensitive to details of the environment that this has been difficult. Yordanov (1994) tabulated some of the values for Mn in CaO, SrO, and MgO. The lore of the field is that samples usually turn out not to be sufficiently reproducible lab-to-lab to make them useful as a magnetic field scan standard. Bruker provides a calibrated Mn(II) sample. The g-value is 2.0011 and the hyperfine coupling constant A is 86.23 G.

To calculate the magnetic field differences for species with two different g values, g_1 and g_2, use the relation between field and frequency:

$$h\nu = g\beta B$$

$$\beta = \frac{e\hbar}{2m_e} = \frac{\left(1.60218\text{x}10^{-19}\text{C}\right)\left(1.05457\text{x}10^{-34}\text{Js}\right)}{2\left(9.10939\text{x}10^{-33}\text{kg}\right)} = 9.2740\text{x}10^{-24}\text{Cs/kg}$$

These units are the same as JT^{-1}, since C = As, and T = kg s^{-2} A^{-1}

Rearrange this to the form

$$B = \frac{h\nu}{g\beta}$$

For a particular case of X-band spectra (assume, e.g., 9.274 GHz) with $g_1 = 2.0023$ and $g_2 = 2.0123$ we have

$$B_1 = \frac{\left(6.62608\text{x}10^{-34}\text{Js}\right)\left(9\text{x}10^{9}\text{s}^{-1}\right)}{\left(2.0023\right)\left(9.2740\text{x}10^{-24}\text{JT}^{-1}\right)} = 0.32115\text{T}$$

$$B_2 = \frac{\left(6.62608\text{x}10^{-34}\text{Js}\right)\left(9\text{x}10^{9}\text{s}^{-1}\right)}{\left(2.0123\right)\left(9.2740\text{x}10^{-24}\text{JT}^{-1}\right)} = 0.31955\text{T}$$

In the more common units of G (1G = 10^{-4} T) $B_1 - B_2 = 16$ G.

9.4 Magnetic Field Homogeneity

The magnetic field homogeneity depends on the magnet diameter and spacing between the poles, so the homogeneous volume is greater for a 10-inch (25 cm) magnet than for a 6-inch magnet. The specification for a 10-inch Bruker magnet is 13 mG in a cylindrical volume 15 mm diameter and 15 mm long. The homogeneity is also achieved and specified only at one magnetic field, because it depends on the degree of saturation of the iron in the magnet pole faces. Since narrow EPR lines and high-resolution spin-spin splitting is usually observed only very close to g = 2, the resolution of the magnetic field is specified at ca. 3400 G for an X-band EPR spectrometer. Magnetic field homogeneity is relevant only over the size of the sample, and at X-band the 3-cm wavelength results in most signal intensity coming from about 1 cm length of sample.

Hysteresis and homogeneity: it is best to saturate the magnet before performing sweeps for very precise measurements. This means that the operator should increase the magnetic field to close to the maximum value achievable with the magnet and power supply combination (limited by the power supply, but for a Bruker 10 inch magnet one might strive for ca. 14 kG), and then reduce the field to the value about which one wants to make accurate field scans.

A good test of the magnetic field homogeneity is to record the CW spectrum of a narrow line signal. One that is commonly used is 50 μM perylene (Aldrich 394475) in sulfuric acid. Bubble with N_2 to remove O_2, and seal in a 0.6 mm i.d. capillary tube. This sample will last a few months at room temperature, so it should be kept cold when not in use. The line widths should be ca. 50 mG. Increases in line width imply magnetic field inhomogeneities of that amount over the length of the sample.

Sweep speed is limited by the physics of electromagnets, and especially by the limitations of iron-core electromagnets. The Xepr software display shows the field position with a red background when the scan speed is too fast for accurate field setting and hence there is an effect on recorded line positions. However, the error in line positions occurs before the red light comes on. About 81 ms conversion time is OK, but faster may cause problems with some wide field sweeps.

When a large magnetic field scan is completed, and the field returns to low field, it could take several seconds to settle to the low-field starting point. If the scan is restarted without waiting for the field to settle, it is possible for false peaks to occur at low field because the field is still sweeping down while the command (and the field scan axis of the recorded spectra) is for increasing magnetic field. Consequently, for signal averaging of spectra over many thousands of gauss, it is necessary to input a waiting time of 5-7 seconds between scans in Xepr.

9.5 Coupling Constants vs. Hyperfine Splittings

The hyperfine coupling constants are characteristics of the paramagnetic species. The experimental hyperfine splittings are approximations to the coupling constants. One has to simulate the spectra to obtain accurate coupling constants, especially at frequencies below X-band or for very large hyperfine couplings, because of the Breit-Rabi effect.

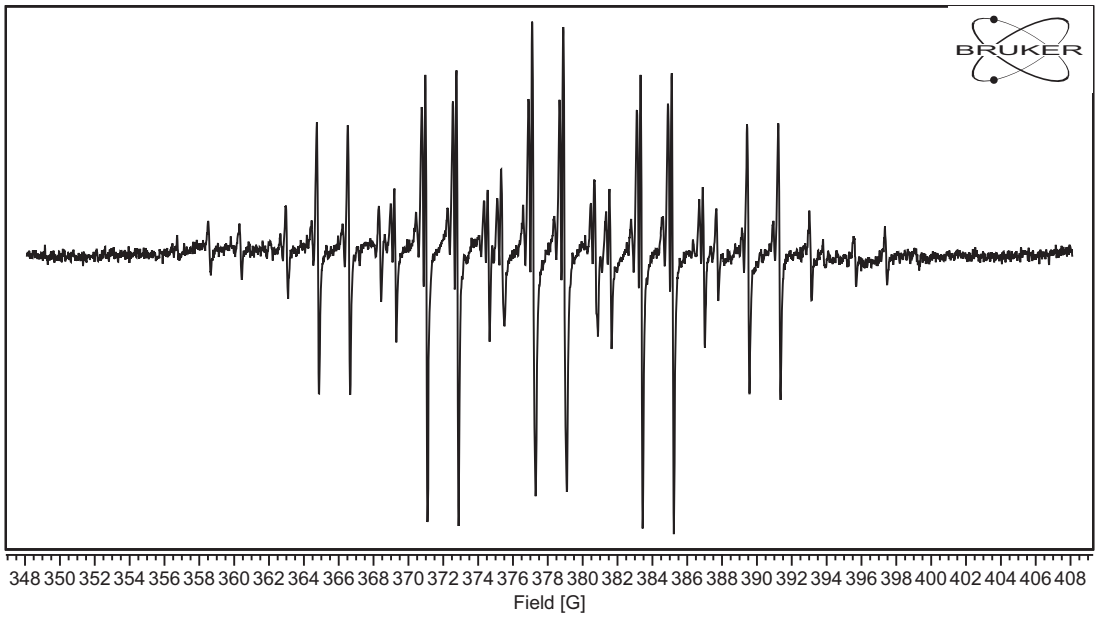

Figure 9-1 Hyperfine splitting of the PNT radical at L-band, exhibiting Breit-Rabi shifts.

Chapter 10 – Standard Samples

10.1 Comparison with a Standard Sample

Absolute quantitation of EPR intensity is very difficult. In most cases, the spectrum of an unknown is compared with the spectrum of a known sample. Many samples proposed as standards for various purposes were discussed in Poole (1967, pages 589-595), Wertz and Bolton (1972, page 462-466); Weil et al. (1994, page 558-562), and Eaton and Eaton (1980).

Extensive discussions of the problem of performing quantitative EPR measurements have provided detailed examination of the issues listed above and have included a focus on the problem of selecting an appropriate reference sample (Auteri et al. 1994; Christova 1994; Czoch 1996; Dyrek et al. 1990; 1994; 1996; Nagy and Placek 1992; Nagy 1994; 1997; Siebert et al. 1994; Nagy et al. 1997a; 1997b; Nagy and Sokolov 1997; Yordanov 1996; Yordanov and Christova 1997; Yordanov and Genova 1997; Yordanov et al. 1999).

Since DPPH has been used as a g-value marker, there has been much discussion of it as a standard also for signal intensity. However, the properties of DPPH depend strongly on the solvent from which it was crystallized (Yordanov 1996; Kolaczkowski et al. 1999), the purity of commercial samples varies, and the stability both as a solid and in solution is less than is needed for an intensity standard (Yordanov and Christova 1994; Yordanov and Christova 1997; Yordanov and Genova 1997). Although DPPH is reasonably stable as the solid, in solution the stability is strongly dependent on the solvent, as reported by Slangen (1970), being much more stable in acetonitrile solution than in toluene solution. The solutions were not de-aerated and were stored in daylight. Yordanov (1996) and Yordanov and Christova (1997) summarized prior literature on stability and molar absorptivity of DPPH and reported a value of 12350±650 l M^{-1} cm^{-1} at 520 nm as a molar absorptivity in ethanol to use to determine the purity of a sample of DPPH.

For transition metal samples, S = ½ Cu(II) and S = 5/2 Mn(II) are commonly used. $MnSO_4 \cdot H_2O$ is available with 99% purity. However, it is somewhat efflorescent, so uncertainty in the degree of hydration could cause uncertainties in spin quantitation. Yordanov and Ivanova (1994b) documented some of the problems with Mn(II) standards. It might be more practical for EPR labs to purchase analytical standard solutions such as Alfa Specpure standards. Some labs try to use $CuSO_4 \cdot 5H_2O$ as a standard, but it is very difficult to prepare it and to store it in an atmosphere of the proper relative humidity to assure that it is really the penta-hydrate. $CuCl_2 \cdot 2H_2O$ has also been cited as a primary standard, but its degree of hydration also depends strongly on the relative humidity of the air in which it is stored. We think that it is better for the most accurate work to dissolve a weighed amount of Cu metal to use as a standard. For non-aqueous samples, compounds of the highest available purity should be used, and for the most accurate results they should be analyzed for metal content.

$VOSO_4 \cdot nH_2O$ also has variable number of waters of hydration, so Dyrek et al. (1990) titrated with $KMnO_4$ in the usual volumetric analysis method to determine the V(IV) content. The compound was used as the solid, and in some cases ground with NaCl or KCl. Dyrek et al. (1994; 1996) found that the choice of diamagnetic diluent for a standard was not simple, and that the main problem is achieving a homogeneous distribution of paramagnetic component in the

diamagnetic diluent. Grinding samples together to try to get a more homogeneous standard sometimes results in chemical reactions that change the EPR spectra. The grinding process itself can produce radicals (Urbanski 1967; More et al. 1980; Adem et al. 1993; Tipikin et al. 1993; 1997). For example, Dyrek et al. (1996) observed that the $CuSO_4$ EPR spectrum changed when it was ground with NaCl, but not when ground with SiO_2 which had been pulverized before the two were ground together. Traces of water in the materials changed a $VOSO_4/K_2SO_4$ sample that was sealed in a quartz tube for a few weeks. The line shape changed, but the integrated intensity did not change. Drying over P_2O_5 resulted in samples that were stable for five years. In spite of sample preparation difficulties, Dyrek et al. (1994) concluded that preparation and measurement of the standard contributed only about 2% error to the overall quantitation of EPR spectra of metals.

Nitroxyl radicals can be obtained in sufficient purity that they can be used as quantitative standards for concentrations of organic radicals in fluid and frozen solutions. Nitroxyl radicals can be selected for solubility in the solvent of interest (ranging from toluene to water) so that the dielectric properties of the known and unknown samples can be matched. We have found that commercial tempol is purer and easier to handle than tempone, since it is a higher-melting more crystalline solid, and it is soluble in both water and alcohols.

As an internal standard for samples to be irradiated, Yordanov et al. (1999) suggest Mn(II) doped into MgO. They concluded that pyrolyzed sucrose and Mn(II) in CaO were less suitable. Irradiation of CaO induced EPR signals that could interfere with measurements of organic radicals, such as in alanine. There was no observable change in the intensity of the EPR signal in pyrolyzed sucrose upon irradiation, but the EPR signal of this material would overlap organic radical signals.

Even an internal standard for relative measurements has uncertainties due to problems of uniform mixing and hence distribution in the sample tube relative to B_1 and modulation field distributions, and hence relative to the sample whose intensity is to be measured.

Attention has to be paid to relaxation times of the samples, especially when quantitating frozen solutions (Eaton and Eaton 2000b).

Note that weak pitch is a spectrometer performance standard, not an intensity standard. The derivative signal amplitude is calibrated under the stated spectrometer conditions for the "weak pitch S/N" test. The integrated area (total signal intensity) is not calibrated. Glarum and Marshall (1970) used a nitroxyl radical to calibrate pitch samples.

The comparison of intensities requires consideration of the spin, since intensity is proportional to S(S+1) (Carrington and Luckhurst 1964).

The importance of careful consideration of transition probabilities for comparison of EPR spectra when the sample and standard differ significantly was demonstrated by Siebert et al. (1994). Chromium in FeS_2 and in $AlCl_3 \cdot 6H_2O$ was measured by EPR and by ICPMS and AAS, with good agreement between methods.

The National Bureau of Standards (now NIST) produced an EPR standard sample using Cr^{3+} in Al_2O_3 in 1978, which some labs still have (Standard Reference Material 2601; Chang et al. (1978)).

Nagy and coworkers discussed choosing reference samples for EPR concentration measurements (Nagy 1997; Nagy et al. 1997a; 1997b; Nagy and Sokolov 1997). The focus was on transition intensity factors obtained by diagonalization of spin Hamiltonian matrices, in order to facilitate comparison of the intensity of e.g., one S = 1 species with the intensity of a different S = 1 center. Specific reference samples were not proposed in these papers.

Cordischi et al. (1999) compared a large series of compounds as possible primary standards for quantitative EPR of S = 1/2, 3/2, and 5/2 species. The S = ½ species (listed in Table 10-1) and S = 5/2 $MnSO_4 \cdot H_2O$ were reliable standards, but "none of the pure Cr^{3+} compounds proved useful as primary standards because of their large fine structure terms or high Néel temperature that invalidated the simple Curie law." Among the Cr compounds tested were $KCr(SO_4)_2 \cdot 12H_2O$, $Cr(acac)_2$, and $(NH_4)_3[CrMo_6O_{24}H_6] \cdot 7H_2O$.

K_3CrO_8 (Dalal et al. 1981b; Cage et al. 1998) has g = 1.97, which is far enough from many organic radical spectra that both can be measured at the same time, which is an aid to reducing uncertainties due to resonator Q, etc.

In all cases, it is important to pay attention to all of the parameters discussed in this booklet as being relevant to quantitative EPR. One anecdote may help one to remember this lesson. There is a paper in the literature, which we will not cite here, in which a small crystal of $CuSO_4 \cdot 5H_2O$, properly prepared, was used as an intensity standard to measure the number of spins in an aqueous protein sample at room temperature, without paying any attention to the differences in resonator Q or B_1 and modulation amplitude distributions for the two samples.

Table 10-1 EPR Intensity and g-Value Standards

Standard	Intensity	g-value	Hyperfine splitting	Reference
DPPH		2.0037 ± 0.0002		(Weil and Anderson 1965)
DPPH	no	2.0036 ± 0.0001		(Yordanov 1996)
DPPH	X			(Cordischi et al. 1999)
Bruker or Varian strong pitch	±10%	2.0028		
Wurster's blue perchlorate		2.00305 ± 0.00002	table of values	(Randolph 1972) p. 98-101
Perylene cation in 98% H_2SO_4		2.00258 ± 0.00002		(Segal et al. 1965)
Tetracene cation in 98% H_2SO_4		2.00260 ± 0.00002		(Segal et al. 1965)

p-benzosemiquinone in butanol-KOH at 290K		2.004679 ± 0.0000129		(Yordanov 1994)
Naphthalene anion radical		2.002757 ± 0.0000006		(Yordanov 1994)
Fremy's salt $K_2NO(SO_3)_2$	X	g = 2.0057	26.182 G between the outer lines	(Randolph 1972) p. 100 and (Yordanov 1994)
Quinhydrone at pH 7.2	X			(Narni et al. 1966)
K_3CrO_8	X	1.97		(Dalal et al. 1981b; Cage et al. 1998)
$CuSO_4 \cdot 5H_2O$	X	$g_1 = 2.27$, $g_2 = 2.08$		(Yordanov 1994)
$CuSO_4 \cdot 5H_2O$ solid Aqueous solution	X	$g_1 = 2.09$, $g_2 = 2.23$, $g_3 = 2.27$ g = 2.18		(Cordischi et al. 1999)
$Cu(acac)_2$ solid or in toluene solution	X	g = 2.13 g = 2.126	A = 78 G	(Cordischi et al. 1999)
Cu metal dissolved in acid	X			Eaton lab
Cr^{3+} in Al_2O_3	X			(Chang et al. 1978)
Mn(II) doped into MgO	X			(Yordanov et al. 1999)
$MnSO_4 \cdot xH_2O$	X	g = 2.0023		(Yordanov 1994)
Tempo	X			(Cordischi et al. 1999)
Tempone	X			
Tempol	X			
3-trimethylamino-methyl-2,2,5,5-tetramethyl-1-pyrrolidinyloxyl iodide	X			Gerald Rosen
3-carbamoyl-2,2,5,5-tetramethylpyrrolinyloxyl	X			
3-carbamoyl-2,2,5,5-tetramethylpyrrolidinyloxyl	X			(Towell and Kalyanaraman 1991)
$VOSO_4 \cdot nH_2O$	X			(Dyrek et al. 1990)
$VOSO_4 \cdot 5H_2O$	X	g = 1.99		(Cordischi et

				al. 1999)
$VO(acac)_2$	X	g = 2.00		(Cordischi et al. 1999)
VOTPP (tetraphenyl porphyrin)	X	g = 1.958	A = 183 G	(Cordischi et al. 1999)
Vanadyl and copper sulfate	X			(Dyrek et al. 1994)
fusinite	X			(Auteri et al. 1994)
$MnSO_4$	X			(Yordanov 1994)
$Cu(diethyldithiocarbamate)_2$	X			(Yordanov 1994)
Pyrolyzed sucrose or dextrose	X	g = 2.0028		(Yordanov 1994)
Ultramarine blue	X	g = 2.0294		(Yordanov 1994)
F-centers in LiF	X			(Yordanov 1994)
Irradiated sucrose				(Yordanov 1994)
γ-irradiated quartz				(Yordanov 1994)
γ-irradiated alanine	X			

10.2 Standard Samples for Q-band

Although in principle any of the standards discussed above could be used for Q-band, each of the problems with sample preparation is much more severe at Q-band (or higher frequency). For example, homogenous distribution of a paramagnetic solid in a diamagnetic host by grinding samples together is very difficult and in a 1 mm o.d. tube the placement of one particle could make a large difference in signal intensity. Atmospheric oxygen (O_2) is a reasonable test of spectrometer performance, but strange problems can occur. For example, when Varian installed a Q-band bridge in our lab in the mid-1970s, the performance test on the amplitude of a line in the gaseous O_2 spectrum of normal air did not meet specification. We were all puzzled until we realized that in mile-high Denver the O_2 concentration is lower than at the sea-level factory where the test was performed by Varian. The lower overall atmospheric pressure causes line width changes as well as amplitude changes. This illustrates the kind of unanticipated problem one can have with a "standard."

As we discussed in our review of standards several years ago (Eaton and Eaton 1980), the primary question is what aspect of performance do you want to measure? Weak pitch has served as an overall spectrometer performance standard, attempting to gather all aspects of performance into one number. Weak pitch, because it is so commonly used at X-band, remains a possibility for Q-band. However, the smaller size tube at Q-band is likely to make the pitch sample preparation cost even greater than at X-band. If you move away from a direct comparison with X-band pitch, and simply want to measure sensitivity in spins per gauss, then the sample

preparation could become less expensive. One approach would be to use pitch or some other carbonaceous radical with a transfer calibration, avoiding the many heating and evacuation steps. There are commercially available carbons, which you could buy in large quantity, dilute as with weak pitch, and simply seal under vacuum without the time-consuming attempt to make a reproducible pitch signal.

Another approach is to seek some other type of sample, such as irradiated alanine. Alanine has some problems as a standard, as is revealed by the long-term task that the international community, including Bruker, has been engaged in to obtain reproducible quantitation of radicals in alanine. The relaxation times of the irradiated alanine sample, are too long to get slow passage spectra at 100 KHz modulation and high power, and there are changes in relative intensities of lines as the power is changed. By selecting a reproducible set of conditions, you can get reproducible spin count, but it is not an optimal sample to use. Alanine is reasonably stable, and the dose and time-dependence has been studied by many groups, especially the lab of Dieter Regula in Munich.

A sample of a persistent nitroxyl radical doped into a diamagnetic solid would be a fairly inexpensive standard sample. We have studied the radical whose trivial name is Tempol doped into the diamagnetic amine analog (Eaton et al. 2001). This spectrum is quite broad, but is a realistic representative of the type of spectrum users might be concerned with.

If the purpose were to monitor background signals, or stability at high modulation amplitudes, or AFC performance, different samples and protocols would be used. Cu doped into Zn diethyldithiocarbamate would be an inexpensive reproducible sample that would test baseline stability and background signals as well as sensitivity. The signal in irradiated fused SiO_2 is a very good measure of AFC performance (Eaton and Eaton, 1993), because it is so sensitive to the mixing of absorption and dispersion contributions (see Figure 3-17 in Chapter 3).

None of these suggestions address the aqueous samples that are of intense interest to many users of Q-band EPR for spin labeling. For this purpose you could seal degassed aqueous solutions of nitroxyl radicals in quartz tubes of the appropriate diameter. This is harder to prepare than a sample of a solid, but more meaningful to many users. In our experience, samples of degassed nitroxyl radicals in reasonably pure toluene solution last for many years, but we have not done quantitative studies as a function of time, and we do not have comparable experience for aqueous solutions.

10.3 Achievable Accuracy and Precision – g Value and Hyperfine Splitting

Older spectrometers – e.g., ER200 and ESP300 could do 4096 steps in the field axis, using a 12 bit digitizer. The Elexsys and EMX spectrometers have 12 bit magnetic field resolution (4096 steps). The EMX-Plus and EMX Micro have 24 bit magnetic field axis digital resolution. The accuracy of the field is determined by the Hall probe. Bruker Hall probes are individually calibrated with the field controller. The NMR Teslameter is somewhat more accurate. For normal EPR line widths, either of these, when the offset discussed above is calibrated, serve as an accurate parameter in g-value and hyperfine measurements.

For the most accurate g value measurements, the operator has to be aware of many subtle small effects, such as are well-described in Segal et al. (1965). For example, it was shown that the magnetic field inside a standard brass EPR cavity is not exactly reproducible when the field outside the cavity is reproduced exactly. A few g values have been measured to high accuracy (see table in Weil et al. (1994, page 558), and Table 10-1). Awareness of the uncertainties of measuring both magnetic field and microwave frequency should caution against reporting any g factor to more than 5 significant figures unless the species of interest was measured simultaneously (e.g., one in a capillary inside the sample tube) with one of the radicals for which the g factor has been measured accurately. For routine g-value measurements, it is handy to attach a speck of DPPH to the outside of a sample tube using tape such as "Scotch" brand transparent tape. Over a long period of time the DPPH partially dissolves and the signal broadens, but for the time of individual measurements this works well to make g value measurements to the accuracy of that of DPPH (± 0.0002).

Chapter 11 - How Good Can It Get? - Absolute EPR Signal Intensities

Throughout this discussion, it has been inherent that the better the S/N, the better the quantitative accuracy possible. The question, then, is what S/N can EPR aspire to? The first quantitative EPR performance criterion was a weak pitch S/N = 20 on the Varian V4502. We have come a long way since then. The S/N for weak pitch under comparable conditions in a TE_{102} cavity has improved roughly linearly in time.

Why did we not start this discussion with a measurement of the absolute EPR signal intensity? Hyde's 1962 statement (as reported by Alger (1968, page 200)) that "of all the measurements one can make with EPR equipment, the determination of absolute spin concentration is the most difficult" remains true 45 years later. In this section we present the background needed to estimate the ultimate sensitivity of spectrometers, and cite papers that illustrate the state of the art in absolute concentration measurements. One task is to measure the "resonator to computer" voltage gain of the spectrometer (Rinard et al. 1999c; 2002b; 2004). In the following discussion we show how to estimate the sensitivity of a perfect spectrometer with known resonator Q, etc., and how real losses and active components prevent achieving this ideal (Eaton et al. 1998; Rinard et al. 1999a; 1999b; 1999c; 2002a; 2002b; 2004).

In prior chapters we have expressed the EPR signal in the form:

$$V_S = \chi'' \eta Q \sqrt{PZ_0}$$

Now, in order to calculate the S/N, we need to define a bit more carefully the way we use χ'', η, and P. Experimentally, the S/N measurement is a ratio of the maximum signal amplitude to the rms noise. In the calculations that follow, the estimate of the ultimate achievable S/N includes a calculation of the thermal noise power. The resultant noise voltage is an rms value, which is appropriate for the denominator of the S/N calculation. Note that the equation for V_s also is expressed in terms of microwave power, so this would yield an rms value for B_1, but we want a peak value, not rms, so we need to multiply by $\sqrt{2}$. As discussed in Chapter 7, the filling factor calculation uses the linearly polarized B_1, but only the circularly polarized component creates the EPR signal. As explained in more detail below, to reduce confusion we include the ½ explicitly in the calculation of V_s, rather than in the calculation of η. The net result of these two factors is that we divide the expression for V_s by $\sqrt{2}$. The third term to discuss is the spin susceptibility. Ideally, one would use the full line shape function, and the fraction that is detected in the CW measurement, in the calculation. In this chapter, we will approximate this by using the expressions from Weil and Bolton for line shapes (pages 539 ff). We will assume a Gaussian line shape, and we assume that the modulation amplitude will be approximately equal to the line width, so that the entire sample magnetization will be measured. We also assume no power saturation of the spin system.

Here we provide more detailed discussion of the multiplicative factor of ½ to account for the fact that only one of the circularly polarized components of B_1 affects the spin magnetization, so that only half of the B_1 calculated from the incident power is used. One might think that the B_1 for the sample in the equation for filling factor should be multiplied by ½; however, this would be equivalent to reducing the efficiency of the resonator by ½ and this is not the case. The effect of

circular polarization is similar to the effect of reducing the source power so that B_1 has half its previous value and we can see that this would reduce the EPR signal by a factor of ½, not ½ squared. Therefore, to reduce confusion, we place the ½ factor in the equation for V_s instead of in the equation for η.

11.1 The Spin Magnetization M for an Arbitrary Spin S – Definitions:

The spin magnetization is $M_0 = H_0\chi_0 = \frac{B_0}{\mu_0}\chi_0$.

One also finds this written as $M = \chi_0 B_0$.

Therefore,

$$M_0 = N_0 \frac{\gamma^2\hbar^2 B_0 S(S+1)}{3k_B T} \quad JT^{-1}m^{-3} \ (= Am^{-1}),$$ so M/H is unitless, as required.

For S = ½, $$M_0 = N_0 \frac{\gamma^2\hbar^2 B_0}{4k_B T} = N_0 \frac{g^2\beta^2 B_0}{4k_B T_{sample}}$$

Definitions and units in these equations:

$g\beta = \gamma\hbar$

$\gamma = 1.7608\text{x}10^{7}$ rad s^{-1} G^{-1}

$\hbar = 1.0546\text{x}10^{-27}$ erg s rad^{-1}

N_0 is the number of spins per unit volume. In some of our publications, the number of spins per unit volume is split into two terms, N, the number of spins in volume V, and V is the volume of sample in m^3.

The static magnetic field $B_0 = \omega_0/\gamma$

S is the electron spin, which will be ½ in all of our calculations.

$k_B = 1.3806\text{x}10^{-16}$ erg K^{-1} is Boltzmann's constant.

T is the temperature of the sample in K.

The permeability of vacuum, $\mu_0 = 4\pi\text{x}10^{-7}$ $T^2J^{-1}m^3$.

The magnetic susceptibility of the sample, χ'' (dimensionless), is the imaginary component of the effective RF susceptibility. We will assume that the line is Gaussian, which is a reasonable approximation for a nitroxyl or weak pitch sample, since there are unresolved hyperfine interactions. The assumption makes the calculation simpler than using a more realistic line shape function.

For a Lorentzian line, with width at half height = $\Delta\omega$ at resonance frequency, ω,

$\chi'' = \chi_0 \frac{\omega}{\Delta\omega}$, where $\Delta\omega$ is the line width.

This formula requires use of the absorption line width, so multiply the peak-to-peak derivative width by $\sqrt{3}$.

At X-band, for ca. 9.4 GHz, B_0 = ca. 3360G = 0.336 T

To get units right in these calculations we have to use the relation (from Wertz and Bolton 1st ed. page 9) that the units of gauss are $\frac{erg}{G\,cm^3}$, and convert to SI units.

Thus, we will use the susceptibility formula in the following form:

$$\chi'' = \chi_0 \frac{\omega}{\Delta\omega} = \frac{N_0 \gamma^2 \hbar^2 \mu_0}{4 k_B T} \frac{\omega}{\Delta\omega}$$

Units for this equation are $\frac{\text{rad s}^{-1}}{\text{G rad s}^{-1}\ \text{G}^{-1}} \frac{\text{m}^{-3}\left(\text{s}^{-1}\text{T}^{-1}\right)^2 (\text{Js})^2 \left(\text{T}^2\text{J}^{-1}\text{m}^3\right)}{\text{JK}^{-1}\text{K}} = \text{unitless}$

It will be convenient to gather all terms that are not specific to a particular sample to simplify multiple calculations.

$$\chi'' = \frac{N\omega}{\Delta\omega} \frac{\left(1.76\text{x}10^{11}\right)^2 \left(1.0546\text{x}10^{-34}\right)^2 \left(4\pi\text{x}10^{-7}\right)}{4\left(1.38\text{x}10^{-23}\right)(295)} = 2.66\text{x}10^{-32} \frac{N\omega}{\Delta\omega}$$

N has units of spins per cubic meter, and frequency and line width are both either Hz or G. For this example we assume room temperature. If the line width does not change and the signal does not saturate, the sensitivity decreases inversely proportional to the temperature. We will calculate for room temperature.

We are going to calculate the signal voltage, V_S, using, based on the above discussion of numerical factors, $V_S = \left(\sqrt{2}/2\right)\chi'' \eta Q_L \sqrt{Z_0 P}$

V_S is the CW EPR signal voltage at the end of the transmission line connected to the resonator. That is, we do not include the spectrometer gains and losses in this calculation. This allows us to calculate for a "perfect" spectrometer, one which does not add noise in the detection system.

η (dimensionless) is the resonator filling factor

Q (dimensionless) is the loaded quality factor of the resonator, sometimes denoted Q_L.

Z_0 is the characteristic impedance of the transmission line (in ohms, usually 50).

P is the microwave power (in W) to the resonator produced by the external microwave source.

A 1 mM S = ½ radical sample has about

$$\left(1\text{x}10^{-3}\,\text{M/L}\right)\left(10^3\,\text{L/m}^3\right)\left(6.022\text{x}10^{23}\,\text{M}^{-1}\right) = 6.022\text{x}10^{23}\ \text{spins/m}^3$$

These are unusual units for chemical concentrations, but we need the spin concentration per m^3 for use in equations in SI units.

The number of spins in a 0.01 mM (10 micromolar) sample in a 1 cm length of a standard 4 mm o.d. sample tube (ca. 3 mm id), which has a sample volume of $7\text{x}10^{-8}$ m^3, is

$(0.01)(6\text{x}10^{23}\ \text{spins/m}^3)(0.07\text{x}10^{-6}\ \text{m}^3) = 4.2\text{x}10^{14}$ spins

Assume a single line with 1 G width.

We seek the maximum signal amplitude (peak of the line). Using the notation of Weil and Bolton, and assuming a Gaussian line with unit area, $Y_{max} = 0.8/\Delta B_{pp}$. For a Lorentzian line the numerator of this expression is 0.368 instead of 0.8.

The susceptibility to be used in the calculation of signal voltage, V_S, is

$$\chi'' = \left(2.66x10^{-32}\right)\frac{2\pi 9.4x10^9}{1x\sqrt{3}x2\pi 2.8x10^6}\left(0.01x6x10^{23}\right)(0.8) = 2.5x10^{-7}$$

Nitroxyl - Note that when we discuss the sensitivity for nitroxyl we have to account for the fact that the intensity is spread over 3 lines due to the ^{14}N hyperfine, so we divide the concentration by 3 and use an effective concentration. For perspective, note that the 2 mm o.d. by 10 mm long irradiated quartz standard sample contains about 10^{16} spins (Rinard et al. 1999c). This is a large numbers of spins relative to the stated sensitivity of a modern EPR spectrometer. There are major differences, though in the microwave power one would assume.

11.2 Signal Voltage

The equation for the signal voltage for CW EPR, for a given sample of given concentration in a resonator with a given Q and a given filling factor for a given input power is (Rinard et al. 1999a; 1999c).

$$V_S = \left(\sqrt{2}/2\right)\chi''\eta Q_L\sqrt{Z_0 P}$$

Recall form the discussion at the beginning of this Chapter that the √2 results from the rms to peak conversion, and the ½ comes from the fact that only half of the total microwave magnetization that is proportional to the square root of the power is effective in causing EPR transitions. One of the circularly polarized components rotates in the opposite direction and has little effect on the spins.

In the calculation we will assume for the 0.0a mM nitroxyl sample
Q = 3000
P = $1x10^{-3}$ W
Z_0 = 50 ohm

The filling factor can be approximated as the ratio of the volumes, but more accurate calculations for a Bruker rectangular TE_{102} cavity resonator are presented in Chapter 7 on Filling Factor. Using those results, we assume that the filling factor, η, is about $6x10^{-3}$ (0.6%).

Putting these values into
$V_S = \left(\sqrt{2}/2\right)\chi''\eta Q_L\sqrt{Z_0 P}$,
we now find for the 0.01mM nitroxyl sample that the signal voltage at the end of the transmission line connected to the resonator is

$$V_S = (1/3)\left(\sqrt{2}/2\right)\left(2.5x10^{-7}\right)\left(6x10^{-3}\right)(3000)\sqrt{(50)\left(1x10^{-3}\right)} = 2.37x10^{-7}V$$

This is the signal voltage for each line of the 0.01 mM nitroxyl sample prior to amplification. The gain of the spectrometer can be ignored for the purpose of this S/N calculation, since signal and noise are amplified equally. This is equivalent to assuming an ideal spectrometer that adds no noise.

11.3 Calculation of Noise

There are several contributions to the noise in the spectrometer. Ideally, the limiting noise would be the noise factor (NF) of the first stage amplifier amplifying thermal noise. However, we know that there are also losses in the path from the resonator to the detector, which can be large

at X-band, source phase noise, and the NF of the detection system. We will calculate the noise at the output of the resonator in order to estimate an ideal S/N.

The thermal noise power in a 50 ohm system, in dBm, is given by

Pn = -174 + 10 log(bandwidth).

Values in dBm are relative to 1 mW power.
We assume a 1 sec. filter time constant, which corresponds to ca 0.125 Hz effective noise bandwidth for a two-pole filter. Thus,

Pn = -174 + 10 log(0.125) = -183 dBm

To convert from dBm to voltage, convert to watts by dividing Pn by 10 and taking the inverse log:
Inverse log(dBm/10) = $5x10^{-19}$ mW = $5x10^{-22}$ W
Since this is power, the noise is calculated as rms V by multiplying by 50 ohm and taking the square root.
$V=\sqrt{WR} = (50 \times 5x10^{-22})^{1/2} = 1.58x10^{-10}$ V

11.4 Calculation of S/N for a Nitroxyl Sample

This pair of calculations suggests a S/N for the 0.010 mM nitroxyl solution of

$$S/N = \frac{\left(2.37x10^{-7}\right)}{\left(1.58x10^{-10}\right)} = 1.5x10^{3}$$

We assumed $4.2x10^{14}$ spins spread over 3 lines that are 1 G wide, and we assume that the magnetic field modulation is chosen to observe all of the EPR line, rather than ca. 1/10 of the line.

11.5 Calculation of S/N for a Weak Pitch Sample

The specification for a modern spectrometer is about 10^{10} spins per G. This is based on a measurement of weak pitch, with a somewhat saturating microwave power and modulation amplitude about equal to line width, conditions chosen to maximize the signal amplitude. Next, we repeat the calculation above for weak pitch with 6 G line width and 200 mW incident power.

The Varian catalog lists strong pitch as $3x10^{15}\Delta H$ spins/cm ±15%. Yordanov and Ivanova (1994a) cited $3x10^{18}$ spins per cm for Bruker strong pitch, but this does not agree with other information.

Weak pitch is diluted by a factor of 300 relative to strong pitch, so it has $1x10^{13}\Delta H$ spins per cm. If the line is 6 G wide, then there are $6x10^{13}$ spins per cm of length. For a Bruker HS (high sensitivity) cavity for the EMX spectrometer, the active length of the resonator is about 2 cm, but with variation in signal over this length such that the effective signal increase is roughly 1.5 times that for a 1 cm sample. The effective filling factor (see table in Chapter 7) will thus be about 1.7% for a 3 mm i.d. weak pitch sample 2 cm long. We will use this factor in the calculation of the signal voltage.

$$\chi'' = \left(2.66x10^{-32}\right)\frac{2\pi 9.4x10^{9}}{6x\sqrt{3}x2\pi 2.8x10^{6}}\left(6x10^{13}\,spins/0.07x10^{-6}\,m^{3}\right)(0.8) = 5.9x10^{-9}$$

$$V_S = \left(\sqrt{2}/2\right)\left(5.9x10^{-9}\right)(0.017)(3000)\sqrt{(50)\left(200x10^{-3}\right)} = 6.73x10^{-7}V$$

$$S/N = \frac{\left(6.73x10^{-7}\right)}{\left(1.58x10^{-10}\right)} = 4.3x10^{3}$$

Thus, we predict S/N = 4300 for weak pitch in a perfect spectrometer.
Note that the noise in the denominator is strongly dependent on the filter time constant and the equivalent noise effective bandwidth of the filter. Losses and the noise of active devices in the signal path might increase the noise relative to the EPR signal by 6 dB. Lacking an actual measurement, assume an effective overall NF = 6 dB, which is a factor of 2 in noise voltage, resulting in a prediction of S/N = 2130 for weak pitch. For conditions comparable to the assumptions of this calculation, but with an optimized high-Q resonator and source, Bruker now meets a 3000:1 S/N specification for weak pitch. Thus, this S/N calculation is fairly realistic, and is probably good to within a factor of two given the various approximations made, especially about filling factor and amount of the long line sample actually observed.

The calculations done here are for the absorption spectrum, with the numerical values adjusted to use the normal experimentally observed derivative peak-to-peak line width, ΔB_{pp}. The line width expressions from Weil and Bolton are normalized for an absorption line area =1. The experimental weak pitch S/N measurement uses the derivative spectrum. In comparing our calculation with experiment, we assume that the noise floor has been established prior to the phase-sensitive detector, and that the derivative spectrum is observed with the same S/N as the absorption.

If we continue to scale the calculations for an integrated area = 1, then, using the Weil and Bolton notation, the peak-to-peak amplitude of the derivative is $1.14/(\Delta B_{pp})^2$ which would replace $0.8/\Delta B_{pp}$ in the expression for the EPR signal voltage. Consistent with the well-known relation that the area of a derivative signal is proportional to width-squared times height, this would predict that the 6-gauss wide weak pitch signal amplitude would be about 25% of the value calculated for the absorption signal. The derivative signal is obtained by the properties of the lock-in amplifier. A full analysis of the output of a lock-in amplifier and its effect on the amplitude of the CW EPR signal is beyond the scope of this chapter.

11.6 Summary of Impact of Parameters on S/N

The following section discusses the contributions of noise other than thermal noise. Here, we review the parameters in the above equations. The signal voltage is given by $V_S = \left(\sqrt{2}/2\right)\chi''\eta Q_L\sqrt{Z_0 P}$. The properties of the sample dominate this – the spin concentration contributes linearly. The more spins the stronger the EPR signal. The narrower the line, the stronger the EPR signal for the same number of spins. The larger the sample, the larger the filling factor, but usually a larger sample lowers the Q, so there is a tradeoff. In addition, as pointed out in an earlier Chapter, the number of spins has to be kept small enough that the EPR signal is a small perturbation on the resonator Q. Increasing modulation amplitude increases S/N up to about an amplitude equal to the line width for narrow lines. Very large modulation amplitudes (more than a few gauss) may increase the noise level. Increasing gain will increase signal amplitude, but will not increase S/N. The other operator-controlled variables are the

microwave frequency and the temperature, but these are usually dictated by the goals of the experiment and by the resources available.

We have ignored relaxation times in this treatment. The electron spin relaxation time will determine the microwave power, P, that can be used. Operator judgment is required here also, trading off partial saturation for better S/N, as discussed in another section.

11.7 How to Improve the Spectrometer – the Friis Equation

We assumed an overall noise figure for the detection system. If we measure each component, we can estimate the effect of each on the overall noise figure.

To understand the importance of various losses and noise sources in a spectrometer, one would know all of the terms in the Friis equation. There are many ways to write the Friis equation. One common way favored by engineers is in terms of the noise temperature of each stage. Noise temperature does not imply physical temperature.

$$T_{e1\ldots n} = T_{e1} + \frac{T_{e2}}{g_1} + \ldots + \frac{T_{en}}{g_1 g_2 \cdots g_{n-1}}$$

where g_i is the power gain of the i^{th} stage and T_{ei} is the noise temperature of the i^{th} stage.

It can be seen from the Friis equation that the overall noise figure of a network is strongly dependent on the gain and noise figure of the first stage amplifier. If the early stages have low enough NF and high enough gain, the later stages are of little importance unless they introduce an enormous noise or interference signal (such as 60 Hz!). It is especially important to recognize that all losses prior to the first amplifier increase the effective noise figure by the amount of the losses.

$T_e = T_0(NF-1)$

The noise factor (NF) is the ratio of the output noise power to the portion of the output noise power that is produced by the input thermal noise when at a standard temperature of 290 K. For a noiseless network NF = 1 (the noise figure would be 0 dB) and $T_e = 0$. $T_0 = 290$ K.

For practical calculations of a spectrometer, recall that a mixer, used as a phase-sensitive detector, has a loss of 1.44 dB (Rinard et al. 1999c).

11.8 Experimental Comparison

Although this seems rather forbidding, it is not impossible to make the necessary calculations and measurements. Starting with the number of spins in the sample, one calculates the signal and compares it with the noise expected for the known (measured) gains, losses, and noise figures of each stage in the signal detection path of the spectrometer. A commercial CW EPR spectrometer is of course the hardest case, because we do not know the gains and losses and noise figures of all of the components in the signal detection path. Consequently, we will give results for two other types of EPR, pulsed and rapid scan. For a particular case an S-band spin echo was calculated to be 3.0 V at the digital oscilloscope, and the measured echo was 2.9 V (Rinard et al. 1999c). Analogous measurements were made for a rapid scan CW 250 MHz spectrometer, using 600 kHz bandwidth and direct detection, with the following results:

Parameter	Calculated theoretical value at the resonator	Measured value at the output of the spectrometer reflected to the resonator
Signal amplitude	1.29×10^{-6} Volts peak	1.24×10^{-6} Volts peak
Thermal noise	3.5×10^{-7} Vrms or -116 dBm	-115.96 dBm
Source phase noise	Use measured value of 0.94 above thermal	0.94 dB above thermal
Total noise	3.9×10^{-7} Vrms or -115 dBm	-115.02 dBm
Signal / Noise	3.25 signal volts / noise Vrms	3.126 signal volts / noise Vrms

These results provide confidence that the approach used is a valid way to identify the major targets for improvement of EPR spectrometer performance. Immediately evident from the Friis equation is that loss prior to the first stage amplifier, and the noise figure of the first stage amplifier can dominate the overall noise figure of the system. In older CW EPR spectrometers, the detector and first stage amplifier had poorer noise figures than is now possible due to technology improvements. From the discussions of η, Q, B_1, and modulation amplitude it is evident that resonators with higher Q and more uniform B_1, and modulation coil systems with more uniform modulation over the sample, all could yield improved signal amplitudes. The Bruker "high-Q" resonators exploit some of these features to provide the user with improved S/N. When everything else is improved, microwave source noise becomes an important contributor. Hence, for the highest-Q resonators, the microwave source has to be specially selected to have the lowest noise among those currently available.

Sometimes, it is necessary to trade off S/N for other experimental goals. For example, there is almost no loss in short lengths of X-band waveguide, but there is not enough room in the normal cryostat that fits in a normal magnet gap to use waveguide to the cavity. Hence, in cryostats coaxial cable is used at X-band (at Q-band, waveguide can be used). A meter of coaxial cable results in a loss of about 16% of the signal voltage (ca. 1.5 dB) at X-band.

The Friis equation points us to another tradeoff. A low-noise preamplifier could greatly improve the EPR S/N by establishing the noise floor before significant losses, such as in the detector crystal. However, a low-noise preamplifier will not survive more than a few mW incident power. Consequently, if a low-noise preamplifier is used in a general-purpose spectrometer, the operator has to switch it out of the circuit whenever the power limits of the amplifier would be exceeded, or it has to be protected by a limiter, which itself increases the noise figure. There is no free lunch. A low-noise preamplifier is used in the Bruker E580 pulsed spectrometer, where it is protected by an active limiter (microwave switch) and can be switched out of the circuit by the operator. If, however, a low-noise preamplifier could be installed at the output of the resonator, as might be possible with a bimodal resonator, a factor of at least two in S/N performance might be possible.

Chapter 12 - Less common measurements with EPR spectrometers

12.1 Multiple Resonance Methods

Irradiation with a second frequency during an EPR experiment can provide much more detailed information about the spin system than the usual single-frequency measurement. The most common of these multiple resonance methods are ENDOR, ELDOR, and TRIPLE. Introductions to ENDOR, TRIPLE, and ELDOR are provided in (Kevan and Kispert 1976; Box 1977; Schweiger 1982; Eachus and Olm 1985; Atherton 1993; Piekara-Sady and Kispert 1994; Bender 2004; Gerson and Gescheidt 2005; Kispert 2005). A convenient table comparing the techniques is in Poole (1983, page 650). Figure 12-1 shows the types of transitions observed in these experiments.

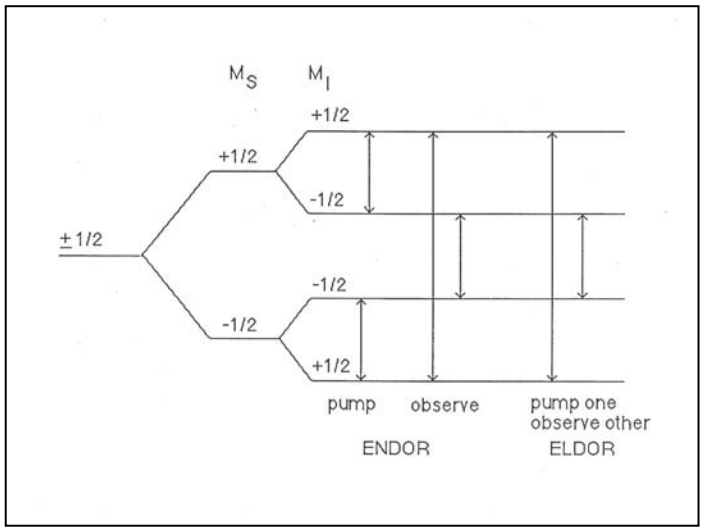

Figure 12-1 ENDOR and ELDOR transitions. The energy level diagram is sketched for the case of S = ½. I = ½, A > 0, $g_n > 0$, and $A/2 > \nu_n$. The allowed EPR transitions have $\Delta m_s = \pm 1$ and $\Delta m_I = 0$. Forbidden EPR transitions with $\Delta m_I = \pm 1$ sometimes have observable intensities. NMR transitions have $\Delta m_I = \pm 1$ and $\Delta m_s = 0$. Observation of a change in the intensity of one of the EPR transitions when one of the NMR transitions is irradiated is the ENDOR experiment. Observation of a change in intensity in one of the EPR transitions when another EPR transition is irradiated is the ELDOR experiment. There are both CW and pulsed methods of performing these measurements.

In ENDOR one adjusts the microwave frequency and magnetic field to a resonance of interest, and then sweeps a radio-frequency signal through the range of nuclear resonant frequencies. It is necessary to operate at a microwave power level that partially saturates the EPR transition (i.e., at microwave power greater than the linear portion of the curve in Figure 3-17), and one must be able to saturate the NMR transition. The radio-frequency field at the nuclear Larmor frequency induces transitions between states such that the overall effect is to decrease the degree of saturation of the electron spin system. This causes an increase in the amplitude of the EPR signal. Thus, there is a 'peak' corresponding to each nuclear transition that is coupled to the electron spin. Electron-nuclear couplings are observed via ENDOR with an effective resolution that is much higher than in conventional EPR. In addition, quadrupolar couplings can be

observed by ENDOR, whereas the quadrupole couplings are not observable, to first order, in EPR transitions. The ENDOR experiment can be extended to the use of two simultaneous radio-frequency fields (TRIPLE). While the ENDOR experiment provides only the magnitudes of the nuclear coupling constant, the TRIPLE experiment provides the signs of the coupling constants.

The ELDOR experiment involves two microwave frequencies. One EPR transition is saturated, and a second EPR transition is observed with a non-saturating microwave field from a second source. Typically, the microwave frequencies differ by about 350 MHz. When one transition is saturated, various relaxation mechanisms make the energy levels for the other (nonsaturated) transition more nearly equally populated. The result is a reduction in the intensity of the second transition.

Note that in both the CW ENDOR and CW ELDOR experiments the experimental observable is a change in the intensity of the EPR line upon irradiation with a second frequency. Thus, the S/N is poorer than for the conventional EPR experiment for the same species. Each of the measurements depends on having relaxation times in an appropriate range, so not every compound can be studied by these techniques over the range of concentrations, temperatures, etc., that might be of interest. This strong dependence on relaxation times translates into a powerful tool for studying relaxation behavior.

The conditions needed to observe ENDOR of various nuclei in organic radicals in solution is discussed in detail in Plato et al. (1981). Illustrations of TRIPLE that provide leading references to the literature are in (Kurreck et al. 1984; Kirste et al. 1985). A wide range of variations on the basic theme of multiple resonance has been developed, with CW and pulsed methods, field sweep and frequency sweep, and various combinations. Poole also describes double resonance experiments in which in addition to the microwave field, there is optical irradiation (optically detected magnetic resonance, ODMR), pulse radiolysis (dynamic electron polarization, DEP), an electric field (Mims 1976), and acoustic or ultrasonic paramagnetic resonance (UPR) (Devine and Robinson 1982).

12.2 Saturation Transfer Spectroscopy

The technique of saturation transfer spectroscopy can be used to measure rates of molecular motion that are a little faster than electron spin relaxation rates (Dalton et al. 1976; Hyde and Thomas 1980; Beth and Hustedt 2005; Marsh et al. 2005). This time-scale is particularly applicable to the study of biological systems labeled with nitroxyl spin labels. Standard conditions for the measurement of saturation transfer EPR spectra have been delineated (Hemminga et al. 1984). For the most common ST-EPR technique, the spectrometer must be capable of phase-sensitive detection at twice the magnetic field modulation frequency. Modern spectrometers have this capability.

12.3 Electrical Conductivity

Since electrical conductivity of a sample affects the magnitude of the EPR signal, it is possible to measure the microwave electrical conductivity of a sample with an EPR spectrometer (Setaka et al. 1970). The conductivity of the walls of a resonant cavity affect the Q of the cavity. This effect has been used to measure surface resistance of nonferromagnetic metals at X-band (Hernandez et al. 1986). Electron spin diffusion rates in conducting crystals have been measured

with electron spin echoes in a magnetic field gradient (Maresch et al. 1984). EPR can be used to monitor aspects of superconductivity in new materials (Emge et al. 1985; Shaltiel et al. 1987). A novel combination of EPR and the ac Josephson effect provided a new type of spectrometer (Baberschke et al. 1984).

12.4 Static Magnetization

The dc magnetization of a sample can be measured by using the EPR of a standard sample attached to the sample whose magnetization is to be measured. The EPR probes the magnetic field outside the sample (Schultz and Gullikson 1983).

12.5 EPR Imaging

With suitable magnetic field gradients, electron paramagnetic resonance (EPR) can provide pictures of spin concentration as a function of the three spatial dimensions x, y, and z. Most of the early work in EPR imaging has emphasized making pictures of objects. In this effort there has been an implied concept that the dimensions of interest were the three cartesian dimensions of the laboratory coordinate system (Eaton and Eaton 1986; Ohno 1986; 1987). However, the properties of the spin systems provide access to several additional dimensions, which may, in some cases, provide more insight into the nature of a sample than the spatial dimensions alone. Many additional features of EPR spectroscopy, including g-values, hyperfine splitting, relaxation times T_1 and T_2, microwave field distribution, spin flip angles, and chemical kinetics (for example, formation and decay of radicals or diffusion) can be dimensions. Our 1991 book comprehensively reviews theory, experiment, image reconstruction, and applications (Eaton et al. 1991). Recent reviews include (Eaton and Eaton 2000a; Fuchs et al. 2003; Halpern 2003; Kuppusamy et al. 2003; Lurie 2003; Subramanian et al. 2003; Zweier et al. 2003; Subramanian and Krishna 2005).

12.6 Zero-Field EPR

When there are multiple unpaired electrons in a species, as in metals with $S > 1/2$, electron spin resonance can be performed in the absence of an external magnetic field. Such an experiment measures directly the zero-field splittings among the unpaired electrons. Together with "normal" field-swept EPR zero-field EPR potentially allows full characterization of the spin system. (Pilbrow 1990) gives a good introduction to the field.

12.7 Rapid Scan EPR

Rapid scan EPR is a new EPR method in which a direct-detected signal (i.e., without magnetic field modulation and phase-sensitive detection) is recorded while the magnetic field is being scanned through the spectrum rapidly relative to electron spin relaxation times. Rapid-scan EPR encompasses the regime in which the magnetic field sweep is fast relative to relaxation times, which is a newly developed intermediate regime between CW and pulsed EPR (Stoner et al. 2004; Joshi et al. 2005a; 2005b; Tseitlin et al. 2006; Tseitlin et al. 2007).

12.8 High Frequency EPR

High frequency EPR is usually defined as higher than a commercial spectrometer, so currently high frequency means above 95 GHz. The state of the art was recently reviewed (Grinberg and Berliner 2004).

Summary

Training
Even after all that has been mentioned in this Workshop has been mastered, constant diligence is required to maintain quantitative accuracy in EPR. In the words of Peter Druker, 'The only things that evolve by themselves in an organization are disorder, friction, and malperformance." As Will Rogers said, "Everybody is ignorant, only on different subjects."

10 Commandments of Quantitative EPR

1. Thou shalt prepare samples carefully.
2. Thou shalt subtract background signals.
3. Thou shalt consider microwave loss.
4. Thou shalt not saturate thine spectra.
5. Thou shalt consider effects of modulation on spectra.
6. Thou shalt adjust microwave phase accurately.
7. Thou shalt allow the spectrometer to achieve thermal equilibrium.
8. Thou shalt calibrate the magnetic field.
9. Thou shalt know resonator Q
10. Thou shalt calibrate microwave power and B_1 at the sample.

Finally, by analogy with certain political slogans, "It is the B_1, stupid!"

Acknowledgments

Some of the figures used in this Workshop were originally prepared for the chapter by Eaton and Eaton in Ewing's Analytical Instrumentation Handbook, and brief portions of the text were adapted from that book. Richard W. Quine and George A. Rinard contributed to estimating the ultimate sensitivity of spectrometers. The Appendix on simulating overmodulated spectra was written by Dr. Colin Mailer.

Since this document is only for teaching purposes, publisher permission for use of figures previously published has not been obtained.

The effort of Gareth R. Eaton, Sandra S. Eaton, was partially supported by NIH NIBIB grants EB002807 and EB000557, and by the Center for Very Low Frequency EPR Imaging In Vivo Physiology, NIH NIBIB grant P41 EB002034, Dr. Howard Halpern, PI.

References

Aasa, R. and T. Vanngard (1975). EPR signal intensity and powder shapes. Reexamination. *J. Magn. Reson.* **19**: 308-315.

Abragam, A. (1961). *The Principles of Nuclear Magnetism*, Oxford, Oxford University Press.

Adem, E., P. E. Munoz, V. R. Gleason, S. H. Murrieta, S. G. Aguilar and R. E. Uribe (1993). Electron paramagnetic resonance studies of γ-irradiated corn. *Appl. Radiat. Isotop.* **44**: 419-422.

Alaouie, A. M. and A. I. Smirnov (2006). Ultra-stable temperature control in EPR experiments: Thermodynamics of gel-to-liquid phase transition in spin-labeled phospholipid bilayers and bilayer perturbations by spin labels. *J. Magn. Reson.* **182**: 229-238.

Alger, R. S. (1968). *Electron Paramagnetic Resonance: Techniques and Applications*, New York, Wiley-Interscience.

Anderson, J. R., R. R. Mett and J. S. Hyde (2002). Cavities with axially uniform fields for use in electron paramagnetic resonance. II. Free space generalization. *Rev. Sci. Instrum.* **73**(8): 3027-3037.

Anderson, W. A. and L. H. Piette (1959). Forbidden $\Delta m_s = \pm 1$, $\Delta m_I = -/+1$ transitions in a vanadyl chelate. *J. Chem. Phys.* **30**: 591-592.

Ardenkjaer-Larsen, J. H., I. Laursen, I. Leunbach, G. Ehnholm, L.-G. Wistrand, J. S. Petersson and K. Golman (1998). EPR and DNP properties of certain novel single electron contrast agents intended for oximetric imaging. *J. Magn. Reson.* **133**: 1-12.

Ashton, G. R., D. K. Hsu and R. G. Leisure (1980). Comparison of multiple-scan direct and lock-in detection in magnetic resonance: Application to nuclear acoustic resonance. *Rev. Sci. Instrum.* **51**: 454-458.

Atherton, N. M. (1993). *Principles of Electron Spin Resonance*, London, Ellis Horwood Prentice Hall.

Auteri, F. P., R. L. Belford, S. Boyer, K. K. Motsegood, A. I. Smirnov, T. Smirnova, N. Vahidi and R. B. Clarkson (1994). Carbon-Based Standards for Electron Paramagnetic Resonance Spectroscopy. *Appl. Magn. Reson.* **6**: 287-308.

Baberschke, K., K. D. Bures and S. E. Barnes (1984). ESR in situ with a Josephson Tunnel Junction. *Phys. Rev. Lett.* **53**: 98-101.

Balan, E., T. Allard, B. Boizot, G. Morin and J.-P. Muller (2000). Quantitative Measurement of Fe^{3+} in Kaolinite. *Clays and Clay Minerals* **48**: 439-445.

Bales, B. L. and L. Kevan (1970). Paramagnetic relaxation of silver species in γ-irradiated frozen aqueous solutions. *J. Chem. Phys.* **52**: 4644-4653.

Belford, R. L., R. B. Clarkson, J. B. Cornelius, K. S. Rothenberger, M. J. Nilges and M. D. Timken (1987). EPR Over Three Decades of Frequency: Radiofrequency to Infrared, in *Electron Magnetic Resonance of the Solid State*. J. A. Weil, M. K. Bowman and K. F. Preston, Eds., Ottawa, Canada, Canadian Society for Chemistry, 21-43.

Bender, C. J. (2004). ENDOR Coils and Related Radiofrequency Circuits, in *EPR: Instrumental Methods*. C. J. Bender and L. J. Berliner, Eds., New York, Kluwer Academic/Plenum Publishers, *Biol. Magn. Reson.* **21**: 155-211.

Bertini, I., G. Martini and C. Luchinat (1994a). Relaxation Data Tabulation, in *Handbook of Electron Spin Resonance: Data Sources, Computer Technology, Relaxation, and ENDOR*. J. Poole, C. P. and H. Farach, Eds., New York, American Institute of Physics, 79-310.

Bertini, I., G. Martini and C. Luchinat (1994b). Relaxation, Background, and Theory, in *Handbook of Electron Spin Resonance*. J. Poole, C. P., Ed., New York, American Institute of Physics, 51-77.

Beth, A., K. Balasubramanian, B. H. Robinson, L. R. Dalton, S. K. Venkataramu and J. H. Park (1983). Sensitivity of V2' saturation transfer electron paramagnetic resonance signals to anisotropic rotational diffusion with [15N]nitroxide spin-labels. Effects of noncoincident magnetic and diffusion tensor principal axes. *J. Phys. Chem.* **87**: 359-367.

Beth, A. and E. J. Hustedt (2005). Saturation transfer EPR: Rotational dynamics of membrane proteins, in *Biomedical EPR, Part B: Methodology, Instrumentation, and Dynamics*. S. S. Eaton, G. R. Eaton and L. J. Berliner, Eds., New York, Kluwer Academic/Plenum Publishers, *Biol. Magn. Reson.* **24**: 369-407.

Blakley, R. L., D. D. Henry, W. T. Morgan, W. L. Clapp, C. J. Smith and D. Barr (2001). Quantitative Electron Paramagnetic Resonance: The Importance of Matching the Q-Factor of Standards and Samples. *Appl. Spectros.* **55**: 1375-1381.

Bloembergen, N. and R. V. Pound (1954). Radiation damping in magnetic resonance experiments. *Phys. Rev.* **95**: 8-12.

Bloembergen, N., E. M. Purcell and R. V. Pound (1948). Relaxation Effects in Nuclear Resonance Absorption. *Phys. Rev.* **73**: 679-712.

Bolton, J. R., D. C. Borg and H. M. Swartz (1972). Experimental Aspects of Biological Electron Spin Resonance Studies, in *Biological Applications of Electron Spin Resonance*. H. M. Swartz, J. R. Bolton and D. C. Borg, Eds., New York, Wiley, ch. 2.

Box, H. C. (1977). *Radiation Effects: ESR and ENDOR Analysis*, Academic Press.

Brändel, R., G. J. Krüger and W. Müller-Warmuth (1970). Impulsspektroskopische Untersuchungen der Elektronenspinrelaxation in freien Radikalen. *Z. Naturforsch.* **25a**: 1-11.

Bryson, W. G., D. P. Hubbard, B. M. Peake and J. Simpson (1975). Applications of Electron Spin Resonance in the Analytical Chemistry of Transition Metal Ions. Part I. Factors Affecting the Signal Amplitude. *Anal. Chim. Acta* **77**: 107-115.

Budil, D. E., S. Lee, S. Saxena and J. H. Freed (1996). Nonlinear least-squares analysis of slow-motion EPR spectra in one and two dimensions using a modified Levenberg-Marquardt algorithm. *J. Magn. Reson. A* **120**: 155-189.

Burgess, J. H. and R. M. Brown (1952). Modulation Effects in Nuclear Magnetic Resonance. *Rev. Sci. Instrum.* **23**: 334-336.

Burns, D. T. and B. D. Flockhart (1990). Application of Quantitative EPR. *Phil. Trans. R. Soc. London A* **333**: 37-48.

Cage, B., P. Cevc, R. Blinc, L. C. Brunel and N. S. Dalal (1998). 1-370 GHz EPR Linewidths for K_3CrO_8: A Comprehensive Test for the Anderson-Weiss Model. *J. Magn. Reson.* **135**: 178-184.

Calvo, R., E. C. Abresch, R. Bittl, G. Feher, W. Hofbauer, R. A. Isaacson, W. Lubitz, M. Y. Okamura and M. L. Paddock (2000). EPR study of the molecular and electronic structure of the semiquinone biradical, $Q_A^{-\cdot}$ $Q_B^{-\cdot}$ in photosynthetic reaction centers from *Rhodobacter sphaeroides*. *J. Am. Chem. Soc.* **122**: 7327-7341.

Carrington, A. and G. R. Luckhurst (1964). Electron spin resonance line widths of transition metal ions in solution. Relaxation through zero-field splitting. *Mol. Phys.* **8**: 125-132.

Casteleijn, G., J. J. TenBosch and J. Smidt (1968). Error analysis of the determination of spin concentration with the electron spin resonance method. *J. Appl. Phys.* **39**: 4375-4380.

Chang, R. (1974). Simple Setup for Quantitative Electron Paramagnetic Resonance. *Anal. Chem.* **46**: 1360.

Chang, T.-T., D. Foster and A. H. Kahn (1978). An Intensity Standard for Electron Paramagnetic Resonance Using Chromium-Doped Corundum (Al_2O_3: Cr^{3+}) *J. Research Natl. Bur. Stand.* **83**: 133 - 164.

Chesnut, D. B. (1977). On the use of AW2 method for integrated line intensities from first-derivative presentations. *J. Magn. Reson.* **25**: 373-374.

Conradi, M. S. (1977). Magnetic resonance signal-to-noise calculations: direct vs. lock-in recording. *Rev. Sci. Instrum.* **48**: 444-448.

Copeland, E. S. (1973). Simple method for estimating H1 [microwave magnetic field strength] in ESR experiments. Microwave power saturation of γ-irradiation induced glycylglycine radicals. *Rev. Sci. Instrum.* **44**: 437-442.

Cordischi, D., M. Occhiuzzi and R. Dragone (1999). Quantitative EPR Spectroscopy: Comparison between Primary Standards and Application to MgO-MnO and α-Al_2O_3-CrO_3 Solid Solutions. *Appl. Magn. Reson.* **16**: 427-445.

Crippa, P. R., E. U. Urbinati and A. Vecli (1971). On the determination of the unpaired spin number by electron spin resonance. *J. Phys. E.* **4**: 1071-1073.

Czoch, R. (1996). Quantitative EPR – Sensitivity to Experimental Conditions and Optimal Setting of Recording Parameters. *Appl. Magn. Reson.* **10**: 293-317.

Dalal, D. P., S. S. Eaton and G. R. Eaton (1981a). The effects of lossy solvents on quantitative EPR studies. *J. Magn. Reson.* **44**(3): 415-28.

Dalal, N. S., M. M. Suryan and M. S. Seehra (1981b). Potassium Perchromate Standard for Determination of Paramagnetic Spin Concentration, g Values, and Magnetic Moments of Fossil Fuels. *Anal. Chem.* **53**: 938-940.

Dalton, L. R., B. H. Robinson, L. A. Dalton and P. Coffey (1976). Saturation Transfer Spectroscopy. *Adv. Magn. Reson.* **8**: 149-259.

Dashnau, J. L., B. Zelent and J. M. Vanderkooi (2005). Tryptophan interactions with glycerol/water and trehalose/sucrose cryosolvents: infrared and fluorescence spectroscopy and *ab initio* calculations. *Biophys. Chem.* **114**: 71-83.

Devine, S. D. and W. H. Robinson (1982). Ultrasonically modulated paramagnetic resonance. *Adv. Magn. Reson.* **10**: 53-117.

Drago, R. S. (1977). *Physical Methods in Chemistry*, Saunders.

Drew, S. C., C. G. Young and G. R. Hanson (2007). A density functional study of the electronic structure and spin Hamiltonian parameters of mononuclear thiomolybdenyl complexes. *Inorg. Chem.* **46**: 2388-2397.

Dyrek, K., E. Bidzinska and A. Adamski (2003). Quantitative EPR- A Versatile Tool in Fundamental and Applied Studies. *Mol. Phys. Reports* **37**: 9-23.

Dyrek, K., A. Madej, E. Mazur and A. Rokosz (1990). Standards for EPR Measurements of Spin Concentration. *Colloids and Surfaces* **45**: 135-144.

Dyrek, K., A. Rokosz and A. Madej (1994). Spin Dosimetry in Catalysis Research. *Appl. Magn. Reson.* **6**: 309-332.

Dyrek, K., A. Rokosz, A. Madej and E. Bidzinska (1996). Quantitative EPR Studies of Transition Metal Ions in Oxide, Aluminosilicate and Polymer Matrices. *Appl. Magn. Reson.* **10**: 319-338.

Eachus, R. S. and M. T. Olm (1985). Electron Nuclear Double Resonance Spectroscopy. *Science* **230**: 268-274.

Eastman, M. P., R. G. Kooser, M. R. Das and J. H. Freed (1969). Heisenberg spin exchange in E.S.R. spectra. I. Linewidth and saturation effects. *J. Chem. Phys.* **51**: 2690-2709.

Eaton, G. R. and S. S. Eaton (1990). Electron Paramagnetic Resonance, in *Analytical Instrumentation Handbook*. G. W. Ewing, 2nd Ed., New York, Marcel Dekker, 467-530.

Eaton, G. R., S. S. Eaton and K. Ohno, Eds. (1991). *EPR Imaging and in Vivo EPR*. Boca Raton, FL, CRC Press.

Eaton, G. R., S. S. Eaton and G. A. Rinard (1998). Frequency dependence of EPR sensitivity. *Spatially Resolved Magnetic Resonance: Methods, Materials, Medicine, Biology, Rheology, Geology, Ecology, Hardware, [Based on Lectures presented at the International Conference on Magnetic Resonance Microscopy], 4th, Albuquerque, Oct., 1997*: 65-74.

Eaton, S. S. and G. R. Eaton (1977). Electron Paramagnetic Resonance Cell for Lossy Samples. *Anal. Chem.* **49**: 1277-1278.

Eaton, S. S. and G. R. Eaton (1980). Signal area measurements in EPR. *Bull. Magn. Reson.* **1**(3): 130-8.

Eaton, S. S. and G. R. Eaton (1982). Measurement of spin-spin distances from the intensity of the EPR half-field transition. *J. Amer. Chem. Soc.* **104**(18): 5002-3.

Eaton, S. S. and G. R. Eaton (1986). EPR imaging. *Spectroscopy (Duluth, MN, United States)* **1**(1): 32-5.

Eaton, S. S. and G. R. Eaton (1992). Quality assurance in EPR. *Bull. Magn. Reson.* **13**(3-4): 83-9.

Eaton, S. S. and G. R. Eaton (1993). Irradiated fused-quartz standard sample for time-domain EPR. *J. Magn. Reson.* **102**(3): 354-6.

Eaton, S. S. and G. R. Eaton (1997). Electron Paramagnetic Resonance, in *Analytical Instrumentation Handbook*. G. W. Ewing, Ed., New York, Marcel Dekker, 2nd ed., 767-862.

Eaton, S. S. and G. R. Eaton (2000a). EPR imaging. *Electron Paramagnetic Resonance* **17**: 109-129.

Eaton, S. S. and G. R. Eaton (2000b). Relaxation times of organic radicals and transition metal ions, in *Distance Measurements in Biological Systems by EPR*. L. J. Berliner, S. S. Eaton and G. R. Eaton, Eds., New York, Kluwer Academic/Plenum Publishers, *Biol. Magn. Reson.* **19**: 29-154.

Eaton, S. S. and G. R. Eaton (2005). Electron paramagnetic resonance, in *Analytical Instrumentation Handbook*. J. Cazes, Ed., New York, Marcel Dekker, 3rd ed., 349-398.

Eaton, S. S., J. Harbridge, G. A. Rinard, G. R. Eaton and R. T. Weber (2001). Frequency dependence of electron spin relaxation for three S = 1/2 species doped into diamagnetic solid hosts. *Appl. Magn. Reson.* **20**(1-2): 151-157.

Eaton, S. S., M. L. Law, J. Peterson, G. R. Eaton and D. J. Greenslade (1979). Metal-nitroxyl interactions. 7. Quantitative aspects of EPR spectra resulting from dipolar interactions. *J. Magn. Reson.* **33**(1): 135-41.

Eaton, S. S., K. M. More, B. M. Sawant and G. R. Eaton (1983). Use of the ESR half-field transition to determine the interspin distance and the orientation of the interspin vector in systems with two unpaired electrons. *J. Am. Chem. Soc.* **105**(22): 6560-7.

Elas, M., K. H. Ahn, A. Parasca, E. D. Barth, D. Lee, C. Haney and H. J. Halpern (2006). Electron paramagnetic resonance oxygen images correlate spatially and quantitatively with OxyLite oxygen measurements. *Clin. Cancer Res.* **12**: 4209-4217.

Emge, T. J., H. H. Wang, M. A. Beno, P. C. W. Leung, M. A. Firestone, H. C. Jenkins, J. D. Cook, K. D. Carlson, J. M. Williams, E. L. Venturini, J. Azevedo and J. E. Schirber (1985). A test of superconductivity vs. molecular disorder in $(BEDT\text{-}TTF)_2X$ synthetic metals: synthesis, structure (298, 120 K), and microwave/ESR conductivity of $(BEDT\text{-}TTF)_2I_2Br$. *Inorg. Chem.* **24**: 1736-1738.

Farrar, T. C. and E. D. Becker (1971). *Pulse and Fourier Transform NMR*, New York, Academic Press.

Fedin, M. V., P. A. Purtov and E. G. Bagryanskaya (2003a). Spin relaxation in low and zero magnetic field. *J. Chem. Phys.* **118**: 192-201.

Fedin, M. V., P. A. Purtov and E. G. Bagyanskaya (2003b). Spin relaxation of radicals in low and zero magnetic field. *J. Chem. Phys.* **118**: 192-201.

Feher, G. (1957). Sensitivity considerations in microwave paramagnetic resonance absorption techniques. *Bell System Technical Journal* **36**: 449-484.

Freed, J. H. (1976). Theory of slow tumbling ESR spectra of nitroxides, in *Spin Labeling: Theory and Applications*. L. J. Berliner, Ed., New York, Academic Press, 53-132.

Froncisz, W., T. Oles and J. S. Hyde (1986). Q-band loop-gap resonator. *Rev. Sci. Instrum.* **57**(6): 1095-9.

Fuchs, M., N. Groth and T. Herrling (2003). Applicaion of in vivo EPR spectroscopy and imaging to skin, in *In Vivo EPR(ESR)*. L. J. Berliner, Ed., New York, Kluwer Academic/Plenum Publishers, *Biol. Magn. Reson.* **18**: 483-515.

Fujita, Y., K. Tsuchiya, S. Abe, Y. Takiguchi, S. Kubo and H. Sakurai (2005). Estimation of the age of human bloodstains by electron paramagnetic resonance spectroscopy: Long-term controlled experiment on the effects of environmental factors. *Forensic Sci. Internat.* **152**: 39-43.

Gancheva, V., N. D. Yordanov, F. Callens, G. Vanhaelewyn, J. Raffi, E. Bortolin, S. Onori, E. Malinen, E. Sagstuen, S. Fabisiak and Z. Peimel-Stuglik (2008). An international intercomparison on 'self-calibrated' alanine dosimeters. *Radiat. Phys. Chem.* **77**: 357-364.

Gerson, F. and G. Gescheidt (2005). Solution-ENDOR of some biologically interesting radical ions, in *Biomedical EPR - Part B: Methodology, Instrumentation, and Dynamics*. S. S. Eaton, G. R. Eaton and L. J. Berliner, Eds., New York, Kluwer Academic/Plenum Publishers, *Biol. Magn. Reson.* **24**: 145-164.

Ginzton, E. L. (1957). *Microwave Measurements*, New York, McGraw-Hill.

Glarum, S. H. and J. H. Marshall (1970). Ethereal Electrons. *J. Chem. Phys.* **52**: 5555-5565.

Goldberg, I. B. (1978). Improving the analytical accuracy of electron paramagnetic resonance spectroscopy. *J. Magn. Reson.* **32**: 233-242.

Goldberg, I. B. and A. J. Bard (1983). Electron-Spin-Resonance Spectroscopy, in *Treatise on Analytical Chemistry*. I. M. Kolthoff and P. J. Elving, Eds., New York, Wiley-Interscience, 2nd ed., **Part I, Vol 10**: 226-289.

Goldberg, I. B. and H. R. Crowe (1977). Effect of cavity loading on analytical electron spin resonance spectrometry. *Anal. Chem.* **49**: 1353-1357.

Goldberg, I. B., H. R. Crowe and W. M. Robertson (1977). Determination of the Composition of Mixtures of Sodium Chromite and Chromic Oxide by Electron Spin Resonance Spectrometry. *Anal. Chem.* **49**: 962-966.

Golumbek, A. P. and M. P. Hendrich (2003). Quantitative analysis of dinuclear manganese(II) EPR spectra. *J. Magn. Reson.* **165**: 33-48.

Grinberg, O. and L. J. Berliner, Eds. (2004). *Very High Frequency (VHF) ESR/EPR*. Biol. Magn. Reson. New York, Kluwer Academic/Plenum Publishers.

Grucker, D., T. Guiberteau and G. Planinšic (1996). Proton-electron double resonance: spectroscopy and imaging in very low magnetic fields. *Res. Chem. Intermed.* **22**: 567-579.

Guiberteau, T. and D. Grucker (1993). Dynamic Nuclear Polarization of Water Protons by Saturation of σ and π EPR Transitions of Nitroxides. *J. Magn. Reson. A.* **105**: 98-103.

Guiberteau, T. and D. Grucker (1996). EPR Spectroscopy by Dynamic Nuclear Polarization in Low Magnetic Field. *J. Magn. Reson. B* **110**: 47-54.

Gunter, T. E., J. S. Puskin and P. R. Russell (1975). Quantitative Magnetic Resonance Studies of Manganese Uptake by Mitochondria. *Biophys. J.* **15**: 319-333.

Hagen, W. R., H. Wassink, R. R. Eady, B. E. Smith and H. Haaker (1987). Quantitative EPR of an S = 7/2 system in thionine-oxidized MeFe proteins of nitrogenase. A redefinition of the P-cluster concept. *Eur. J. Biochem.* **169**: 457-465.

Halpern, H. J. (2003). Applications of in vivo EPR spectroscopy and imaging in cancer research, in *In Vivo EPR (ESR)*. L. J. Berliner, Ed., New York, Kluwer Academic/Plenum Publishing, *Biol. Magn. Reson.* **18**: 469-482.

Halpern, H. J., M. Peric, C. Yu and B. L. Bales (1993). Rapid quantitation of parameters from inhomogeneously broadened EPR spectra. *J. Magn. Reson. A* **103**(1): 13-22.

Halpern, H. J., C. Yu, M. Peric, E. Barth, D. J. Grdina and B. A. Teicher (1994). Oxymetry deep in tissues with low-frequency electron paramagnetic resonance. *Proc. Natl. Acad. Sci. U. S.* **91**(26): 13047-51.

Harbridge, J. R., G. R. Eaton and S. S. Eaton (1998). Impact of spectral diffusion on apparent relaxation times for the stable radical in irradiated glycylglycine. *Modern Applications of EPR/ESR: From Biophysics to Materials Science, Proceedings of the Asia-Pacific EPR/ESR Symposium, 1st, Kowloon, Hong Kong, Jan. 20-24, 1997*: 220-225.

Harbridge, J. R., S. S. Eaton and G. R. Eaton (2003). Electron Spin-Lattice Relaxation Processes of Radicals in Irradiated Crystalline Organic Compounds. *J. Phys. Chem. A* **107**(5): 598-610.

Hemminga, M. A., P. A. deJager, D. Marsh and P. Fajer (1984). Standard Conditions for the Measurement of Saturation-Transfer ESR Spectra. *J. Magn. Reson.* **59**: 160.

Hendrich, M. P. and P. G. DeBrunner (1989). Integer-spin electron paramagnetic resonance of iron proteins. *Biophys. J.* **56**: 489-506.

Hernandez, A., E. Martin, J. Margineda and J. M. Zamarro (1986). Resonant Cavities for Measuring the surface resistivities of metals at X-band frequencies. *J. Phys. E.* **19**: 222-225.

Herrington, J. R., L. A. Boatner, T. J. Aton and T. L. Estle (1974). Electron paramagnetic resonance investigation of the dynamic Jahn-Teller effect for Sc^{2+} in BaF_2, SrF_2, and CaF_2 *Phys. Rev. B* **10**: 833-843.

Hill, H. D. W. and R. E. Richards (1968). Limits of measurement in magnetic resonance. *J. Sci. Instrum.* **2**: 977-83.

Horasan, N., M. M. Sünnetçioğlu, R. Sungur and G. Bingöl (1997). A Weak Field EPR Study of TANOL in Water and Water-Oil Using Dynamic Nuclear Polarization. *Z. Naturforsch.* **52a**: 485-489.

Hyde, J. S. (1972). A new principle for aqueous sample cells for EPR. *Rev. Sci. Instrum.* **43**: 629-631.

Hyde, J. S. (1978). Saturation-Transfer Spectroscopy. *Methods in Enzymology* **XLIX**: 480-511.

Hyde, J. S. and W. Froncisz (1982). The role of microwave frequency in EPR spectroscopy of copper complexes. *Ann. Rev. Biophys. Bioeng.* **11**: 391-417.

Hyde, J. S., A. Jesmanowicz, J. J. Ratke and W. E. Antholine (1992). Pseudomodulation: a computer-based strategy for resolution enhancement. *J. Magn. Reson.* **96**(1): 1-13.

Hyde, J. S. and R. R. Mett (2002). Aqueous sample considerations in uniform field resonators for electron paramagnetic resonance spectroscopy. *Curr. Topics Biophys.* **26**: 7-14.

Hyde, J. S., R. R. Mett and J. R. Anderson (2002). Cavities with axially uniform fields for use in electron paramagnetic resonance. III. Re-entrant geometries. *Rev. Sci. Instrum.* **73**(11): 4003-4009.

Hyde, J. S. and D. D. Thomas (1980). Saturation-Transfer Spectroscopy. *Ann. Rev. Phys. Chem.* **31**: 293-317.

Ilangovan, G., J. L. Zweier and P. Kuppusamy (2004). Mechanism of oxygen-induced EPR line broadening in lithium phthalocyanine microcrystals. *J. Magn. Reson.* **170**: 42-48.

Jardetzky, O. and G. C. K. Roberts (1981). *NMR in Molecular Biology*, New York, Academic Press.

Jeschke, G. (2007). Instrumentation and Experimental Setup. *Biol. Magn. Reson.* **27**: 17-47.

Joshi, J. P., J. R. Ballard, G. A. Rinard, R. W. Quine and G. R. Eaton (2005a). Rapid-Scan EPR with Triangular Scans and Fourier Deconvolution to Recover the Slow-Scan Spectrum. *J. Magn. Reson.* **175**: 44-51.

Joshi, J. P., G. R. Eaton and S. S. Eaton (2005b). Impact of Resonator on Direct-Detected Rapid-Scan EPR at 9.8 GHz. *Appl. Magn. Reson.* **29**: 239-249.

Juarez-Garcia, C., M. P. Hendrich, T. R. Holman, L. J. Que and E. Münck (1991). Combined Mossbauer and EPR Studies of the S = 3 State of an Exchange-Coupled FeIIICuII Complex: Test for Quantitative EPR Analysis of Integer Spin Systems. *J. Amer. Chem. Soc.* **113**: 518-525.

Kälin, M., I. Gromov and A. Schweiger (2003). The continuous wave electron paramagnetic resonance experiment revisited. *J. Magn. Reson.* **160**: 166-182.

Kevan, L. and L. D. Kispert (1976). *Electron Spin Double Resonance Spectroscopy*, Wiley.

Kirste, B., W. Harrer and H. Kurreck (1985). ENDOR Studies of Novel Di- and Triphenylmethyl Radicals Generated from Galvinols. *J. Amer. Chem. Soc.* **107**: 20-28.

Kispert (2005). Electron-electron double resonance, in *Biomedical EPR- Part B: Methodology, Instrumentation, and Dynamics*. S. S. Eaton, G. R. Eaton and L. J. Berliner, Eds., New York, Kluwer Academic/Plenum Publisher, *Biol. Magn. Reson.* **24**: 165-197.

Kolaczkowski, S. V., J. T. Cardin and D. E. Budil (1999). Some Remarks on Reported Inconsistencies in the High-Field EPR Spectrum of DPPH. *Appl. Magn. Reson.* **16**: 293-298.

Kooser, R. G., W. V. Volland and J. H. Freed (1969). E.S.R. relaxation studies on orbitally degenerate free radicals. I. Benzene anion and tropenyl. *J. Chem. Phys.* **50**: 5243-5257.

Kuppusamy, P., M. Chzhan and J. L. Zweier (2003). Principles of Imaging, in *In Vivo EPR (ESR)*. L. J. Berliner, Ed., New York, Kluwer Academic/Plenum Publisher, *Biol. Magn. Reson.* **18**: 99-152.

Kurreck, H., M. Bock, N. Bretz, M. Elsner, W. Lubitz, F. Muller, J. Geissler and P. M. H. Kroneck (1984). Fluid Solution and Solid-State Electron Nuclear Double Resonance of Flavin Model Compounds and Flavoenzymes. *J. Amer. Chem. Soc.* **106**: 737-746.

Lloyd, J. P. and G. E. Pake (1954). Spin relaxation in free radical solutions exhibiting hyperfine structure. *Phys. Rev.* **94**: 579-591.

Ludowise, P., S. S. Eaton and G. R. Eaton (1991). A convenient monitor of EPR automatic frequency control function. *J. Magn. Reson.* **93**(2): 410-12.

Lurie, D. J. (2003). Proton-electron double-resonance imaging (PEDRI), in *In Vivo EPR(ESR)*. L. J. Berliner, Ed., New York, Kluwer Academic/Plenum Publishers, *Biol. Magn. Reson.* **18**: 547-578.

Lurie, D. J., I. Nicholson and J. R. Mallard (1991). Low-field EPR measurements by field-cycled dynamic nuclear polarization. *J. Magn. Res.* **95**: 405-409.

Mailer, C., B. H. Robinson, B. B. Williams and H. J. Halpern (2003). Spectral fitting: The extraction of crucial information from a spectrum and a spectral image. *Magn. Reson. Med.* **49**: 1175-1180.

Mailer, C., T. Sarna, H. M. Swartz and J. S. Hyde (1977). Quantitative studies of free radicals in biology: corrections to ESR saturation data. *J. Magn. Reson.* **25**: 205-210.

Maresch, G. G., M. Mehring, J. U. von Schutz and H. C. Wolf (1984). Time-resolved ESR Investigation of Electron-spin Diffusion in the Radical Cation Salt (fluoranthenyl)$^{2+}AsF_6^-$. *Chem. Phys. Lett* **85**: 333-340.

Marsh, D., L. I. Horváth, T. Páli and V. Livshits (2005). Saturation Transfer Spectroscopy of Biological Membranes. *Biol. Magn. Reson.* **24**: 309-367.

Mazúr, M. (2006). A dozen useful tips on how to minimize the influence of sources of error in quantitative electron paramagnetic resonance (EPR) spectroscopy – A review *Anal. Chim. Acta* **561**: 1-15.

Mazúr, M., J. Moncol, M. Valko and H. Morris (2004). Analysis of the Radial and Longitudinal Effect of a Planar Sample in a Single TE_{102} Rectangular Electron Paramagnetic Resonance (EPR) Cavity. *Anal. Chim. Acta* **526**: 163-176.

Mazúr, M., J. Moncol, M. Valko and H. Morris (2005). Analysis of the longitudinal "sloping plateau" effect in a single TE_{102} rectangular cavity. *Anal. Chim. Acta* **538**(165-174).

Mazúr, M., H. Morris and M. Valko (1997a). Analysis of the movement of line-like samples of variable length along the x-axis of a double TE_{104} and a single TE_{102} rectangular resonator. *J. Magn. Reson.* **129**: 188-200.

Mazúr, M. and M. Valko (1999). Radial Effect of the EPR Signal Intensity in a Bruker Single TE_{102} Rectangular Cavity. *Bruker Report* **147**: 43-45.

Mazúr, M., M. Valko, R. Klement and H. Morris (1996a). Quantitative Electron Paramagnetic Resonance (EPR) Spectrometry with a TE_{104} Double Rectangular Cavity. Part 1. A Simple Alignment Procedure for the Precision Positioning of the Sample. *Anal. Chim. Acta* **333**: 249-252.

Mazúr, M., M. Valko, M. Micov and H. Morris (1998). Analytical Solution for the Electron Paramagnetic Resonance Signal Intensity of a Line-Like Sample of Variable Length Whose Centre is Situated at an Arbitrary Position along the Common Sample-Cavity x-Axis. *Anal. Chim. Acta* **373**: 107-109.

Mazúr, M., M. Valko and H. Morris (1997b). A Simple Alignment Procedure for the Precision Positioning of the Sample at Arbitrary Points of the Intracavity Space of a TE_{104} Double Rectangular Cavity. *Rev. Sci. Instrum.* **68**: 2514-2517.

Mazúr, M., M. Valko and H. Morris (2000). Analysis of the radial and longitudinal effect in a double TE_{104} and a single TE_{102} rectangular cavity. *J. Magn. Reson.* **142**: 37-56.

Mazúr, M., M. Valko and H. Morris (2001). Influence of the movement of "over full-length cavity" cylindrical samples along the x-axis of a double TE_{104} and a single TE_{102} rectangular cavity on the electron paramagnetic resonance An unusual effect analysis. *Anal. Chim. Acta* **443**: 127-141.

Mazúr, M., M. Valko and H. Morris (2003). Influence of the Variable Wall Thickness of the Sample Tube and a Quartz Dewar on an EPR Signal Intensity in a Single TE_{102} and Double TE_{104} Rectangular Cavities. *Anal. Chim. Acta* **482**: 229-248.

Mazúr, M., M. Valko, H. Morris and R. Klement (1996b). Quantitative Electron Paramagnetic Resonance (EPR) Spectrometry with a TE_{104} Double Rectangular Cavity. Part 2. Analysis of Sample and TE_{104} Cavity Error Sources Associated with the Movement of Line-like Samples into the TE_{104} Cavity *Anal. Chim. Acta* **333**: 253-265.

Mazúr, M., M. Valko and P. Pelikan (1997c). Quantitative EPR spectroscopy in solid state chemistry. *Chem. Papers* **51**: 134-136.

Mett, R. R., W. Froncisz and J. S. Hyde (2001). Axially uniform resonant cavity modes for potential use in electron paramagnetic resonance spectroscopy. *Rev. Sci. Instrum.* **72**(11): 4188-4200.

Mett, R. R. and J. S. Hyde (2003). Aqueous flat cells perpendicular to the electric field for use in electron paramagnetic resonance spectroscopy. *J. Magn. Reson.* **165**: 137-152.

Mims, W. B. (1976). *The Linear Electric Field Effect in Paramagnetic Resonance*, Oxford.

Molin, Y. N., V. M. Chibrikin, V. A. Shabalkin and V. F. Shuvalov (1966). Accuracy of the E. P. R. (electron paramagnetic resonance) measurement of paramagnetic-particles concentration. *Zavod. Lab.* **32**: 933.

More, K. M., G. R. Eaton and S. S. Eaton (1980). Magnetic susceptibility and EPR changes caused by grinding of samples. *J. Magn. Reson.* **37**(2): 217-22.

More, K. M., G. R. Eaton and S. S. Eaton (1984). Determination of T_1 and T_2 by simulation of EPR power saturation curves and saturated spectra. Application to spin-labeled iron porphyrins. *J. Magn. Reson.* **60**(1): 54-65.

Nagy, V. (1994). Quantitative EPR: Some of the most difficult problems. *Appl. Magn. Reson.* **6**: 259-285.

Nagy, V. Y. (1997). Choosing reference samples for electronic paramagnetic resonance (EPR) spectrometric concentration measurements. Part 1. General introduction and systems of S = 1/2. *Anal. Chim. Acta* **339**: 1-11.

Nagy, V. Y., P. N. Komozin and M. F. Desrosiers (1997a). Choosing reference samples for EPR concentration measurements. Part 3. Systems of S = 3/2. *Anal. Chim. Acta* **339**: 31-51.

Nagy, V. Y. and J. Placek (1992). Improvement of analytical accuracy of EPR spectrometer by taking into account variations in the shapes of samples. *Fresenius J. Anal. Chem.* **343**: 863-872.

Nagy, V. Y. and D. P. Sokolov (1997). Choosing reference samples for EPR concentration measurements. Part 2. Systems of S = 1. *Anal. Chim. Acta* **339**: 13-29.

Nagy, V. Y., D. P. Sokolov and M. F. Desrosiers (1997b). Choosing reference samples for EPR concentration measurements. Part 4. Systems of S = 5/2. *Anal. Chim. Acta* **339**: 53-62.

Narni, G., H. S. Mason and I. Yamazaki (1966). Quinhydrone as a Quantitative Standard for Electron Spin Resonance Spectrometry of Biological Systems. *Anal. Chem.* **38**: 367-368.

Noble, G. A. and J. J. Markham (1962). Analysis of paramagnetic resonance properties of pure and bleached F-centers in potassium chloride. *J. Chem. Phys.* **36**: 1340-1353.

Ohno, K. (1986). ESR imaging and its applications. *Appl. Spectros. Rev.* **22**: 1-56.

Ohno, K. (1987). ESR Imaging. *Magn. Reson. Rev.* **11**: 275-310.

Piekara-Sady, L. and L. D. Kispert (1994). ENDOR Spectroscopy, in *Handbook of Electron Spin Resonance*. J. C. P. Poole and H. A. Farach, Eds., New York, American Institute of Physics, **1**: Ch. V.

Pierce, B. S., T. E. Elgren and M. P. Hendrich (2003). Mechanistic implications for the formation of the diiron cluster in ribonucleotide reductase provided by quantitative EPR spectroscopy. *J. Am. Chem. Soc.* **125**: 8748-8759.

Pilbrow, J. R. (1990). *Transition Ion Electron Paramagnetic Resonance*, London, Oxford.

Plato, M., W. Lubitz and K. Mobius (1981). A solution ENDOR sensitivity study of various nuclei in organic radicals. *J. Phys. Chem.* **85**: 1202-1219.

Poole, C. P. (1967). *Electron Spin Resonance: A Comprehensive Treatise on Experimental Techniques*, New York, Interscience Publishers.

Poole, C. P. (1983). *Electron Spin Resonance: A Comprehensive Treatise on Experimental Techniques*, 2nd Ed., New York, Wiley.

Poole, C. P. and H. Farach (1971). *Relaxation in Magnetic Resonance*, New York, Academic Press.

Poole, J., C. P. and H. A. Farach (1974). Electron Spin Resonance, in *CRC Handbook of Spectroscopy*, **II**: 215.

Poole, J., C. P. and H. Farach, Eds. (1994). *Handbook of Electron Spin Resonance*. New York, AIP Press.

Presley, T., P. Kuppusamy, J. L. Zweier and G. Ilangovan (2006). Electron Paramagnetic Resonance Oximetry as a Quantitative Method to Measure Cellular Respiration: A Consideration of Oxygen Diffusion Interference. *Biophys. J.* **91**: 4623-4631.

Rages, K. A. and R. E. Sawyer (1973). Properties of Microwave Cavities Containing Magnetic Resonant Samples. *Rev. Sci. Instrum.* **44**(830-834).

Randolph, M. L. (1972). Quantitative Considerations in Electron Spin Resonance Studies of Biological Materials, in *Biological Applications of Electron Spin Resonance*. H. M. Swartz, J. R. Bolton and D. C. Borg, Eds., New York, Wiley, ch. 3.

Rataiczak, R. D. and M. T. Jones (1972). Investigation of the cw [continuous wave] saturation technique for measurement of electron spin-lattice relaxation. Application to the benzene anion radical. *J. Chem. Phys.* **56**: 3898-3911.

Rinard, G. A., S. S. Eaton, G. R. Eaton, C. P. Poole, Jr. and H. A. Farach (1999a). Sensitivity in ESR measurements. *Handbook of Electron Spin Resonance* **2**: 1-23.

Rinard, G. A., R. W. Quine, S. S. Eaton and G. R. Eaton (2002a). Frequency dependence of EPR signal intensity, 248 MHz to 1.4 GHz. *J. Magn. Reson.* **154**(1): 80-84.

Rinard, G. A., R. W. Quine, S. S. Eaton and G. R. Eaton (2002b). Frequency dependence of EPR signal intensity, 250 MHz to 9.1 GHz. *J. Magn. Reson.* **156**(1): 113-121.

Rinard, G. A., R. W. Quine, S. S. Eaton and G. R. Eaton (2004). Frequency dependence of EPR sensitivity. *Biol. Magn. Reson.* **21**: 115-154.

Rinard, G. A., R. W. Quine, J. R. Harbridge, R. Song, G. R. Eaton and S. S. Eaton (1999b). Frequency Dependence of EPR Signal-to-Noise. *J. Magn. Reson.* **140**(1): 218-227.

Rinard, G. A., R. W. Quine, R. Song, G. R. Eaton and S. S. Eaton (1999c). Absolute EPR Spin Echo and Noise Intensities. *J. Magn. Reson.* **140**(1): 69-83.

Robinson, B. H., C. Mailer and A. W. Reese (1999a). Linewidth analysis of spin labels in liquids. I. Theory and data analysis. *J. Magn. Reson.* **138**: 199-209.

Robinson, B. H., C. Mailer and A. W. Reese (1999b). Linewidth analysis of spin labels in liquids. II. Experimental. *J. Magn. Reson.* **138**: 210-219.

Russell, A. M. and D. A. Torchia (1962). Harmonic analysis in systems using phase sensitive detection. *Rev. Sci. Instrum.* **33**: 442-444.

Saraceno, A. J., D. T. Fanale and N. D. Coggeshall (1961). An Electron Paramagnetic Resonance Investigation of Vanadium in Petroleum Oils. *Anal. Chem.* **33**: 500-505.

Schell-Sorokin, A. J., F. Mehran, G. R. Eaton, S. S. Eaton, A. Viehbeck, T. R. O'Toole and C. A. Brown (1992). Electron spin relaxation times of fullerene ion (C_{60}^-) in solution. *Chem. Phys. Lett.* **195**: 225-32.

Schreurs, J. W. H., G. E. Blomgren and G. K. Fraenkel (1960). Anomalous relaxation of hyperfine components in electron spin resonance. *J. Chem. Phys.* **32**: 1861-1869.

Schreurs, J. W. H. and G. K. Fraenkel (1961). Anomalous relaxation of hyperfine components in electron spin resonance. II. *J. Chem. Phys.* **34**: 756-758.

Schultz, S. and E. M. Gullikson (1983). Measurement of static magnetization using electron spin resonance. *Rev. Sci. Instrum.* **54**: 1383-1385.

Schweiger, A. (1982). *Electron Nuclear Double Resonance of Transition Metal Complexes with Organic Ligands*, Springer-Verlag.

Segal, B. G., M. Kaplan and G. K. Fraenkel (1965). Measurement of g values in the electron spin resonance spectra of free radicals. *J. Chem. Phys.* **43**: 4191-4200.

Sert, I., M. M. Sünnetçioğlu, R. Surgur and G. Bingöl (2000). Dynamic Nuclear Polarization Studies of TANOL/water-glycerol Solutions. *Z. Naturforsch.* **55a**: 682-686.

Setaka, M., K. M. Sancier and T. Kwan (1970). Electron Spin Resonance Investigation of Electrical Conductivity Parameters of Zinc Oxide during Surface Reactions. *J. Catal.* **16**: 44-52.

Shaltiel, D., J. Genossar, A. Grayevsky, Z. H. Kalman, B. Fisher and N. Kaplan (1987). ESR in new high temperature superconductors. *Solid State Commun.* **63**: 987-990.

Sidabras, J. W., R. R. Mett and J. S. Hyde (2005). Aqueous flat cells perpendicular to the electric field for use in electron paramagnetic resonance spectroscopy, II: design. *J. Magn. Reson.* **172**: 333-341.

Siebert, D., J. Dahlem and V. Nagy (1994). Importance of Transition Probability Values for Accurate EPR Concentration Measurements. *Anal. Chem.* **66**: 2640-2646.

Slangen, H. J. M. (1970). Determination of the spin concentration by electron spin resonance. *J. Phys. E. Sci. Instrum.* **3**: 775-778.

Smirnov, A. I., S. W. Norby, T. Walczak, K. J. Liu and H. M. Swartz (1994). Physical and instrumental considerations in the use of lithium phthalocyanine for measurements of the concentration of oxygen. *J. Magn. Reson. B* **103**: 95-102.

Smith, G. W. (1964). Modulation Effects in Magnetic Resonance: Widths and Amplitudes for Lorentzian and Gaussian Lines. *J. Appl. Phys.* **35**: 1217-1221.

Stesmans, A. and A. VanGorp (1989). Improved measurement of the g factor of conduction electrons in lithium particles embedded in lithium-doped lithium fluoride. *Phys. Lett. A* **139**: 95-98.

Stoner, J. W., D. Szymanski, S. S. Eaton, R. W. Quine, G. A. Rinard and G. R. Eaton (2004). Direct-detected rapid-scan EPR at 250 MHz. *J. Magn. Res.* **170**: 127-135.

Subramanian, S. and M. C. Krishna (2005). Time-Domain Radiofrequency EPR Imaging, in *Biomedical EPR - Part A: Free Radicals, Metals, Medicine, and Physiology*. S. S. Eaton,

G. R. Eaton and L. J. Berliner, Eds., New York, Kluwer Academic, *Biol. Magn. Reson.* **23**: 321-383.

Subramanian, S., J. B. Mitchell and M. C. Krishna (2003). Time-domain radio frequency EPR imaging, in *In Vivo EPR (ESR)*. L. J. Berliner, Ed., New York, Kluwer Academic/Plenum Publisher, *Biol. Magn. Reson.* **18**: 153-197.

Sünnetçioğlu, M. and G. Bingöl (1993). An investigation of tanol/benzene solutions in weak and strong fields by EPR. *Phys. Chem. Liq.* **26**: 47-58.

Sünnetçioğlu, M., G. Bingöl and R. Sungur (1991). Hyperfine Structure and Relaxation Times of 4-Oxo-TEMPO/Methyl Alcohol Solutions in Weak and Strong Fields. *Z. Naturforsch.* **46a**: 976-982.

Swallen, S. F., K. L. Kearns, M. K. Mapes, Y. S. Kim, R. McMahon, M. D. Ediger, T. Wu, L. Yu and S. Satija (2006). Organic Glasses with Exceptional Thermodynamic and Kinetic Stability. *Science* **315**: 353-356.

Swartz, H. M., A. Iwasaki, T. Walczak, E. Demidenko, I. Salikhov, N. Khan, P. Lesniewski, J. Thomas, A. Romanyukha and D. S. Schauer, P. (2006). In Vivo EPR Dosimetry to Quantify Exposures to Clinically Significant Doses of Ionizing Radiation. *Radiat. Protect. Dosimetry* **120**: 163-170.

Tipikin, D. S., G. G. Lazarev and Y. S. Lebedev (1993). Mechanochemical generation of stable radical pairs. *Z. Fizich. Khim.* **67**: 176-9.

Tipikin, D. S., Y. S. Levbedev and A. Rieker (1997). Mechanochemical generation of stable radical species. Oxidation of pyrocatechols. *Chem. Phys. Lett.* **272**: 399-404.

Towell, J. and B. Kalyanaraman (1991). Detection of radical adducts of 5,5-Dimehtyl-1-Pyrroline N-oxide by the Combined Use of High-Performance Liquid Chromatography with Electrochemical Detection and Electron Spin Resonance. *Anal. Biochem.* **196**.

Tseitlin, M., A. Dhami, S. S. Eaton and G. R. Eaton (2007). Comparison of Maximum Entropy and Filtered Back-Projection Methods to Reconstruct Rapid-Scan EPR Images. *J. Magn. Res.* **184**: 157-168.

Tseitlin, M., A. Dhami, R. W. Quine, G. A. Rinard, S. S. Eaton and G. R. Eaton (2006). Electron Spin T_2 of a Nitroxyl Radical at 250 MHz Measured by Rapid Scan EPR. *Appl. Magn. Reson.* **30**: 651-656.

Urbanski, T. (1967). Formation of solid free radicals by mechanical action. *Nature* **216**: 577-8.

Vigouroux, B., J. C. Gourdon, P. Lopez and J. Pescia (1973). Broadening of the ESR line, caused by the variation of the cavity Q factor across the magnetic resonance. *J. Phys. E.* **6**: 557-558.

Wada, T., M. Yamanaka, T. Fujihara, Y. Miyazato and K. Tanaka (2006). Experimental and Theoretical Evaluation of the Charge Distribution over the Ruthenium and Dioxolene Framework of [Ru(OAc)(dioxolene)(terpy)] (terpy) 2,2':6',2”-terpyridine) Depending on the Substituents. *Inorg. Chem.* **45**: 8887-8894.

Wahlquist, H. (1961). Modulation Broadening of Unsaturated Lorentzian Lines. *J. Chem. Phys.* **35**: 1708-1710.

Watanabe, T., T. Sasaki and S. Fujiwara (1982). Phase Dependence of Saturation Transfer EPR Signals and Estimated Rotational Correlation Times. *Applied Spectrosc.* **36**: 174.

Weger, M. (1960). Passage Effects in Paramagnetic Resonance Experiments. *Bell System Technical J.* **39**: 1013-1112.

Weil, J. A. and J. K. Anderson (1965). The determination and reaction of 2,2-diphenyl-1-picrylhdrazyl with thiosalicylic acid. *J. Chem. Soc.* : 5567-5570.

Weil, J. A., J. R. Bolton and J. E. Wertz (1994). *Electron Paramagnetic Resonance: Elementary Theory and Practical Applications.*, New York, John Wiley & Sons, Inc.

Wertz, J. E. and J. R. Bolton (1972). *Electron Spin Resonance: Elementary Theory and Practical Applications*, McGraw-Hill.

Westenberg, A. A. (1975). Use of ESR for the quantitative determination of gas phase atom and radical concentrations. *Prog. Reaction Kinetics* **7**: 23-84.

Wilson, G. V. H. (1963). Modulation broadening of nuclear magnetic resonance and electron spin resonance line shapes. *J. Applied Phys.* **34**: 3276-3285.

Wright, A. C., H. K. Song and F. W. Wehrli (2000). In Vivo MR Micro Imaging with Conventional Radiofrequency Coils Cooled to 77 ^{o}K. . *Magn. Reson. Med.* **43**: 163-169.

Yordanov, N. D. (1994). Quantitative EPR Spectroscopy - "state of the art". *Appl. Magn. Reson.* **6**: 241-257.

Yordanov, N. D. (1996). Is our knowledge about the chemical and physical properties of DPPH enough to consider it as a primary standard for quantitative EPR spectrometry. *Appl. Magn. Reson.* **10**: 339-350.

Yordanov, N. D. and A. G. Christova (1994). DPPH as a Primary Standard for Quantitative EPR Spectrometry. *Appl. Magn. Reson.* **6**: 341-345.

Yordanov, N. D. and A. G. Christova (1997). Quantitative Spectrophotometric and EPR-Determination of 1,1-diphenyl-picryl-hydrazyl (DPPH) *Fresenius J. Anal. Chem.* **358**: 610-613.

Yordanov, N. D., V. Gancheva and V. A. Pelova (1999). Studies on some materials suitable for use as internal standards in high energy EPR dosimetry. *J. Radioanal. Nuclear Chem.* **240**: 619-622.

Yordanov, N. D. and B. Genova (1997). Analysis of Some Non-Linear Effects in Quantitative Electron Paramagnetic Resonance Spectrometry. Non-Linear Effects Due to the Use of Cavities with TE_{102} and TM_{110} Modes. *Anal. Chim. Acta* **353**: 99-103.

Yordanov, N. D. and M. Ivanova (1994a). The Present State of Quantitative EPR Spectrometry: The Results from an International Experiment. *Appl. Magn. Reson.* **6**: 333-340.

Yordanov, N. D. and M. Ivanova (1994b). Test Studies of Some Conventional CW EPR Spectrometer Settings. *Appl. Magn. Reson.* **6**: 347-357.

Yordanov, N. D., B. Mladenova and P. Petkov (2002). Studies on the uncertainties in quantitative EPR estimations due to the construction of the cavities used. *Anal. Chim. Acta* **453**: 155-162.

Yordanov, N. D. and P. Slavov (1996). Influence of the Diameter and Wall Thickness of a Quartz Pipe Inserted in the EPR Cavity on the Signal Intensity. *Appl. Magn. Reson.* **10**: 351-356.

Zecevic, A., G. R. Eaton, S. S. Eaton and M. Lindgren (1998). Dephasing of electron spin echoes for nitroxyl radicals in glassy solvents by non-methyl and methyl protons. *Mol. Phys.* **95**(6): 1255-1263.

Zweier, J. L., A. Samouilov and P. Kuppusamy (2003). Cardiac applications of in vivo EPR spectroscopy and imaging, in *In Vivo EPR (ESR)*. L. J. Berliner, Ed., New York, Kluwer Academic/Plenum Publishing, **18**: 442-468.

Part II – Practical Guides

Practical Guide 1: Obtaining the preliminary EPR scan
Practical Guide 2: Effect of microwave power, modulation amplitude, and field sweep width on your EPR spectrum.
Practical Guide 3: Post processing EPR spectra for optimal quantitative results.
Practical Guide 4: Quantitating nitroxide radical adducts using TEMPOL

Appendix Materials

CW EPR Starting from Pulsed EPR

S. S. Eaton and G. R. Eaton, Signal Area Measurements in EPR Bull Magn. Reson. 1 (3) 130-138 (1980)

S. S. Eaton and G. R. Eaton, Quality Assurance in EPR. Bull Magn. Reson. 13 (3/4) 83-89 (1992)

Patrick Carl and Peter Höfer, Quantitative EPR Techniques

M. Mazur and M. Valko, EPR Signal Intensity in a Bruker Single TE_{102} Rectangular Cavity. Bruker Spin Report 150/151, 26-30 (2002)

C. Mailer and B. Robinson Line width measurements and over-modulation.

Glass-forming solvents, from R. Drago Physical Methods in Chemistry, Saunders, 1977, page 318

CW EPR Starting from Pulsed EPR

The Spin Physics of CW EPR

The series of Workshops started with pulsed EPR, in part because pulsed EPR is much easier to understand than CW EPR. We will introduce CW EPR by starting with pulsed EPR.

Spin Magnetization and Its Representations

The spin magnetization of an ensemble of spins at a particular temperature, T, and magnetic field strength, B_0, is given by:

$M_0 = N_0 \frac{\gamma^2\hbar^2 B_0 S(S+1)}{3k_B T}$ $JT^{-1}m^{-3}$ (= Am^{-1}), so M/H is unitless, as required.

For S = ½, $M_0 = N_0 \frac{\gamma^2\hbar^2 B_0}{4k_B T} = N_0 \frac{g^2\beta^2 B_0}{4k_B T_{sample}}$

Definitions and units in these equations:

$g\beta = \gamma\hbar$

$\gamma = 1.7608 \times 10^7$ rad s^{-1} G^{-1}

$\hbar = 1.0546 \times 10^{-27}$ erg s rad^{-1}

N_0 is the number of spins per unit volume.

The static magnetic field $B_0 = \omega_0/\gamma$

S is the electron spin, which will be ½ in all of our calculations.

$k_B = 1.3806 \times 10^{-16}$ erg K^{-1} is Boltzmann's constant

T is the temperature of the sample in K.

The permeability of vacuum, $\mu_0 = 4\pi \times 10^{-7}$ $T^2J^{-1}m^3$.

In pictures, the familiar diverging lines (spin energy levels) represent the net populations of spins precessing around the magnetic field direction (Figure A-1)

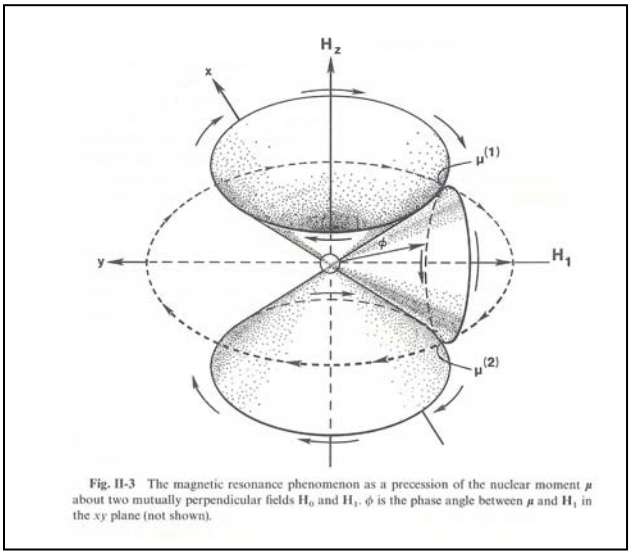

Fig. II-3 The magnetic resonance phenomenon as a precession of the nuclear moment μ about two mutually perpendicular fields H_0 and H_1. ϕ is the phase angle between μ and H_1 in the xy plane (not shown).

Figure A-1 The spins precess in cones with axes parallel with and antiparallel with the main magnetic field. At thermal equilibrium there are slightly more spins in one direction than the other. From Jardetzky and Roberts (1981).

The two cones of precession in this picture are the two energy levels we plot in a picture such as

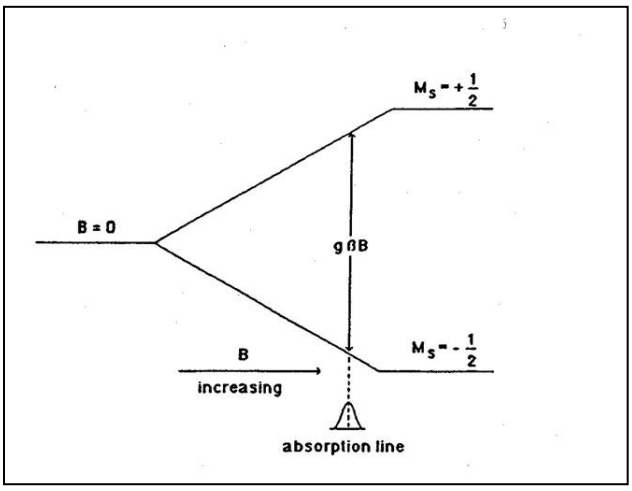

Figure A-2, which is the same as Figure 2-1.

The numbers of spins in each cone are the populations of these two energy levels. This picture can be elaborated to multiple spin states, hence multiple cones of precession, and multiple energy levels among which transitions can take place.

In a pulsed EPR (or NMR) experiment, the cones are oriented by the RF/microwave magnetic field vector.

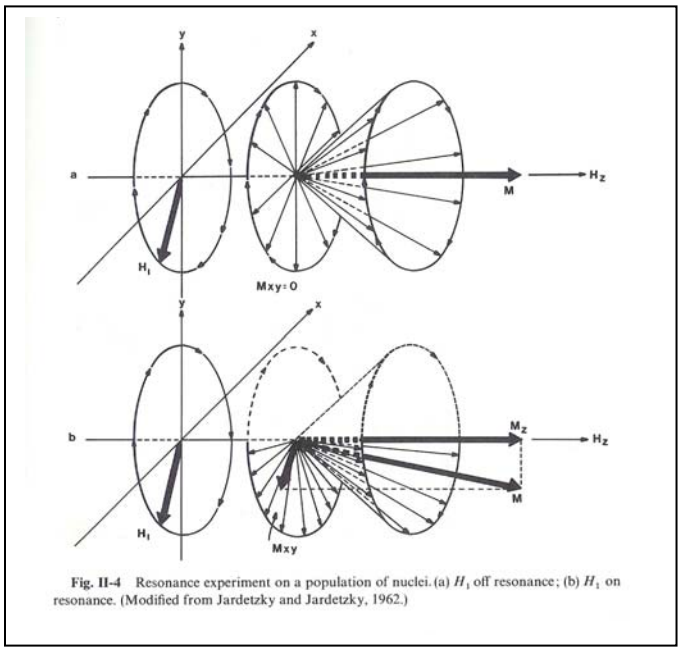

Fig. II-4 Resonance experiment on a population of nuclei. (a) H_1 off resonance; (b) H_1 on resonance. (Modified from Jardetzky and Jardetzky, 1962.)

Figure A-3 We modify the prior cone picture to now focus only on the net spins, and see that when the field/frequency is on resonance the cone tips from being symmetric (no net

magnetization) in the xy plane to having net magnetization in the xy plane. From Jardetzky and Roberts (1981).

It is awkward to keep drawing the actual cones of precession, so it has become customary to show only the net magnetization vector, but one should recall that the spins are not really on the field axis but rather are precessing around this axis. The vector model is a useful and reasonably accurate way to describe the spin physics. We will from this point on assume that this is obvious, and just use the vector picture. In terms of the vector picture the simplest possible magnetic resonance experiment is to turn the spins 90 degrees into the xy plane, and watch the recovery to equilibrium by monitoring the xy magnetization (Figure A-4).

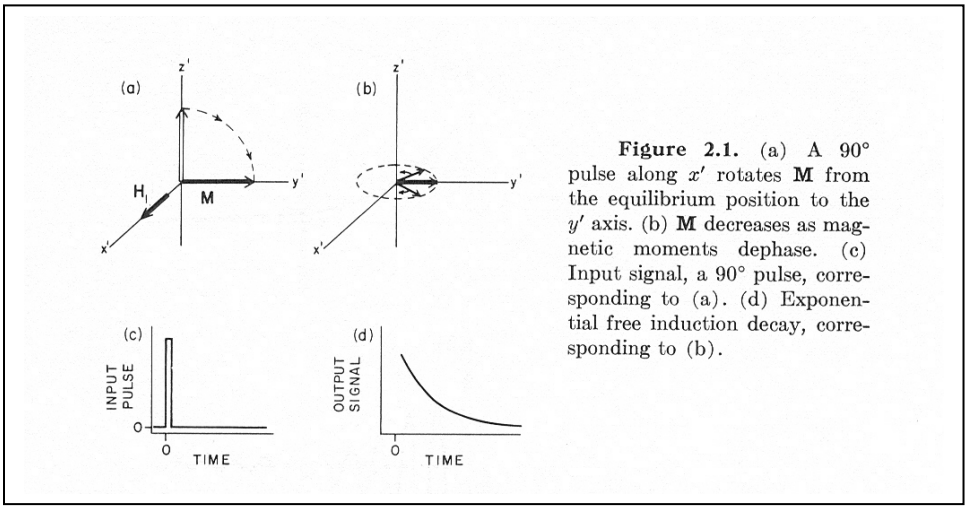

Figure 2.1. (a) A 90° pulse along x' rotates **M** from the equilibrium position to the y' axis. (b) **M** decreases as magnetic moments dephase. (c) Input signal, a 90° pulse, corresponding to (a). (d) Exponential free induction decay, corresponding to (b).

Figure A-4 Net magnetization vector picture of a pulse turning the M_z magnetization into the xy plane, and the recovery to the z axis, resulting in an FID. From Farrar and Becker (1971).

The turning angle, θ, of the spins is calculated with the formula:

$$\theta = \gamma B_1 t_p$$

For example, θ = π/2 (90-degree pulse) is achieved with a 20 ns pulse that has B_1 = ca. 4.46 G:

$$B_1 = \frac{\pi/2}{\gamma t_p} = \frac{\pi/2}{\left(1.7608\text{x}10^7 \text{ rad G}^{-1}\text{ s}^{-1}\right)\left(20\text{x}10^{-9}\text{s}\right)} = 4.46\text{G}$$

Now, let's gradually approach a CW experiment. If the incident power were, say, 1 mW, an approximate relation for a TE_{102} X-band cavity is

$$B_1 = 0.02\sqrt{QP} = 0.02\sqrt{(3000)(0.001)} = 0.0346$$

This B_1 would yield a 90-degree pulse if t_p = 2.6 μs. Hence in ca. 10 μs the spins rotate about 360 degrees. Continuing this argument, the spins rotate a full 360 degrees about 10^5 times per second. If the sample has a long relaxation time, the multiple rotations as the pulse length is increased at constant B_1, or as B_1 is increased at constant t_p, can be observed on a pulse spectrometer. Now we add another fact, that in a microwave radiation field the transitions from the low energy level to the high energy level are equally probable with the transitions from the

high energy level to the low energy level. Thus, if there is no relaxation pathway, the energy levels will become equally populated. This is what is called saturation. However, there are relaxation pathways that tend to return the spin system to thermal equilibrium, as sketched in Figure A-5.

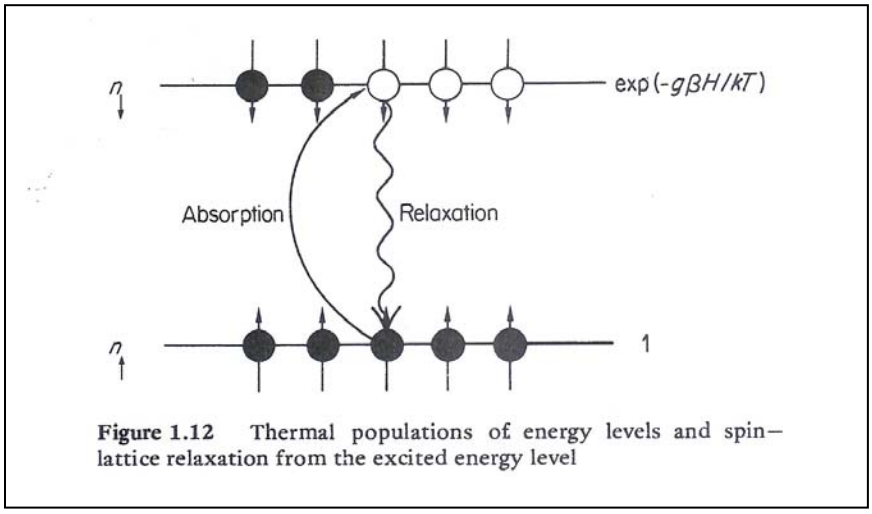

Figure 1.12 Thermal populations of energy levels and spin–lattice relaxation from the excited energy level

Figure A-5 The microwave field causes transitions between the energy levels that tend to equalize the populations in the two energy levels, and spin-lattice relaxation tends to return the populations to the thermal equilibrium.

Part of the expression for the shape of an EPR line is a factor that we call the saturation factor, S,

$$S = \frac{1}{1+\gamma^2 B_1^2 T_1 T_2}$$

If the T_1 and T_2 relaxation times were 1 μs each, then using the B_1 example calculated above for 1 mW incident power,

$$S = \frac{1}{1+\left(1.76\text{x}10^7\right)^2 (0.0346)^2 \left(1\text{x}10^{-6}\right)\left(1\text{x}10^{-6}\right)} = \frac{1}{1+0.37} = 0.73$$

Since S is much less than 1, a species with 1 μs relaxation times would be partially saturated at 1 mW in a high-Q cavity resonator.

The power absorbed by the spin system is due to spin-lattice relaxation (T_1) of the spins. The dynamic (RF) susceptibility of the spin system is defined in terms of power absorption. The magnetic susceptibility of the sample, χ'' (dimensionless), is the imaginary component of the effective RF susceptibility. It is χ'' that one measures in a CW EPR spectrum.

It is in fact the spin-lattice relaxation that makes it possible to perform CW EPR.

Tabulated values of relaxation times (Bertini et al. 1994a; 1994b; Eaton and Eaton 2000b) for many species would make the saturation term, S, too small relative to the practical experience that it is possible to obtain CW EPR spectra of many species with long T_1. There are two parts

to the explanation of this observation. First, many spectra are actually run substantially saturated. Second, there are spectral diffusion processes in many species that are faster than T_1 and T_2, and in such cases the T_1T_2 product should be replaced with a product in which one or both of these relaxation times is replaced by the spectral diffusion time. Irradiated alanine is an important example of such a case. Irradiated SiO_2 is an example of a species for which the relaxation times are so long that it is almost impossible to obtain an unsaturated CW EPR spectrum. This case is discussed in more detail later in these notes.

In summary, CW EPR works only because spin-lattice relaxation relieves saturation of the populations of the spin energy levels. The power absorption due to this spin relaxation is what is detected in CW EPR.

Why CW Instead of Pulse?

Given this approach of morphing pulsed EPR into CW EPR, and the greater difficulties of understanding the CW experiment, we should ask why we should not just perform pulsed EPR instead of performing CW EPR. This answer is also in terms of B_1 and relaxation times. First, it is very difficult to create pulses with B_1 large enough to excite the entire spin system, so the analog of the pulsed, FID-detected, FT NMR spectrum works for only a limited range of compounds with needed long relaxation times and narrow spectral extent. Many spectra are wide relative to the resonator Q, so even if the FID experiment is feasible, the resulting spectrum will have intensity distortions. Even with low Q, the ring-down time after a pulse, and other contributions to the dead time are long enough that many species relax during the dead time and cannot be observed with either FID or spin echo type experiments. Consequently, there will always be a role for CW EPR.